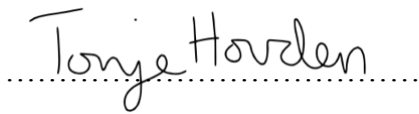




University of
Stavanger

Faculty of Science and Technology

MASTER'S THESIS

Study program/Specializations: Master's in Industrial Economics/ Specializations: Risk analysis, Project management, Contract administration	Spring semester, 2018 Open
Writer: Tonje R. Hovden	 (Writer's signature)
Faculty supervisor: Aksel Hiorth Internal supervisors Merete Vadla Madland and Reidar Inge Korsnes	
Thesis title: Compaction of fine granular calcite by pressure solution at high temperature and stress with and without organic additive in pore fluid	
Credits (ECTS): 30	
Key words: Pressure solution Calcite powder Organic additive Uniaxial strain loading and creep Ion concentrations SEM – scanning electron microscope	Pages: 88 + enclosure: 13 Stavanger, 15.06/2018 Date/year

Acknowledgement

First and foremost, I am very grateful towards the National IOR Centre of Norway at the University of Stavanger for making me feel welcome and cared for throughout the semester. I feel very lucky to have been allowed to spend so much time in their office locations, working on my thesis for all these months. This is very much appreciated.

I would also like to use this opportunity to thank my supervisors Professor Aksel Hiorth and Professor Merete Vadla Madland for help and guidance. I also want to give a big thank you to my supervisor Dr. Reidar Inge Korsnes for helping and supporting me in the lab throughout the semester, always in a good mood and giving great advice. In addition, having weekly meetings with Aksel and Reidar have been very useful.

Also, a big thank you to Mona Minde for providing SEM images.

Abstract

Pressure solution is a compaction mechanism that reduces both porosity and permeability. It is a common and important water-rock interaction process and it is a widespread phenomenon that influences many essential natural processes. It is an important mechanism, but it is poorly understood. Especially when there are organic molecules present. It often leads to materials having a stronger and more resilient structure and texture, compared to the absence of the organic molecules. Obtaining a good understanding of the mechanism and the rate of compaction in calcite under upper crust conditions are therefore of major interest.

The objective of this study has been to make artificial cores out of calcite powder and performing uniaxial strain tests with loading to an axial stress of 30 MPa at 130 °C, where basic quantities like stress-strain relationship and axial creep over time were measured. Two different brines were used to flood the artificial cores, one with and one without organic additive, too see how this affected the results. Also, two tests were performed at lower stress, to see how the cores and grains behaved with a smaller amount of stress applied. Chemical analysis and scanning electron microscope (SEM) analysis were conducted to investigate the ion concentrations and their potential changes. A novel contribution in this thesis compared to previous work is that we used the SEM images to quantify the grain size distribution, and changes in grain size distribution when the various tests were performed.

All tests performed with an axial stress of 30 MPa showed a similar behavior for both the axial strain loading phase with values laying between 12.7-15.5% and for the creep phase with values between 8.2-12.0%. A minor difference was seen on the creep, as the presence of oxalic acid seemed to make the cores stronger. This was supported by SEM investigations, the presence of oxalic acid made the occurrence of tiny grain size almost nonexistent compared to the cores being flooded without an organic additive. Comparing the high pressure tests to the low pressure tests, the grain distribution in low-pressure tests were more evenly distributed throughout the cores, with small variations. For the chemical analysis in the tests, there were only observed changes for the Ca^{2+} concentrations. A loss in calcium throughout the test durations was observed, and there were indications that the loss seemed to be greater with the presence of oxalic acid.

This study revealed or at least point to differences in the mechanical behavior and microstructure in the cores flooded with and without organic additives, and with and without overburden pressure. In order to further quantify the differences and draw some solid conclusions regarding the nature of pressure solutions, we believe that the tests should have been performed for longer period of times. However, the results in this thesis indicates that the presence of oxalic acid preserves the grain distribution to a larger degree compared to the cores flooded without oxalic acid, which should be investigated further.

Table of contents

Acknowledgement.....	2
Abstract	3
List of tables	7
List of figures.....	8
List of symbols.....	12
1. Introduction	13
1.1. Structure of the thesis	13
1.2. Background.....	13
1.3. Objectives and tasks.....	15
2. Theory	16
2.1. Porosity.....	16
2.2. Permeability.....	17
2.3. Darcy's law	17
2.4. Stress, strain and creep	20
2.5. Pressure solution.....	25
3. Procedure and equipment	27
3.1. Test material - calcite-powder	27
3.2. Making core samples.....	27
3.3. Brines.....	28
3.4. Equipment	30
3.5. Test-setup.....	32
3.6. Post experiments	34
3.6.1. Chemical analysis by ion chromatography.....	34
3.6.2. Sampling for SEM – scanning electron microscope.....	34

4.	Results	36
4.1.	Uniaxial strain tests.....	37
4.1.1.	Experiment without organic additive and low stress	37
4.1.2.	Experiments without organic additive, but with axial stress of 30 MPa.....	39
4.1.3.	Experiment with organic additive and axial stress of 30 MPa	47
4.1.4.	Experiments with oil leakage	50
4.2.	Chemical analysis.....	53
4.2.1.	Experiment without organic additive and low stress	54
4.2.2.	Experiments without organic additive, but with axial stress of 30 MPa.....	54
4.2.3.	Experiment with organic additive and axial stress of 30 MPa	55
4.1.4.	Experiments with oil leakage	56
4.2.5.	pH - values	56
4.3.	Calcite microstructure morphology - SEM.....	58
4.2.1.	Experiment without organic additive, but with axial stress of 30 MPa.....	59
4.3.2.	Experiments without organic additive and low stress	66
4.3.3.	Experiments with organic additive and axial stress of 30 MPa	67
5.	Discussion	69
5.1.	Uniaxial strain loading	69
5.2.	Creep phase.....	71
5.3.	Chemical analysis.....	77
5.4.	SEM - Scanning Electron Microscope	77
5.5.	Sources of error.....	83
6.	Conclusion	84
6.1.	Future recommendations	86
7.	References	87
	Appendix	89

List of tables

Table 3. 1: Overview of values for each test before tests have began.....	28
Table 3. 2: Fluids purpose and composition.....	28
Table 4.1. 1: Overview of LP5.....	37
Table 4.1. 2: Values for LP5	38
Table 4.1. 3: Overview of different values for HP1, HP2, HP3 and HP4. * indicates that the tests failed.....	39
Table 4.1. 4: Values for HP1.....	40
Table 4.1. 5: Values for HP2.....	42
Table 4.1. 6: Values for HP3.....	44
Table 4.1. 7: Values for HP4.....	46
Table 4.1. 8: Overview of HPA7.....	48
Table 4.1. 9: Values for HPA7.....	49
Table 4.1. 10: Overview of HPA6 and LP9.....	50
Table 4.1. 11: Values for HPA6.....	51
Table 4.1. 12: Values for LP9.....	52
Table 4.2. 1: A table showing the pH values for each test on different days in the test period. The values marked with * means that the tests are being flooded with DW. Note that the Ca ²⁺ values seem to be lower for the test containing oxalic acid (HPA6 and HPA7, marked with a darker grey color) for all the different days compared to the rest.....	57
Table 5. 1: Overview of different values for all tests performed	69

List of figures

Figure 2. 1: forces acting on three different cross-sectional areas. (Fjær, et al. 2008)	20
Figure 2. 2: decomposition of a force acting on a cross-section (Fjær, et al. 2008).	21
Figure 2. 3: Stress acting on a square in two dimensions (Fjær, et al. 2008).....	22
Figure 2. 4: Stress-strain curve for uniaxial strain test showing strain on the x-axis and stress on the y-axes.....	24
Figure 2. 5: Strain against time for uniaxial strain test. We here clearly see the different stages in a creep process. (Fjær, et al. 2008).....	25
Figure 3. 1: a); rod with a drainage plate and filters in the lower part of the shrinking sleeve. b): powder filled into the sleeve. c): the full length of the core.	27
Figure 3. 2: The artificial core is placed on the underbody with an extensometer around it (a). A cap was placed on top after each test has been assembled (b). The assembled Triaxial cell (c).....	31
Figure 3. 3: a) is the piston cell used for each experiment. B) is the piston- and confining pump, and c) is the flooding pump.	32
Figure 3. 4: a) show the dilution of water samples taken during a test. This was done with a Gilson GX-271 Liquid Handler. When this was completed, the samples were placed in smaller glasses and put in a black stand (b), before finally being put into the machine (c). This was a Dionex ICS 5000+.....	34
Figure 3. 5: Sketched drawing of how the core from test 1 was cut and where three samples were collected.....	35
Figure 3. 6: a): the core from HP1 as a whole, b) the core in halves and c) one of the halves cut into two pieces.....	35
Figure 4.1. 1: Axial creep strain [%] and permeability as a function of creep time [days] for LP5.	38
Figure 4.1. 2: Axial stress [MPa] as a function of Axial strain [%] for HP1.	40
Figure 4.1. 3: Axial creep strain [%] and permeability as a function of creep time [Days] for HP1.....	41
Figure 4.1. 4: Axial stress [MPa] as a function of axial strain [%] for HP2.	42

Figure 4.1. 5: Axial creep strain [%] and permeability as a function of creep time [Days] for HP2.....	43
Figure 4.1. 6: Axial stress [MPa] as a function of Axial strain [%] for HP3.....	44
Figure 4.1. 7: Axial creep strain [%] and permeability as a function of creep time [Days] for HP3.....	45
Figure 4.1. 8: Axial stress [MPa] as a function of axial strain [%] for HP4.	46
Figure 4.1. 9: Axial creep strain [%] and permeability as a function of creep time [Days] for HP4.....	47
Figure 4.1. 10: Axial stress [MPa] as a function of Axial strain [%] for HP7.	48
Figure 4.1. 11: Axial creep strain [%] and permeability as a function of creep time (days). .	49
Figure 4.1. 12: Axial stress [MPa] as a function of Axial strain [%] for HPA6.	50
Figure 4.1. 13: Axial creep strain [%] and permeability as a function of creep time [Days] for HPA6.....	51
Figure 4.1. 14: Axial creep strain [%] and permeability as a function of creep time [Days] for LP9.	52
Figure 4.2. 1: Sodium, chloride and calcium concentrations [mol/l] as a function of flow time [days] for LP5.....	54
Figure 4.2. 2: Sodium, chloride and calcium concentrations [mol/l] as a function of flow time [days] for HP1 (a), HP2 (b), HP3 (c) and HP4 (d).....	55
Figure 4.2. 3: Sodium, chloride and calcium concentrations [mol/l] as a function of flow time [days] for HPA7.	55
Figure 4.2. 4: Sodium, chloride and calcium concentrations [mol/l] as a function of flow time [days] for HPA6 (a) and LP9 (b).....	56
Figure 4.3. 1: The different locations the samples investigated in SEM are collected from for HP1.....	59
Figure 4.3. 2: SEM image of inlet for HP1.	60
Figure 4.3. 3: SEM image of inlet for HP1.	60
Figure 4.3. 4: SEM image of the middle location for HP1.	61
Figure 4.3. 5: SEM image of outlet for HP1.	61
Figure 4.3. 6: The frequency of the grains as a function of different grain sizes for HP1. The ufl indicates the original and unflooded powder. (tiny: 0.87x0.87 μm , very small: 0.87x0.87 – 1.74x1.74 μm , small: 1.74x1.74-2.9x2.9 μm , medium: 2.9x2.9-6.38x6.38 μm , large: 6.38x6.38 μm)	62

Figure 4.3. 7: The locations of where samples were collected from the core in HP2.....	63
Figure 4.3. 8: The frequency of the grains as a function of different grain sizes for HP2. (tiny: 0.87x0.87 μm , very small: 0.87x0.87 – 1.74x1.74 μm , small: 1.74x1.74-2.9x2.9 μm , medium: 2.9x2.9-6.38x6.38 μm , large: 6.38x6.38 μm)	63
Figure 4.3. 9: The locations of where samples were collected from the core in HP4.....	64
Figure 4.3. 10: The frequency of the grains as a function of different grain sizes for HP4. (tiny: 0.87x0.87 μm , very small: 0.87x0.87 – 1.74x1.74 μm , small: 1.74x1.74-2.9x2.9 μm , medium: 2.9x2.9-6.38x6.38 μm , large: 6.38x6.38 μm)	65
Figure 4.3. 11: The locations of where samples were collected from the core in LP5.	66
Figure 4.3. 12: The frequency of the grains as a function of different grain sizes for LP5. (tiny: 0.87x0.87 μm , very small: 0.87x0.87 – 1.74x1.74 μm , small: 1.74x1.74-2.9x2.9 μm , medium: 2.9x2.9-6.38x6.38 μm , large: 6.38x6.38 μm)	66
Figure 4.3. 13: The locations of where samples were collected from the core in HPA7.....	67
Figure 4.3. 14: The frequency of the grains as a function of different grain sizes for HPA7. (tiny: 0.87x0.87 μm , very small: 0.87x0.87 – 1.74x1.74 μm , small: 1.74x1.74-2.9x2.9 μm , medium: 2.9x2.9-6.38x6.38 μm , large: 6.38x6.38 μm)	68
Figure 5.1. 1: An overview of all the tests plotted for axial stress [MPa] as a function of axial strain [%].	70
Figure 5.2. 1: Axial creep strain [%] as a function of creep time [Days] for all the high-pressure tests without organic additive. The black dots indicate DW.	71
Figure 5.2. 2: Axial creep strain [%] as a function of creep time [Days] for all the high-pressure tests. The black color indicated flooding with DW.	73
Figure 5.2. 3: Axial creep strain [%] as a function of creep time [Days] for low-pressure tests	76
Figure 5.2. 4: Radial creep strain [%] as a function of creep time [Days] for low-pressure tests	76
Figure 5.4. 1: the distribution for the unflooded powder. (tiny: 0.87x0.87 μm , very small: 0.87x0.87 – 1.74x1.74 μm , small: 1.74x1.74-2.9x2.9 μm , medium: 2.9x2.9-6.38x6.38 μm , large: 6.38x6.38 μm)	78
Figure 5.4. 2: Overview of the grain distributions for all the cores from the inlet samples. (tiny: 0.87x0.87 μm , very small: 0.87x0.87 – 1.74x1.74 μm , small: 1.74x1.74-2.9x2.9 μm , medium: 2.9x2.9-6.38x6.38 μm , large: 6.38x6.38 μm)	79

Figure 5.4. 3: Overview of the grain distributions for all the cores from the middle samples. (tiny: 0.87x0.87 μm , very small: 0.87x0.87 – 1.74x1.74 μm , small: 1.74x1.74-2.9x2.9 μm , medium: 2.9x2.9-6.38x6.38 μm , large: 6.38x6.38 μm)	80
Figure 5.4. 4: Overview of the grain distributions for all the cores from the outlet samples. (tiny: 0.87x0.87 μm , very small: 0.87x0.87 – 1.74x1.74 μm , small: 1.74x1.74-2.9x2.9 μm , medium: 2.9x2.9-6.38x6.38 μm , large: 6.38x6.38 μm)	81
Figure A. 1: The HP1 core was clearly white (a), while P6 was brown in color (b).	90
Figure A. 2: SEM image of inlet for HP1.	90
Figure A. 3: SEM image of inlet for HP1.	91
Figure A. 4: SEM image of the middle for HP1.	91
Figure A. 5: SEM image of outlet for HP1.	92
Figure A. 6: SEM image of inlet for HP2.	92
Figure A. 7: SEM image of the middle for HP2.	93
Figure A. 8: SEM image of outlet for HP2.	93
Figure A. 9: SEM image of rim for HP2.....	94
Figure A. 10: SEM image of the powder used to make the core.	94
Figure A. 11: SEM image of inlet for HP4.	95
Figure A. 12: SEM image of inlet for HP4.	95
Figure A. 13: SEM image of the middle for HP4.	96
Figure A. 14: SEM image of outlet for HP4.	96
Figure A. 15: SEM image of rim for HP4.....	97
Figure A. 16: SEM image of inlet for LP5.....	97
Figure A. 17: SEM image of the middle for LP5.....	98
Figure A. 18: SEM image of outlet for LP5.....	98
Figure A. 19: SEM image of rim for LP5.	99
Figure A. 20: SEM image of inlet for HPA7.	99
Figure A. 21: SEM image of inlet for HPA7.	100
Figure A. 22: SEM image of the middle for HPA7.	100
Figure A. 23: SEM image of outlet for HPA7.	101

List of symbols

ϕ	porosity
V_b	bulk volume
V_s	solid volume
V_p	pore volume
r	radius
h	height
g	weight
ρ	density
D	Darcy
q	flow rate
K	permeability
A	cross sectional area
μ	viscosity
ΔP	pore pressure
L	length
LVDT	Linear Voltage Displacement Transducer
HP1	High-pressure test - Powder 1
HP2	High-pressure test - Powder 2
HP3	High pressure test - Powder 3
HP4	High pressure test - Powder 4
LP5	Low-pressure test - Powder 5
HPA6	High-pressure test with oxalic acid - Powder 6
HPA7	High-pressure test with oxalic acid - Powder 7
LP9	Low-pressure test - Powder 9
o.l.	oil leakage
DW	distilled water
SEM	scanning electron microscope
Na^+	Sodium
Cl^-	Chloride
Ca^{2+}	Calcium

1. Introduction

1.1. Structure of the thesis

The thesis contains a total of 7 chapters. In addition, there is a section of acknowledgement, abstract and lists of tables, figures and symbols. Chapter 1 is the introduction. Here, there is a description of the background for this thesis and a description of the objectives and tasks performed. In chapter 2 we present some of the underlying theory, and this is followed by chapter 3 which contains the procedure for the uniaxial strain tests and equipment used. Further, chapter 4 is the results where all the tests are presented. They are all presented in an order decided in advance, so not in a numerical or chronological order. Chapter 5 is the discussion part where the results are discussed, and it is followed by chapter 6 which contains the conclusion made from working on this thesis. Chapter 7 is the references used. At the end of the thesis there is an appendix section. This contains the SEM images from the cores that are not presented in the thesis but were used to count the grains on different locations on the various cores.

1.2. Background

About 60% of the world's oil reserves and 40% of the world's gas reserves are found in carbonate reservoirs. Acquiring a detailed understanding of the process and rate of compaction in calcite under upper crust conditions is therefore of big interest in both reservoir and fault zone carbonates. Pressure solution is an important phenomenon in many environmental and geological systems. It reduces the porosity and permeability of rocks, both clastic and carbonate rocks under diagenetic conditions. Compaction by pressure solution is accomplished by stress-driven dissolution of material from contact by grains that comprise the load-bearing framework in the aggregate. Material that has been dissolved is transported out of the contacts by diffusion. This is transported through a fluid film or a microscale channel network at the grain boundary. Then, it is precipitated on the pore walls or it is removed from the system by diffusion. Pressure solution is believed to play an important role in controlling the quality of hydrocarbon reservoirs, sealing capacity of reservoir-bounding faults and evolution of the strength properties of fault zones. It has been considered to be the most important ductile deformation mechanism in the upper crust (Ben-Itzhak, Erez og Aharonov 2015). It controls the oil and gas reservoir

productivity. With that said, the phenomenon is poorly understood in many ways. And particularly when organic molecules are involved. The existence of organic molecules makes the characteristics and conditions differ compared to if they were not present. They can affect the precipitation, the dissolution and the morphology of the surfaces. Often, it will make the materials stronger and having more resilient structures and textures compared to if the organisms were absent (Ben-Itzhak, Erez og Aharonov 2015).

The purpose of this master thesis has been to get a deeper understanding of pressure solution. We have chosen to use a simplified system, to better analyze the results. The system investigated is artificial core samples made out of calcite powder. The uniaxial strain loading- and creep phase of uniaxial strain tests and other key controlling variables have been investigated. The effluent samples of the fluid passing through the cores have been analyzed and the changes in concentrations throughout the test-durations have been measured. The tests include the introduction of change in the fluid composition being flooded through the cores, adding oxalic acid for some of the tests. Also, the cores have been further investigated by Scanning Electron Microscopy (SEM), and the grains in the cores have been studied. Before performing any of the experiments, we had the hypothesis that there should be some differences for the tests with and without oxalic acid, and that this difference could be linked to changes in the pore scale texture.

In order to compare the tests at high stress (to observe pressure solutions), we chose to also do some tests at low confining stress. These tests were then performed without adding oxalic acid. The same investigations were done on these two tests, as for those exposed to high stress.

Experimental work with powder has been done prior to this thesis, but with some distinct differences. One example is uniaxial creep experiments with crushed limestone and analytical grade calcite powders. This was done at a temperature of 150 °C, pore fluid pressure of 20 MPa and effective axial stresses of 30 and 40 MPa. The intent was to determine the inter-relationship between pore fluid chemistry, compaction rate and the rate-controlling process of intergranular pressure solution (Zhang, Spiers og Peach 2011). Also, some similar uniaxial compaction experiments have been carried out by the same people, using milled limestone, analytical grade calcite and superpure calcite. These tests were performed with a temperature between 28°C-150°C, pore pressure of 20 MPa and effective stresses of 20-47 MPa. The intent was to

determine if creep would occur by intergranular pressure solution under the mentioned conditions and to find the rate-controlling process (Zhang, Spiers and Peach 2010).

1.3. Objectives and tasks

This master thesis was divided into three tasks. Task 1: perform long-term compaction creep experiments on fine granular calcite by using a Triaxial cell. During the different test-durations, controlling, monitoring and adjusting setups like confining, piston and pore pressure have been conducted. Data have been logged constantly so that one could measure axial creeps over time and stress-strain relations. Task 2: collect effluent water samples regularly so that the ion concentration could be analyzed. Furthermore, the pH value was measured on a regular basis to observe how it changed over time. Task 3: take images of the cores by SEM, investigating the calcite microstructure morphology, including counting and classifying the grains. Investigating how the distribution of different grain sizes changes throughout each core and between different cores.

These three tasks were conducted by performing a total of 8 tests. All the experiments were conducted under controlled conditions. The temperature was 130°C, the tests were loaded to an axial stress of 30 MPa, except for two, before they were left to creep. The two other tests were performed at a confining pressure of 1.2 MPa. Two different brines were used, one without organic additive and one with organic additive – oxalic acid (HOCCOOH).

2. Theory

2.1. Porosity

Porosity is a measure of the part of a rock that does not consist of rock grains or fine mud rock, i.e. the voids in the material. It is usually given as a percentage of how much it represents out of the total volume, and it is a static parameter defined locally as an average over the volume of the rock. It can be written as:

$$\phi = \frac{V_b - V_s}{V_b} = \frac{V_p}{V_b}, \quad (2.1)$$

where ϕ is porosity, V_b is the bulk volume, V_s is solid volume and V_p is the pore volume.

One can differentiate between absolute and effective porosity. Absolute porosity is the ratio of the total void space in a rock, regardless if the void spaces are interconnected or not, to the bulk volume of that rock. Effective porosity is the ratio of the total volume of interconnected voids in a rock to the bulk volume of that rock. There are numerous factors that affect the effective porosity like type of rock, the heterogeneity of grain sizes, how the grains are packed and cemented, weathering and leaching, type of clay, etc. (Ursin og Zolotukhin 2000) It is the effective porosity value that is used in reservoir engineering calculations. This is due to the petroleum that occupies non-connected void spaces, it cannot be produced, and is therefore of little interest. An important exception is the production of shale gas and oil, where almost all the oil and gas are located in nonconnected pores and is being produced by fracturing (Tiab og Donaldson 2004).

2.2. Permeability

When a rock is capable of transporting fluids through interconnected pores, the rock is permeable. The lack of interconnected pores would make the rock impermeable, and this way we can assume that there is a correlation between permeability and porosity (Ursin og Zolotukhin 2000). With zero porosity, no fluids can be transported and therefore a change in the porosity will then often affect the permeability, even though there are a few exceptions (like for pumice stone, clay and shale.)

As can be seen below, the permeability is part of the Darcy's law equation, having the symbol k . The permeability is measured in Darcy (D), and the majority of the petroleum reservoir rocks are less than one Darcy. It is also common to use millidarcy (mD) which is a smaller unit → 1D is the same as 1000 mD.

One can distinguish between absolute and relative permeability. If there is only one fluid that saturates a rock a 100%, then we use the term "absolute" permeability. The term "relative" permeability is used when there is more than one fluid present.

There are different factors that can have an impact on the permeability. It can be the shape and size of the sand grains, lamination, cementation and fracturing and solution (Tiab og Donaldson 2004).

2.3. Darcy's law

Darcy's law, originating from Henry Darcy, describes the flow of fluids through a porous rock and it applies to both compressible and incompressible fluids. The difference between the two, is that for a compressible fluid, the measure of the volume change will be reduced with the presence of an external pressure and in reality, all fluids that we encounter in our daily lives are compressible. While for incompressible fluids, the term is introduced as a hypothetical type of fluid to make it easier to do calculations. It does not change its volume due to external pressure.

The law is:

$$q = \frac{k \cdot A}{\mu} \frac{\Delta P}{L}, \quad (2.2.)$$

Where: q = flow rate, k = permeability of the porous rock, A = (total) cross sectional area, μ = viscosity of the fluid, ΔP = pore pressure, L = length.

It is possible to derive an expression between the permeability and porosity, by assuming that the porous medium can be represented with a bundle of tubes. Poiseuille's law, tells us the pressure drop of a fluid that is flowing with a laminar flow through a pipe with a cylindrical shape with a cross section that is constant. It is possible to combine this to Darcy's law to get an expression for permeability. The Poiseuille's law is as followed:

$$q = \frac{\pi R^4}{8\mu} \frac{\Delta p}{Lc}, \quad (2.3.)$$

This small q indicates that the equation is for a small cylindrical pipe, that is one part of numerous ones which constitutes a larger pipe Q .

We have N small pipes:

$$Q = Nq = \frac{N\pi R^4}{8\mu} \frac{\Delta p}{Lc}, \quad (2.4.)$$

As seen above, the equation (equation 2.1.) for the porosity is: $\phi = \frac{V_p}{V_b}$

Which then can be written as:

$$\phi = \frac{N\pi R^2 \cdot Lc}{Vb}, \quad (2.5.)$$

$$N = \frac{\phi \cdot Vb}{\pi R^2 \cdot Lc}, \quad (2.6.)$$

Putting this N into Q (equation 2.4):

$$Q = \frac{\phi \cdot Vb}{\pi R^2 Lc} \frac{\pi R^4 \Delta p}{8\mu Lc} = \frac{\phi R^2 \cdot Vb}{8\mu} \frac{\Delta p}{Lc^2}, \quad (2.7.)$$

Further, $V_b = A \cdot L$ and we can then set this equal to Darcy's law, and gets (per definition):

$$Q = \frac{\phi R^2 \cdot A \cdot L}{8\mu} \frac{\Delta p}{Lc^2} = \frac{k \cdot A \Delta p}{\mu L}, \quad (2.8.)$$

$$k = \frac{\phi R^2 \cdot A \cdot L}{8\mu} \frac{\Delta p}{Lc^2} \frac{\mu \cdot L}{A \Delta p} = \frac{\phi R^2 \cdot L^2}{8 \cdot Lc^2} = \frac{\phi R^2}{8 \cdot \left(\frac{Lc}{L}\right)^2}, \quad (2.9.)$$

$$k = \frac{\phi R^2}{8\tau^2}, \quad (2.10.)$$

(Tiab og Donaldson 2004)

2.4. Stress, strain and creep

2.4.1. Stress

Stress [σ] is defined as force (F) acting through a cross-section area (A). The SI unit for stress is Pa, which is Newton per square meters (Pascal = N/m^2).

$$\sigma = \frac{F}{A} \quad (2.11.)$$

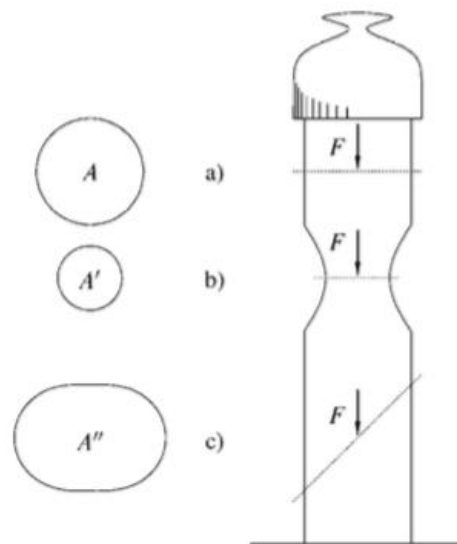


Figure 2. 1: forces acting on three different cross-sectional areas. (*Fjær, et al. 2008*)

Figure 2.1 shows a pillar with a weight on top. Because of the weight, there is a force acting on the pillar. The pillar reacts with an equal and reversely directed force and the pillar is supported by the ground. The force acting at top of the pillar must be acting through any cross-section of the pillar. Looking at the cross section for a) and b), they are not similar in size. But the force acting through the cross sections at a) and b) is equal. Putting these two areas in the stress equation 2.11, the stress at b) will be larger than the stress at a). I.e. the stress is dependent on the position within the stress sample. When the cross-sectional area is reduced, the stress will increase.

Dividing any cross section into sub-sections, could make the force acting on the different areas vary from one sub-section to another. Then you can get a point P, where the stress is local.

Point c) in figure 2.1 has the cross-section A'' . The force is not normal to the cross section. Dividing the force into two components, F_n and F_p are then possible. The force F_n is normal to the cross section and is called the normal stress, while F_p is parallel to the cross section and is called the shear stress, see figure 2.2.

$$\sigma = \frac{F_n}{A''} \quad (2.12.)$$

$$\tau = \frac{F_p}{A''} \quad (2.13.)$$

Equation 2.12 is the normal stress and equation 2.13 is the shear stress.

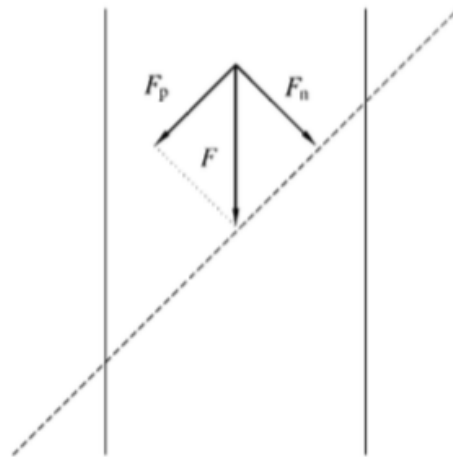


Figure 2. 2: decomposition of a force acting on a cross-section (*Fjær, et al. 2008*).

The magnitude of the two types of stresses are dependent on the orientation of the surface.

The stress state at point P should be described related to the surface orientated in three orthogonal directions. For a surface normal to the x-axis, the stresses can be called σ_x , τ_{xy} , and τ_{xz} . They represent the normal stress, shear stress related to a force in the y-direction and the shear stress related to a force in the z-direction. For point P, there are in total nine stress components:

$$\begin{pmatrix} \sigma_{xx} & \tau_{xy} & \tau_{xz} \\ \tau_{yx} & \sigma_y & \tau_{yz} \\ \tau_{zx} & \tau_{zy} & \sigma_z \end{pmatrix} \quad (2.14)$$

The expression (2.14) is called stress tensor. It describes the stress state at point P. Figure 2.3. shows stress components acting in two dimensions. For an object at rest (figure 2.3.), it is possible to reduce the number of stress components from nine to six. There are no net translational or rotational forces that can act on it. For there to be no rotational force, the following must be met:

$$\tau_{xy} = \tau_{yx} \quad (2.15)$$

$$\tau_{xz} = \tau_{zx} \quad (2.16)$$

$$\tau_{yz} = \tau_{zy} \quad (2.17)$$

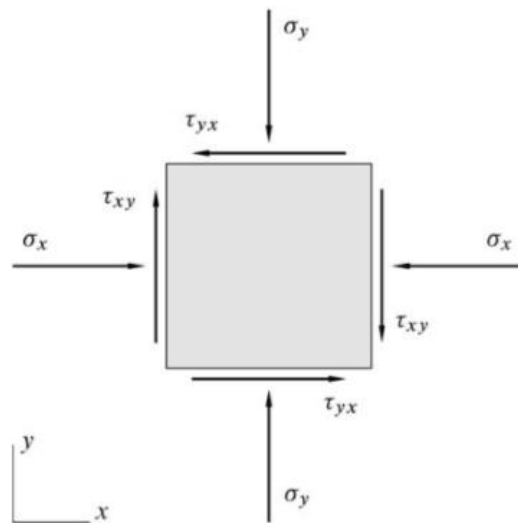


Figure 2. 3: Stress acting on a square in two dimensions (*Fjær, et al. 2008*).

Expression 2.14 can be re-written as:

$$\begin{pmatrix} \sigma_{11} & \sigma_{12} & \sigma_{13} \\ \sigma_{12} & \sigma_{22} & \sigma_{23} \\ \sigma_{13} & \sigma_{23} & \sigma_{33} \end{pmatrix} \quad (2.18)$$

Both normal and shear stress are denoted by σ_{ij} . Numbers 1, 2 and 3 represent the x-axis, y-axis and z-axis. This can be done to minimize having different notations (Fjær, et al. 2008).

2.4.2. Strain

Strain is a measure of the deformation of a material. This comes as a result of being exposed to stress (external forces), it's like a response to the applied stress. The formula for strain is:

$$\varepsilon = \frac{\Delta L}{L_i}, \quad (2.19.)$$

The change in length (elongation), ΔL , is divided on the original length, L_i , and it is dimensionless.

One can differentiate between elastic and plastic strain. Elastic strain is usually when the stress is small, and the material will only deform a small amount before returning to its original size when the applied stress is released. Usually this only occurs when the stress applied is smaller than the yield strength, which is then called critical stress. If the stress applied is higher than the critical stress, the material will not return to its original size when the stress load is removed. It then exceeds the yield, and this is called plastic strain and then also called plastic deformation. (Fjær, et al. 2008)

2.4.3. Stress-strain relationship

There is a relationship between stress and strain if the elastic material is linear. This applies regardless of the magnitude of the stress and strain applied. This can be shown in a stress-strain curve which gives a direct indication of the material properties. A curve like that can give us knowledge about many of the properties of a material and the curves for different materials can vary. It can also vary for the same material due to temperature and speed of loading (Fjær, et al. 2008).

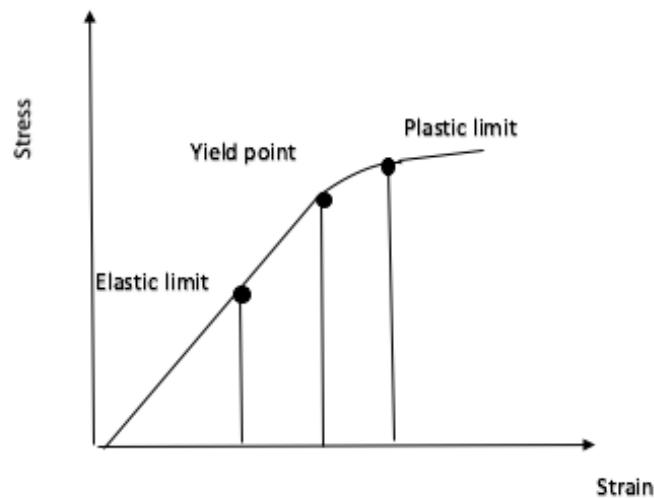


Figure 2. 4: Stress-strain curve for uniaxial strain test showing strain on the x-axis and stress on the y-axes.

The elastic deformation region, the yield point and plastic deformation region can be placed in a curve. The regions are shown in figure 2.4 and the yield point marks where the elasticity region ends and where the plastic region begins. After yielding has ended, the curve can rise continuously but also become flatter until it reaches a maximum, a so called ultimate stress. This is called the strain hardening and it is a consequence of plastic deformation (Fjær, et al. 2008).

2.4.4. Creep

Creep is a deformation of materials that is time-dependent, and it can occur when the materials are under constant stress. Creep can be divided into three stages, depending of the level of stress the material is exposed to (figure 2.5). The first stage is called the transient (primary) creep stage. Here, the rate of deformation decreases with time. If the stress applied to the material is reduced to zero, then the deformation of the material will gradually also be reduced to zero. The next stage is called the steady state (secondary) creep. In this stage, the deformation becomes more constant and steady. If here the applied stress is reduced to zero, then the deformation will not reduce to zero, as it would in the previous stage. It will remain. The third stage is the accelerating (tertiary) creep. Here, the deformation increases rapidly within a short matter of time. This can lead to failure.

The creep behavior is dependent on the magnitude of the stress applied. If the material is exposed to low or moderate stress, it may virtually stabilize after a period of transient creep. If the stress applied is higher, then the material could rapidly move through all the stages of the creep phase and then fail. The creep is dependent on more than just applied stress, it is also dependent on temperature because it is a molecular process. The time scale is dependent on the temperature and one can say that in general the process will speed up when the temperature increases (Fjær, et al. 2008) (Jaeger og Cook 1976).

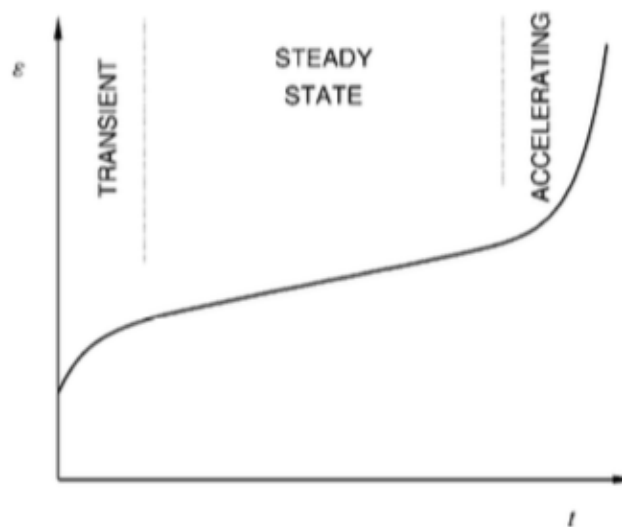


Figure 2. 5: Strain against time for uniaxial strain test. We here clearly see the different stages in a creep process. (Fjær, et al. 2008)

2.5. Pressure solution

Pressure solution is a mechanism that reduces porosity and permeability due to compaction in clastic and carbonate rocks. It is a common and important water-rock interaction process and it is a widespread phenomenon that influences many essential natural processes. It has been considered to be the most essential ductile deformation mechanism in the upper crust. It occurs in rocks where solid surfaces are exposed to pore fluids and it is a creep process involving microscale dissolution and precipitation reactions mediated by diffusion of solutes in the fluid phase. Minerals dissolve where there is a higher chemical potential. Then the solutes are transported within the fluids surrounding them and the minerals are then precipitated in regions of lower chemical potential (Ben-Itzhak, Erez og Aharonov 2015). In other words, the mechanism contains the transfer of mineral grains by diffusion, dissolution and precipitation

processes. The slowest of these three processes determine the rate of pressure solution. It may be controlled by the kinetics of dissolution or precipitation reactions, or by the rate of diffusion along the grain boundary. Along the grains contact, the diffusive transport is driven by chemical potential gradient that exist between the liquid in the contact and the one on the pore space. The rate of transport is dependent on thickness and microstructure of the grain-to-grain contact (Croize, et al. 2010).

It is dependent on different elements, like grain size, porosity, stress, temperature, chemistry of the fluids and time (Croizet, Renard og Gratier 2013). Therefore, it is believed that the amount of pressure solution increases with depth and it occurs in geological environments in the upper crust that are characterized by moderate levels of stress and fluid that are present. The mineral grains are deformed individually, and the material is precipitated in pore spaces. This compacts the rock and decreases the permeability (Hellmann, Renders, et al. 2002).

Within this deformation mechanism, it is possible to see some characteristic microstructures, like stylolites, sutured grain contacts and clay seams (Croizet, Renard og Gratier 2013). Stylolites are the most common feature, and are the most distinct feature in limestones, sandstones and evaporites. Other features are pressure solution cleavage, differentiated crenulation cleavage and secondary mineral growth found in pressure shadows and along fault planes. What determines the microstructure in correlation with pressure solution is a function of the structural resistance along with the rock lithology (Hellmann, Gaviglio, et al. 2002).

Several analytical models have been suggested, which describe its constitutive behavior. Assumptions are required for these models, regarding the geometry of the aggregate and the grain size distribution. This is required in order to solve for the contact stresses and often neglect shear tractions. Analytical models have a tendency to overestimate experimental compaction rates at low porosities (van den Eide, M.P.A, et al. 2017).

Despite the importance of pressure solution and despite all the decades of research done related to the mechanism, it is poorly understood along with the processes controlling pressure solution (Ben-Itzhak, Erez og Aharonov 2015). So, the origin of pressure solution and other dissolution processes related to the mechanism remain elusive (Kristiansen, et al. 2011).

3. Procedure and equipment

3.1. Test material - calcite-powder

The experimental work performed in this thesis was with powder, contrary to drilled cores from blocks which is often used. The powder was a fine granular calcite powder (Calcium Carbonate 99,95 Suprapur – CaCO_3). The manufacturer is EMD Millipore Corporation. This was used to make multiple artificial core samples to be placed in a Triaxial cell (see figure 3.2.) when conducting the experiments.

3.2. Making core samples

When making the artificial core samples, a steel rod with diameter 37 mm was fitted with a shrinking sleeve. A heating gun was used to fit the shrinking sleeve tightly around the steel rod. The rod was then fitted with a draining plate and filter in the lower part of the shrinking sleeve, figure 3.1 (a). Then powder was filled in the sleeve with a spoon and for each second spoonful the powder was compressed tightly together with a steel rod, figure 3.1 (b). When the desired lengths and weights of each core were reached, figure 3.1(c), a second drainage plate and filter were placed on top. The core samples were then ready to be used and placed in the Triaxial cell. It can be noted that only one core sample was made at a time, prior to each test start-up.

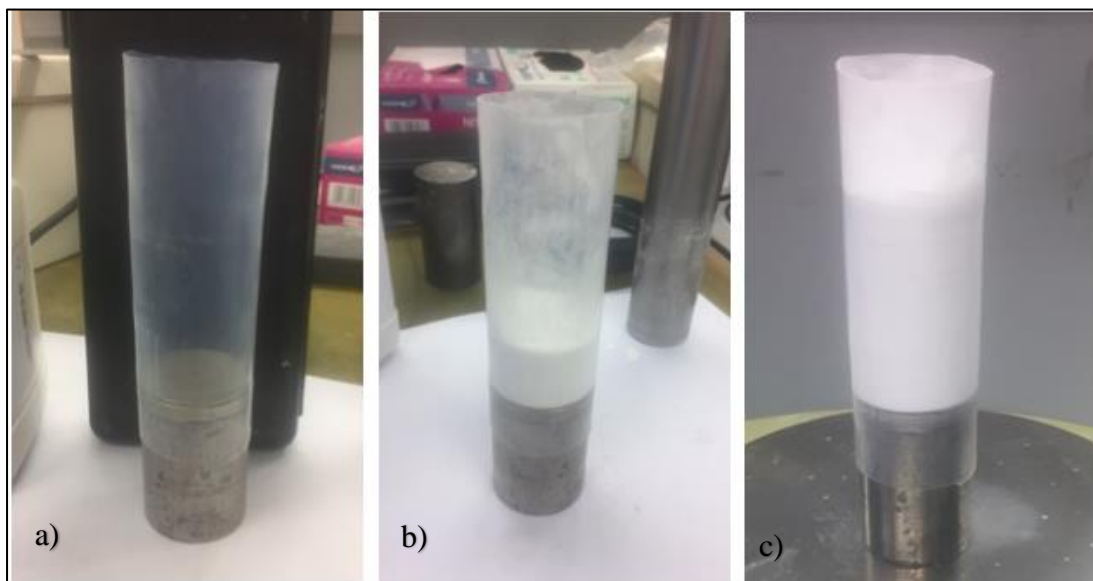


Figure 3. 1: a); rod with a drainage plate and filters in the lower part of the shrinking sleeve. b); powder filled into the sleeve. c): the full length of the core.

In total 8 artificial cores were made. In table 3.1, there is an overview of pre-test measurements. To calculate the porosity, equation 2.1 was used. The density value for calcite is 2.71 g/cm^3 .

Table 3. 1: Overview of values for each test before tests have began

	Length [mm]	Diameter [mm]	Dry weight [g]	Porosity [%]
HP1	68.6	36.6	99.0	49.4
HP2	58.0	36.6	90.1	45.5
HP3	57.2	36.8	86.1	47.8
HP4	58.9	36.8	87.7	48.3
LP5	58.1	36.9	87.6	48.2
HPA6	58.6	36.8	87.4	48.3
HPA7	59.8	36.7	87.9	49.0
LP9	58.2	36.9	87.1	48.6

3.3. Brines

All cores were flooded with brine, so a brine mixture was made for each experiment. For HP1-HP4, LP5 and LP9 a brine mixture without additive was prepared. For HPA6 and HPA7, a brine containing organic additive (Oxalic acid – HOOCCOOH) was used, see table 3.2.

Table 3. 2: Fluids purpose and composition

Flooding fluid	Purpose	Composition	
Brine without additive	Used to saturate and to flood the cores during the uniaxial strain loading and creep phase	DW NaCl $\text{CaCl}_2 \cdot 2\text{H}_2\text{O}$ NaHCO_3 NaOH	1000 ml 5.843 g 0.02499 g 0.4410 g 1.33 - 2.01 ml
Brine with additive – oxalic acid (HOOCCOOH)	Used to saturate and to flood the cores during the uniaxial strain loading and creep phase	DW Oxalic acid $\text{CaCl}_2 \cdot 2\text{H}_2\text{O}$ NaCl NaHCO_3 NaHCO_3 NaOH	1000 ml 0.09230 g 0.03381 g 5.844 g 2.797 g (HPA6) 0.5417 g (HPA7) 12.14 – 16.2 ml
DW	Clean the cores	Clean water without any impurities	

3.3.1. Brine preparation without additive:

Before making the brine, two stock solutions were made. They were both used in the preparation for all brines.

1. Started measuring up 0.1249 g of $\text{CaCl}_2 \cdot 2\text{H}_2\text{O}$, even though only 1/5 of this amount was needed – 0.02499 g. The reason was that it can be quite difficult measuring up such a small measurement as 0,02499 g, which was the needed amount. Further, poured the 0.1249g of $\text{CaCl}_2 \cdot 2\text{H}_2\text{O}$ into a 500 ml flask and added DW up until the line. The reason for using the 500 ml flask was to compensate for taking 5 times the needed amount of $\text{CaCl}_2 \cdot 2\text{H}_2\text{O}$. This was then stored with a cap.
2. Next measured up 2.0022g of NaOH and poured it into a 500 ml flask. Added DW until the line. Used a magnet to stir the solution, and this was also stored with a cap.

Making the final solution - the brine. Took a 1liter flask. Poured approximately 250 ml of DW into the flask and measured up 5.843 g of NaCl and added this. Then added 100 ml of $\text{CaCl}_2 \cdot 2\text{H}_2\text{O}$ from the first of the two stored solutions. Here, a 100ml flask was used to get the desired amount. Next measured up 0.4410 g of NaHCO_3 and added this. Filled the flask with DW until the line and used a magnet to stir it.

Measured the pH value of the final solution. For all five brines the pH was below 8.5, which was the desired value for the brines prior to each test. The values lay between 7.94 and 8.16. To increase the pH, the second of the two stock solutions, NaOH 0.1 Mol, was added. Ended up adding between 1.33 ml and 2.01 ml for each brine mixture. Poured it in a bottle and closed it using a cap.

3.3.2. Brine preparation with additive (oxalic acid - HOOCCOOH):

Stock solutions were also required here. The NaOH 0.1 Mol stock solution described above could also be used for this brine. For the $\text{CaCl}_2 \cdot 2\text{H}_2\text{O}$ stock solution on the other hand, it required a different concentration of the substance, so this stock solution had to be prepared.

1. Measured up 0.16905 g of $\text{CaCl}_2 \cdot 2\text{H}_2\text{O}$, and again, only 1/5 of this amount was needed. Poured this into a 500 ml flask and added DW up until the line and stored this with a cap.

Making the final solution – the brine with additive. Took a 1 liter volumetric flask and filled it with approximately 250 ml of DW. Measured up 0.0923 g of Oxalic acid and added this. Then added 100 ml of the new stock solution - $\text{CaCl}_2 \cdot 2\text{H}_2\text{O}$, used a 100 ml flask to get this amount. Then, measured up 5.844 g of NaCl and added this. Then, 2.797 g of NaHCO_3 was added for HPA6 and 0.5417 g of NaHCO_3 was added for HPA7. There is a big difference in these two amounts. For the brine made for HPA6 the fluid did not look clear. It had a white looking color and was grainy. For this reason, when making the brine for HPA7, the amount got adjusted to a lower value. This did not help, also here, the fluid looked unclear. Filled up the flask with DW and used a magnet to stir it for a while before closing it with a cap.

Next, the pH values of the solutions were measured to be 7.59 and 6.73 for HPA6 and HPA7, respectively. To increase the pH to the desired value of 8.43, 12.14 ml and 16.2 ml of 0.1 M NaOH was added to HPA6 and HPA7, respectively. Unlike for PHA6, the brine for HPA7 was filtered to achieve a clear fluid. After filtering the brine, the pH was 8.42. This was then used.

3.4. Equipment

3.4.1. Triaxial cell

With this cell, it was possible to replicate reservoir conditions for the cores in the different experiments. The cell also made it possible for the conditions for each core to be kept somewhat stable and equal, with minimal differences. The cell consisted of an underbody where the core was placed with an extensometer around it for radial strain measurements, figure 3.2 (a), steel chamber that was filled with confining oil, heating jacket, a top cap mounted to the underbody with six bolts, and a Linear Voltage Displacement Transducer (LVDT) for axial displacement measurements, figure 3.2 (c). A computer software (LabView) was used to log data recorded throughout all the tests, keeping track of the mechanical behavior.

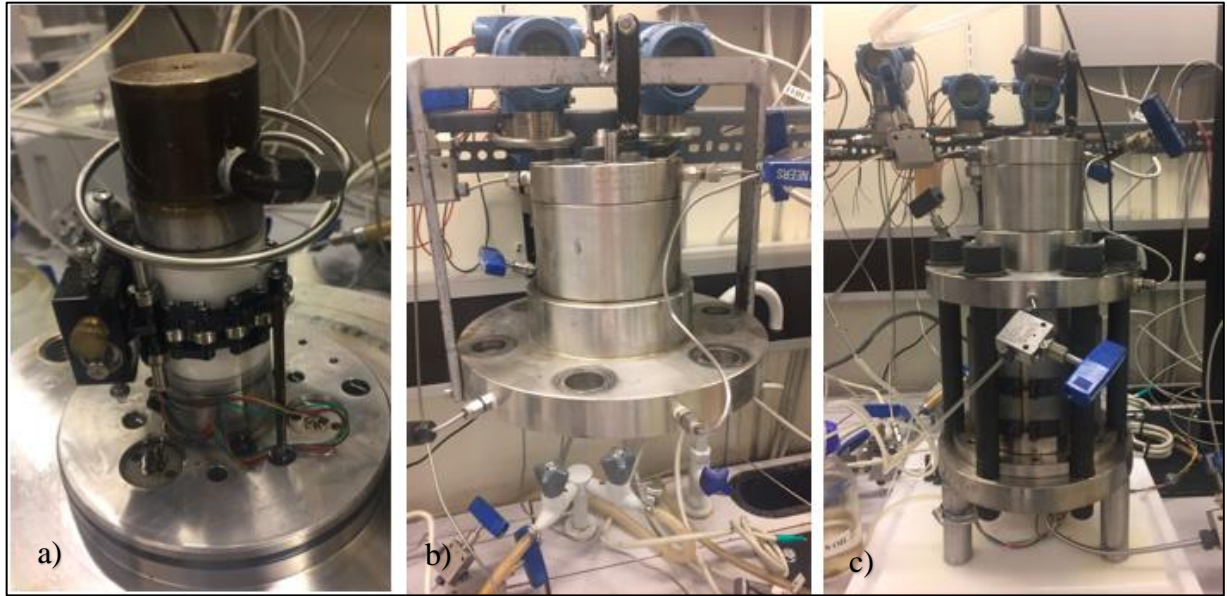


Figure 3. 2: The artificial core is placed on the underbody with an extensometer around it (a). A cap was placed on top after each test has been assembled (b). The assembled Triaxial cell (c).

3.4.2. Piston cell and high-pressure pumps

Brine mixture was filled into the piston cell in one end and distilled water was filled into the opposite end separated by a piston, figure 3.3 (a). The brine was flooded from this cell through the core inside the Triaxial cell.

There were three different high-pressure pumps in use for all the tests performed. It was possible to control all the pumps individually, so both flooding rates and pressure values could be set and changed throughout the test-durations as desired. Pump 1 and pump 2 were Quizix QX pumps, figure 3.3 (b), and they were used to regulate the axial pressure and confining pressure. Pump 3 was a Gilson 307 pump, figure 3.3 (c). It was the flooding pump used to control the flow rate.

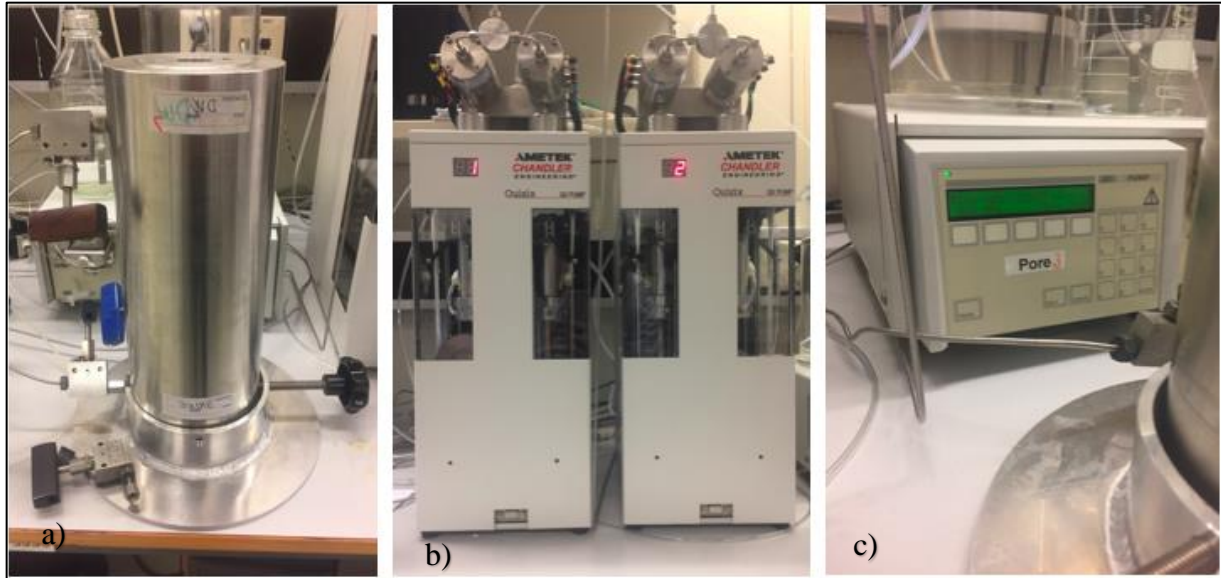


Figure 3. 3: a) is the piston cell used for each experiment. B) is the piston- and confining pump, and c) is the flooding pump.

3.4.3. Water sampling and pH measurements

Water samples from the effluent that had flooded through the cores were collected regularly for each experiment. This was carried out so that the pH could be measured frequently, and these measurements were conducted on a SevenCompact pH Meter from Mettler Toledo. Samples were also collected so that one could do a chemical analysis after the experiments were completed.

3.5. Test-setup

It took a few days to get each uniaxial strain-test up and running. The set-up can be divided into three steps and the same steps were conducted on all experiments, except for LP5 and LP9. For these two tests, the last step was skipped.

A. Assembling the Triaxial cell

As mentioned above, a core sample and a brine mixture were made for each test. The brine was poured into the piston cell in one end and distilled water was poured into the other. The core sample was placed in the middle of the underbody of the cell and a chain was placed around it. To make sure it was attached properly and to prevent any leakages, a heating gun was used at the top and the bottom of the core on the shrinking sleeve. After it was attached, a steel cylinder was placed around it. The diameter of the cylinder was a lot bigger than the diameter of the core, so in the gap that followed, marcol oil was filled to the top of the cylinder resulting in the

core being completely covered in the oil. A heating jacket was placed around the cylinder and on top of this, a steel cap was placed and bolted with 6 bolts. Further, the LVDT (linear voltage displacement transducer) was attached at the top of the cap. And at last, a fan was placed over the cell making the assemble of the Triaxial cell complete.

B. Confining pressure, pore pressure and temperature

Starting on the second step, the confining pressure was increased to 0.5 MPa. Next, push piston down. When piston landed on sample, the piston pressure was set to 0.6 MPa. The flooding of the core was started by the flooding pump. The core had to be saturated, so one waited for a couple of hours before continuing this second step.

When the core was saturated, the by-pas was opened. It was opened so that the pore pressure could increase quickly, because when it is open, there is no pressure drop over the core and one can increase the pressure quickly. The confining pressure had to be increased to 1.2 MPa and the pore pressure had to increase to 0.7 MPa. This was done gradually. It was desirable to keep approximately 0.5 MPa in between the two pressure measurements as they both increased. When the two pressures reached 1.2 MPa and 0.7 MPa, the by-pass valve was closed, and the heating jacket was switched on to increase the temperature slowly towards 130 °C. While this was increasing, the confining pressure was kept stable at 1.2 MPa by using a relief valve such that excess oil due to the temperature increase was expelled from the cell. When the desired 130 °C was reached, the confining valve was closed.

C. Uniaxial strain program and overburden

The final step was the uniaxial strain loading- and following creep phase. Here, the uniaxial strain program was started. The axial stress was increased up to 30 MPa before the creep phase started. During the uniaxial strain test, a program was run so that the radial strain would stay at zero. When the creep phase began, the constant overburden program was started so that the axial stress and overburden was 30 MPa during the creep phase. The confining pressure varied during the creep phase to keep the radial strain at zero. At the end of the creep phase a minimum of 3 pore volumes of distilled water were injected to displace the saturation brine. This was done in order to clean and prepare the core for SEM studies after the Triaxial test. After cleaning, the pressures were reduced down to its initial values prior to the uniaxial strain loading phase before the temperature was turned off.

3.6. Post experiments

3.6.1. Chemical analysis by ion chromatography

All the water samples collected throughout each experiment were analyzed by a Dionex ICS 5000+. Before analyzing them, they had to be diluted and filtrated before they were transferred into glasses used for ion chromatographic testing. The samples were all diluted 500 times and then placed in a black stand and further placed in Dionex ICS 5000+, see figures 3.4. (a), (b) and (c). Here, the ion concentrations were measured. This was done to analyze and compare the concentrations of the samples to the original brine made for each test.

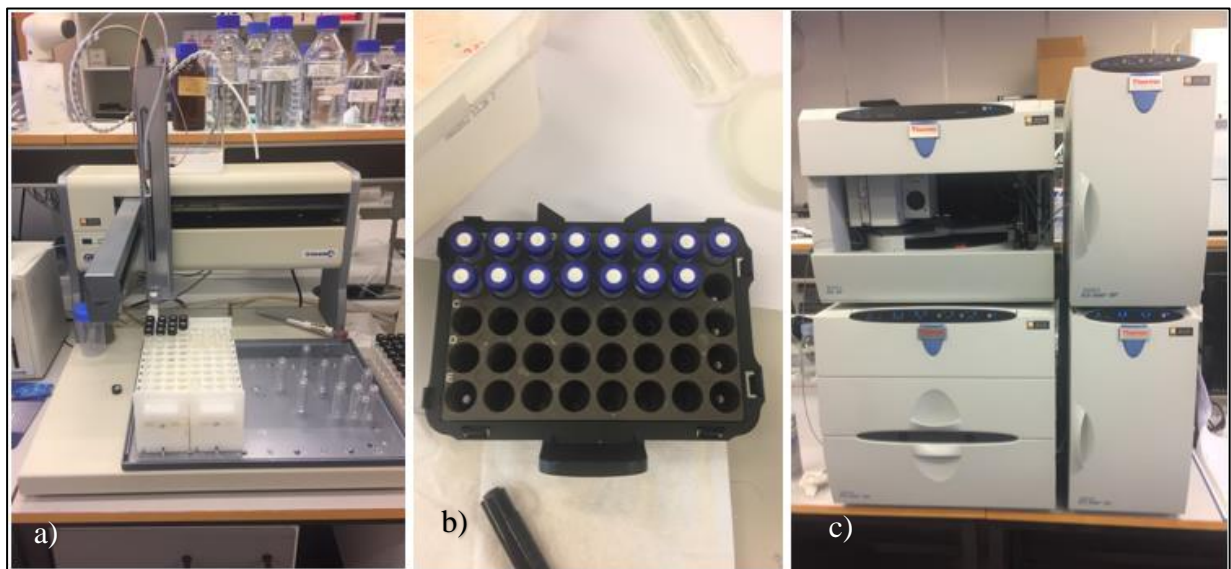


Figure 3. 4: a) shows the dilution of water samples taken during a test. This was done with a Gilson GX-271 Liquid Handler. When this was completed, the samples were placed in smaller glasses and put in a black stand (b), before finally being put into the machine (c). This was a Dionex ICS 5000+.

3.6.2. Sampling for SEM – scanning electron microscope

After each experiment had finished, the cores had to be dried up in a heating cabinet before being investigated in a scanning electron microscope (SEM). Samples were taken at different parts of the cores so that it would be possible to look at the calcite microstructure morphology from different areas. This was done to determine the influence of compaction and fluid-rock interactions on structure of grains. A SEM is an electron microscope that can take images of samples from cores, and their surfaces are scanned with a focused beam of electrons. It is a powerful method for investigating surfaces and its structures. It gives a large depth of field,

meaning that the area of a sample that is viewed in focus at the same time is quite large. It has a relatively wide range of magnification, and it allows the investigator to easily focus on an area of interest (Stadtländer 2007).

For all the cores, samples were collected at inlet, middle, outlet, and for some of the cores it was also collected from the outside rim. In figure 3.5 it is shown precisely where the samples were taken for HP1. The core was first cut into four parts and then small pieces from three different areas on the core were collected. One sample was taken from inlet, one from the middle and one from outlet. Figure 3.6 (a) shows the core from HP1 as a whole, (b) shows the core cut into two halves and (c) shows one of the halves further cut into two pieces.

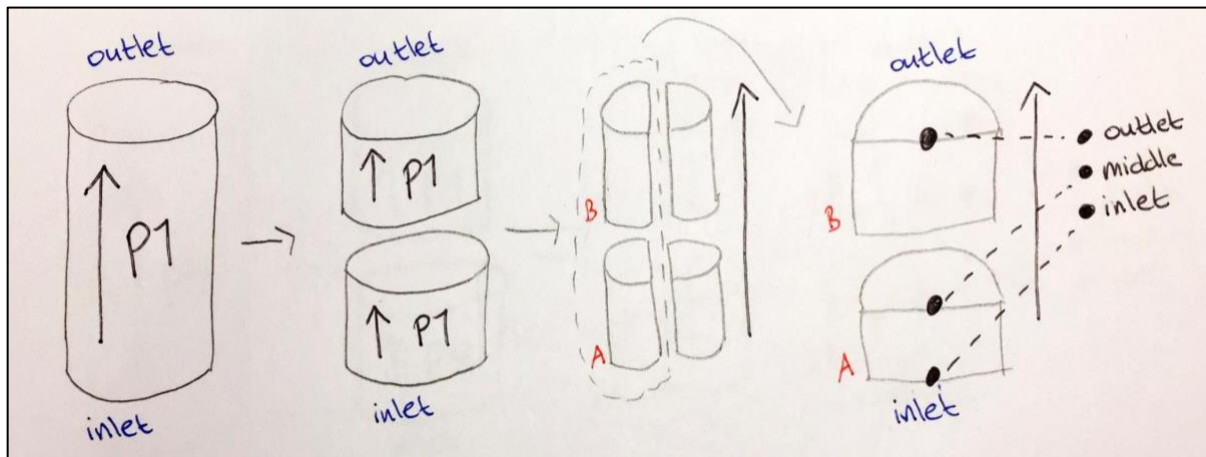


Figure 3. 5: Sketched drawing of how the core from test 1 was cut and where three samples were collected.

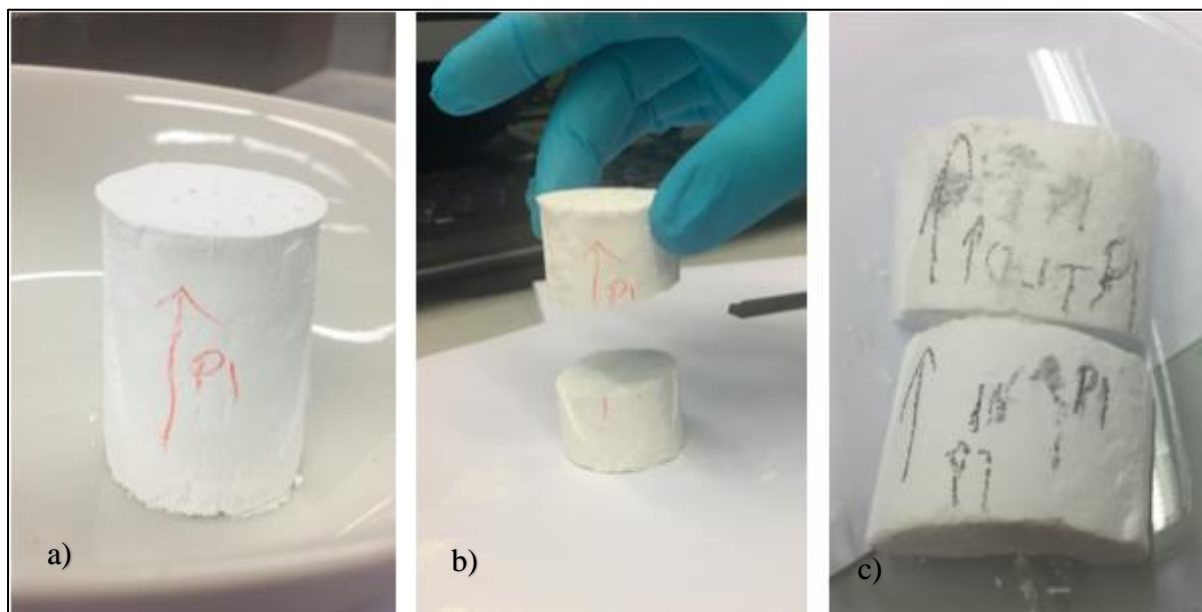


Figure 3. 6: a): the core from HP1 as a whole, b) the core in halves and c) one of the halves cut into two pieces.

4. Results

In total, eight uniaxial strain tests were conducted. HP1-HP4, LP5 and LP9 were carried out using a brine without organic additive, while HPA6-HPA7 used a brine with organic additive - HOOC-COOH. There is no test 8. It failed after just a couple of hours and had to be stopped, and test 9 was started right away, including having to make a new artificial core sample. All tests were performed with a temperature of 130 °C. All tests, except for LP5 and LP9, were loaded to an axial stress of 30 MPa before the creep phase followed. They were performed at low confining pressure of 1.2 MPa and pore pressure 0.7 MPa. They were done to see how the cores and the grains behaved without being exposed to the same stress as the others. Data were constantly logged for different values for all the tests, so that stress, strain and creep could be plotted. The ion concentrations were analyzed and plotted to see losses or increased amounts of the ions in different effluent samples collected from all the cores.

The names of the tests are shortened to HP1 for Powder 1, LP5 for Powder 5 and HPA6 for Powder 6 and so on in the following. HP stands for high-pressure, LP for low-pressure and HPA for high-pressure with oxalic acid.

It has to be mentioned that HP3 and HP4 did not run as planned. For HP3, there was a problem with the equipment. When disconnecting a confining valve, the pipe connected to the valve broke and the confining pressure dropped to zero. For this reason, the test could not be carried on further. For HP4, filters were not placed on top and bottom of the core, and the test had to be stopped due to clogging of the outlet tubing when flooding brine to saturate the core. The test was dismantled, and filters were fitted on the same core. When restarting the test, the core was shorter than it was original. It was forgotten to place a spacer above the core to compensate for that, and due to this the axial piston reached maximum displacement after just a couple of days, and the test could not be carried on further.

4.1. Uniaxial strain tests

In the following, two graphs are presented for each of the tests performed.

- 1) The first graph is showing the uniaxial strain loading phase, with the axial stress [MPa] as a function of axial strain [%]. For LP5 and LP9, this graph is not included.
- 2) The uniaxial strain phase is followed by the creep phase. The second graph is then the axial creep strain [%] and the permeability [mD] as a function of creep time [days] and it is showing the deformation of the cores under constant axial stress.

Toward the end of each test, the cores were flooded with DW. This was done to clean the cores, prior to investigating them in SEM. The flooding rate was the same for all tests, 0.05 ml/min, both for the flooding of the brines and DW.

4.1.1. Experiment without organic additive and low stress

LP5 was performed without organic additive and without an axial stress of 30 MPa, to see how the grains would react and behave throughout the test duration and then conduct a SEM investigation. The brine used is described in section 3.3.1. *Brine preparation without additive.*

Table 4.1. 1: Overview of LP5.

	Original length [mm]	New length [mm]	Original mass weight [g]	Saturated mass weight [g]	New dry weight [g]	Porosity before test [%]	Porosity after test [%]	Total axial creep strain [%]
LP5	58.1	56.0	87.6	108.73	87.5	48.2	44.6	0.56

When calculating the porosity after the test had finished, the same equation was used as for the calculations done prior to performing the tests (equation 2.1) but now with the new radius, length and dry weight. The porosity after the test was 44.6% (see table 4.1.1), which is lower compared to before the test meaning that there are less voids in the material. The total axial creep strain was 0.56%, as presented.

LP5

The creep phase

The creep phase lasted approximately 13 days. The core was flooded with brine for about 10 days, before being flooded with DW the remaining time. In the transient creep phase, the axial creep strain reached approximately 0.5%. The axial creep strain in the steady state phase reached 0.55% towards the end of flooding with the brine. At the end of the creep phase, after starting to flood DW, the axial creep strain was 0.56%. It was expected that the total axial creep strain would have a low value, as this test was not left to creep at an axial stress of 30 MPa.

Due to the absence of a loading phase prior to the creep phase, it was decided to start the creep phase approximately two hours after the temperature increase started. By then, the cell had reached 130 °C. The same was done for LP9 which is presented further down in figure 4.1.14.

Table 4.1. 2: Values for LP5

	Total creep time [days]	Flooding brine [days]	Flooding DW [days]	Axial creep strain brine [%]	Total axial creep strain [%]
LP5	12.8	10.2	2.6	0.55	0.56

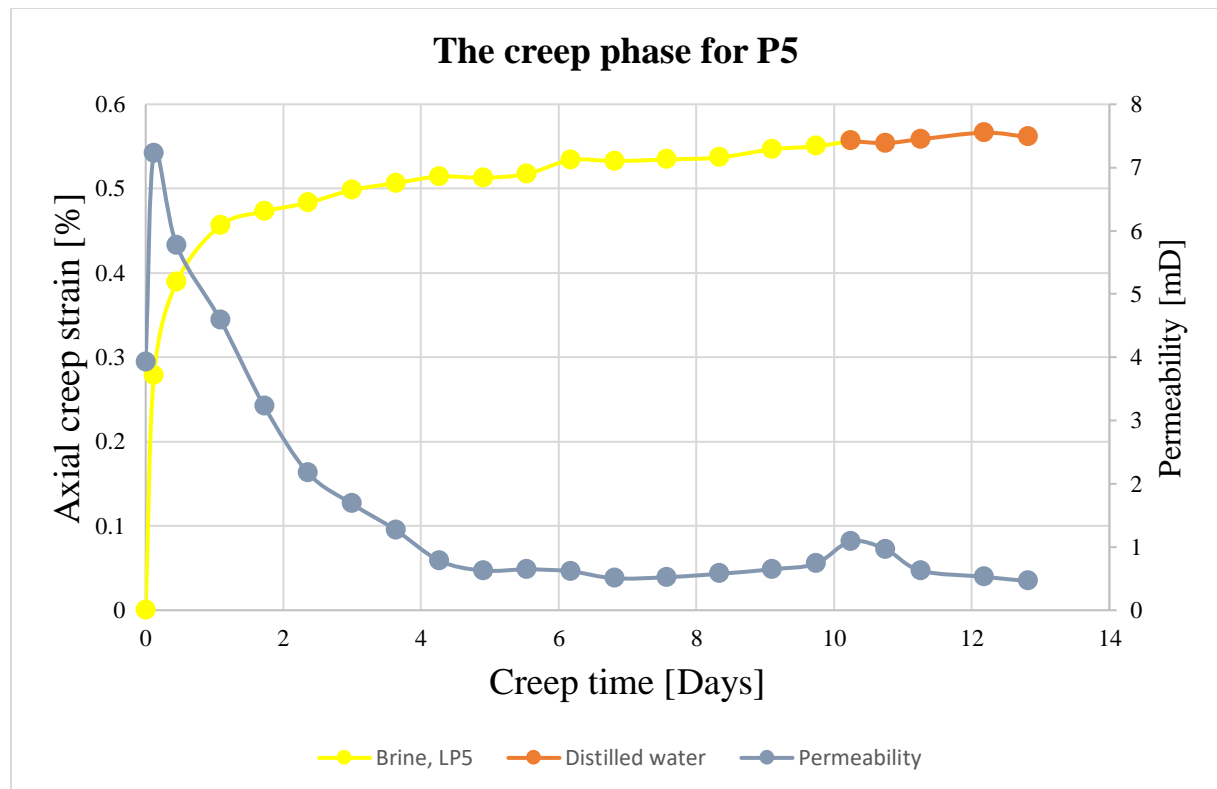


Figure 4.1. 1: Axial creep strain [%] and permeability as a function of creep time [days] for LP5.

4.1.2. Experiments without organic additive, but with axial stress of 30 MPa

The tests performed without organic additive, but with an axial stress of 30 MPa were HP1, HP2, HP3 and HP4. They were flooded with the same brine as LP5. After the uniaxial strain loading phase, all the cores were left to creep when the axial stress reached 30 MPa.

Table 4.1. 3: Overview of different values for HP1, HP2, HP3 and HP4. * indicates that the tests failed.

	Original length [mm]	New length [mm]	Original mass weight [g]	Saturated mass weight [g]	New dry weight [g]	Porosity before test [%]	Porosity after test [%]	Total axial creep strain [%]
HP1	68.6	49.0	99.0	106.7	98.8	49.4	27.3	10.0
HP2	58.0	43.6	90.1	100.4	89.7	45.5	25.8	12.0
HP3*	57.2	-	86.1	-	-	47.8	-	9.8
HP4*	58.9	39.9	87.7	92.4	83.9	48.3	22.9	9.0

HP1

Uniaxial strain loading and creep

HP1 lasted for a total of 9 days. The stress and strain were measured, and the yield point can be found during the uniaxial strain loading phase. This can normally be found by adding two linear trend lines, one through the elastic phase and one through the plastic phase on the curve. They would then extrapolate into a cross section and here the yield point would be located. As seen in the theory part in chapter 2, the curve from figure 2.5. does not look like the curve below in figure 4.1.2. The curve in figure 4.1.2. does not show the elastic behavior and it does not show the yielding. What is seen in the graph is a continuously rise in the curve and this is the strain hardening region. This comes after the yielding. Towards the end, the line gets steeper. It indicates that the core is getting stiffer at the end of the uniaxial strain loading phase as the line increases more rapidly. The total axial strain for the core in HP1 was 14.3% which was achieved by an implied axial stress of 29.3 MPa.

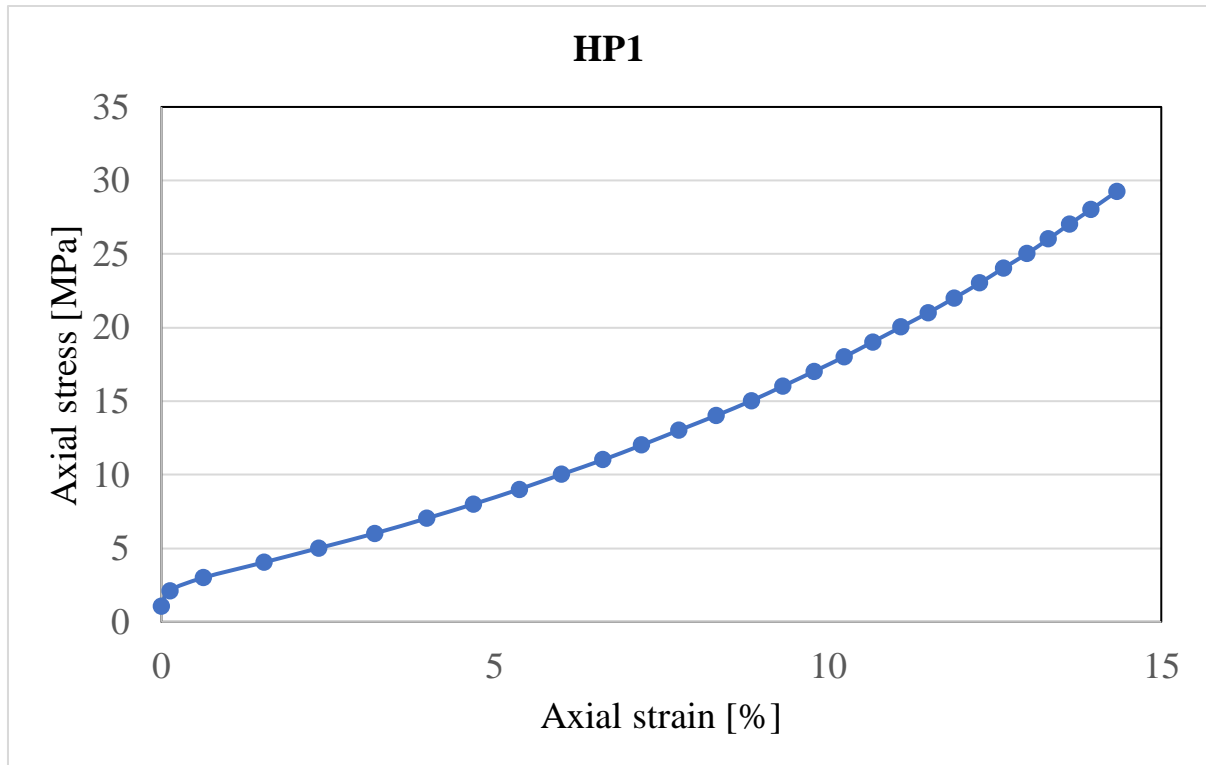


Figure 4.1. 2: Axial stress [MPa] as a function of Axial strain [%] for HP1.

The following creep phase lasted approximately 5.6 days. The creep can be seen in Fig. 4.1.3. The core was flooded with brine for the entire period. In the transient creep phase, the axial creep strain started to reduce. The core reached an axial creep strain of approximately 7-8%. Here, the rate of deformation decreased with time. Further, in the secondary or steady state phase the deformation was constant and steady. The total axial creep strain reached was 10.0%. The permeability has a downward trend that follows the creep, as the core gets shorter, the permeability drops. The fluctuations may be present because the material in the core is unconsolidated, grains can have some movements, causing some areas to get a higher permeability. There may be local variations in the core.

Table 4.1. 4: Values for HP1.

	Total creep time [days]	Flooding brine [days]	Flooding DW [days]	Axial creep strain brine [%]	Total axial creep strain [%]
HP1	5.6	5.6	-	-	10.0

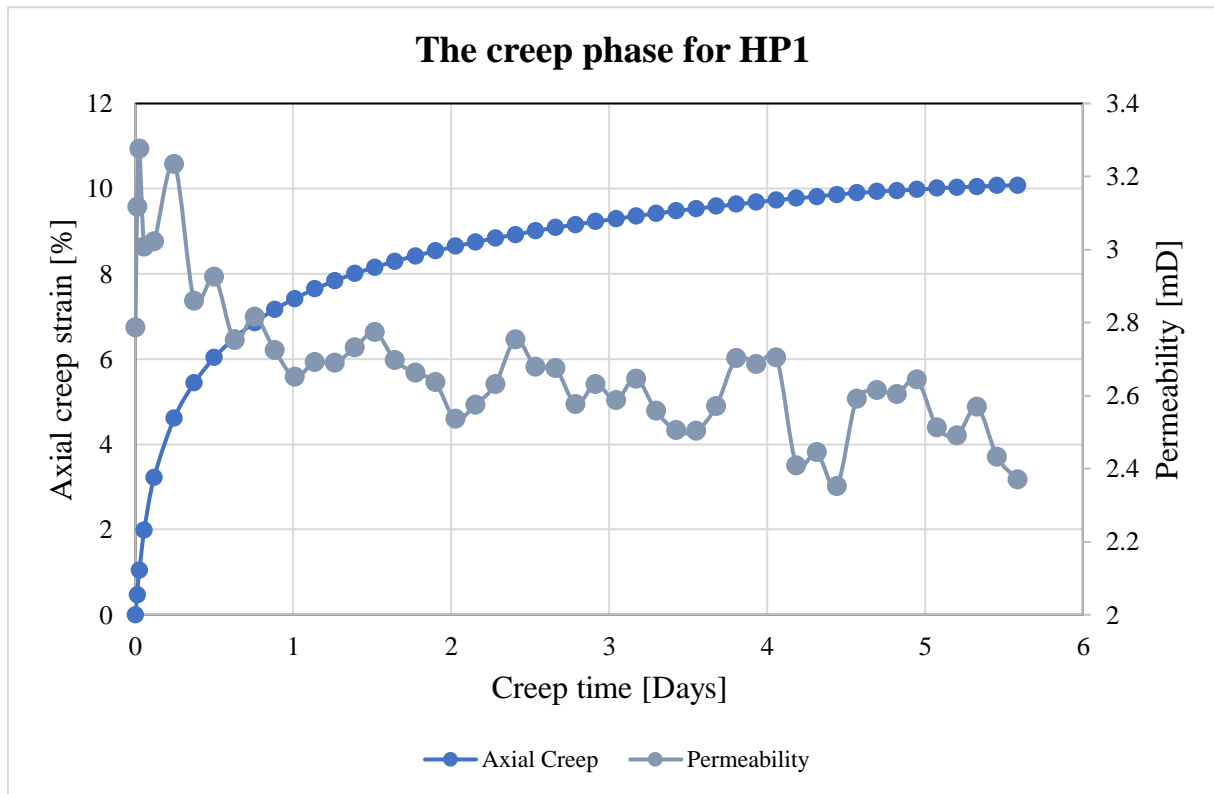


Figure 4.1. 3: Axial creep strain [%] and permeability as a function of creep time [Days] for HP1.

HP2

Uniaxial strain loading and creep

HP2 lasted a total of 15 days. Figure 4.1.4 is showing the strain hardening of the core. The axial strain for the core was 12.7% and the axial stress applied was 29.3 MPa.

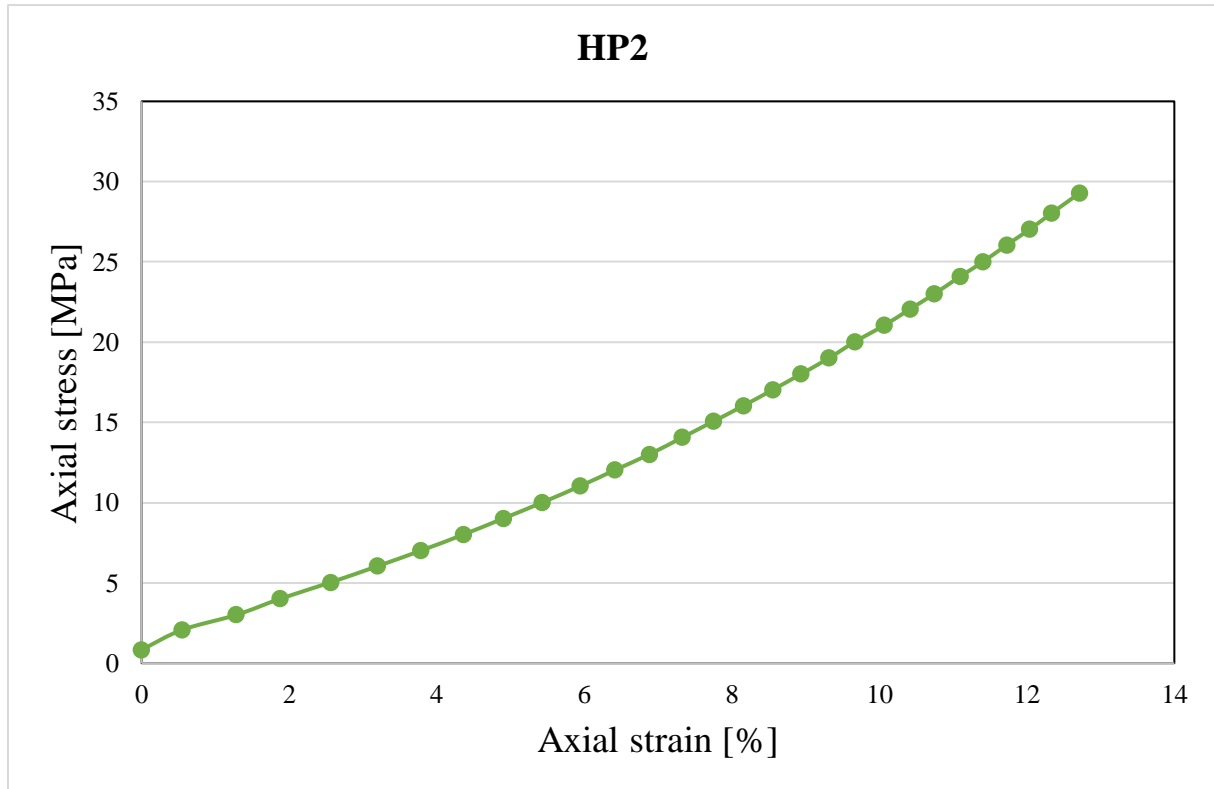


Figure 4.1. 4: Axial stress [MPa] as a function of axial strain [%] for HP2.

The creep phase lasted 12.4 days in total, where the core was flooded with brine the first 9.8 days, see table 4.1.5. The remaining days, the core was flooded with DW. As seen in figure 4.1.5, the flooding of DW did not have an impact on the line on the graph. In the transient creep phase, the core reached an axial creep strain of approximately 9%. Further, in the steady state phase when starting to flood the core with DW, the core reached an axial creep strain of 11.5%. The total axial creep strain, including DW, was 12.0%. The permeability has a downward trend without any fluctuations, except toward the end where there is a rise.

Table 4.1. 5: Values for HP2

	Total creep time [days]	Flooding brine [days]	Flooding DW [days]	Axial creep strain brine [%]	Total axial creep strain [%]
HP2	12.4	9.8	2.6	11.5	12.0

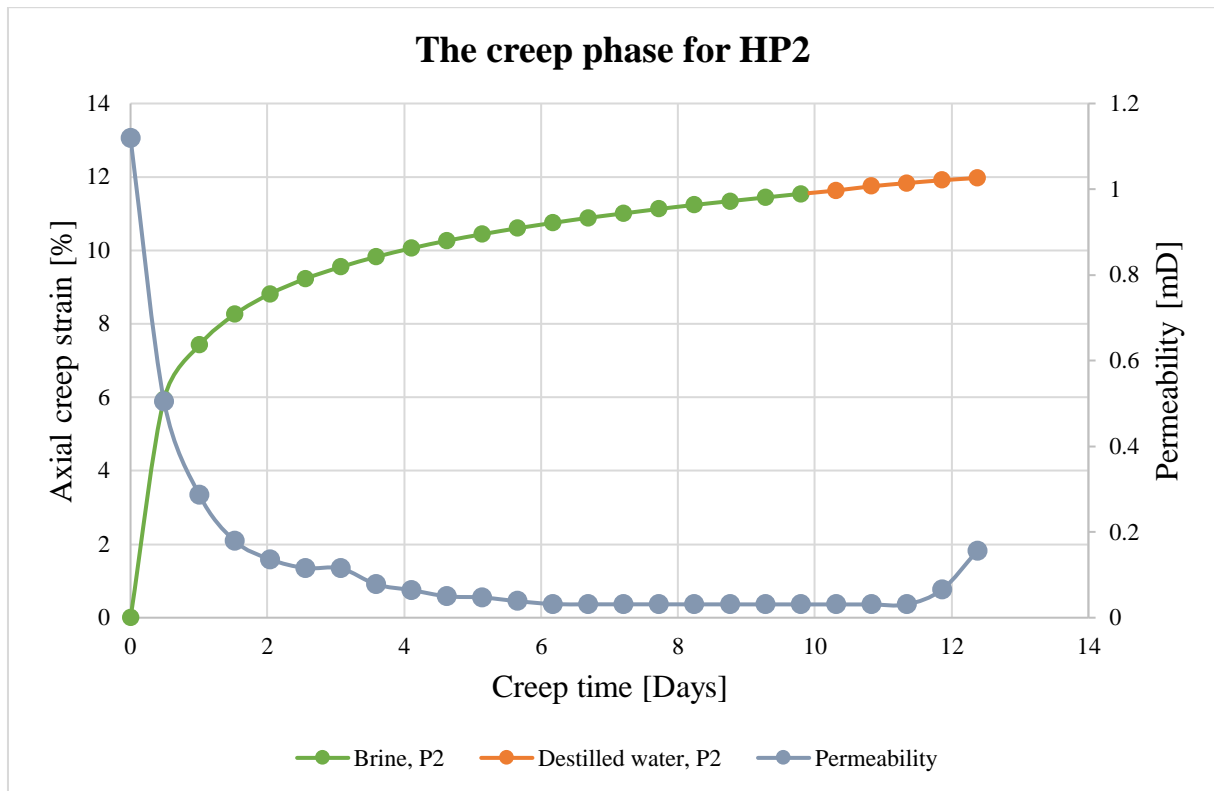


Figure 4.1. 5: Axial creep strain [%] and permeability as a function of creep time [Days] for HP2.

HP3

Uniaxial strain loading and creep

HP3 lasted 4 days in total. The axial strain and axial stress reached in the uniaxial strain loading phase were 14.4% and 29.1 MPa, (figure 4.1.6).

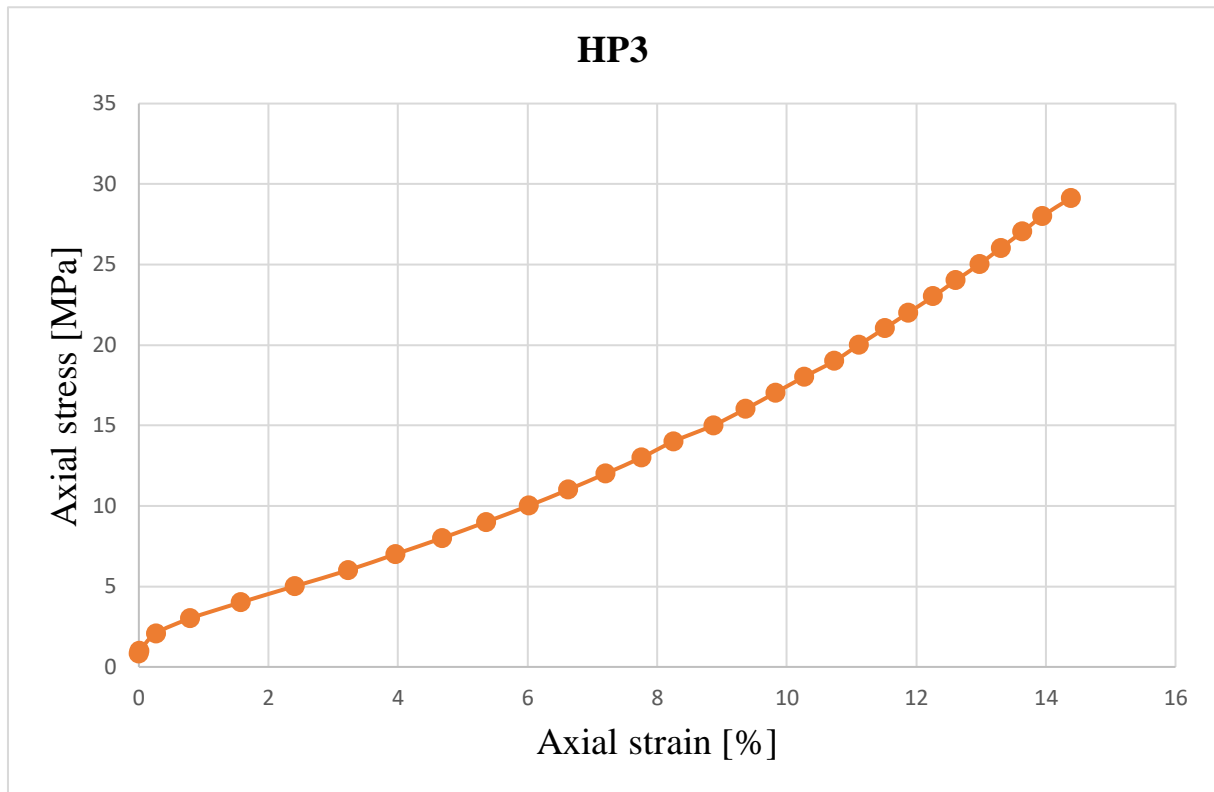


Figure 4.1. 6: Axial stress [MPa] as a function of Axial strain [%] for HP3.

The core was not flooded with DW in the creep phase. The core reached a total axial creep strain of 9.8% and this was reached after 2.7 creep days. During the transient phase, the axial creep strain reached 7.5%. In figure 4.1.7, the permeability has a downward trend, but with some fluctuations. This is most likely due to movements of the grains in the core.

Table 4.1. 6: Values for HP3

	Total creep time [days]	Flooding brine [days]	Flooding DW [days]	Axial creep strain brine [%]	Total axial creep strain [%]
HP3	2.7	2.7	-	-	9.8

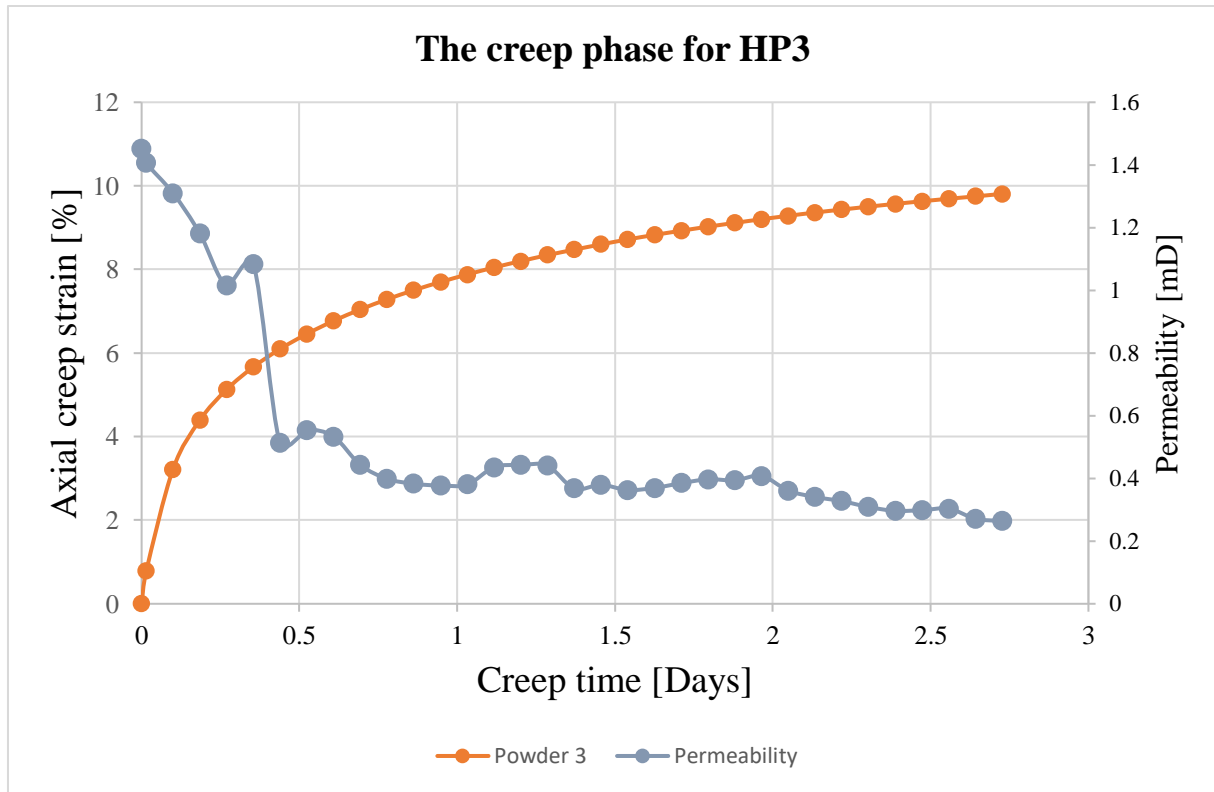


Figure 4.1. 7: Axial creep strain [%] and permeability as a function of creep time [Days] for HP3.

HP4

Uniaxial strain loading and creep

HP4 lasted for approximately 6 days. The axial strain reached in the uniaxial strain loading phase was 13.7% and the axial stress was 29.0 MPa, as seen in figure 4.1.8. There is a drop towards the end of the curve. This could be a result of core fatigue or leakage from the Triaxial cell effecting the inflation rate.

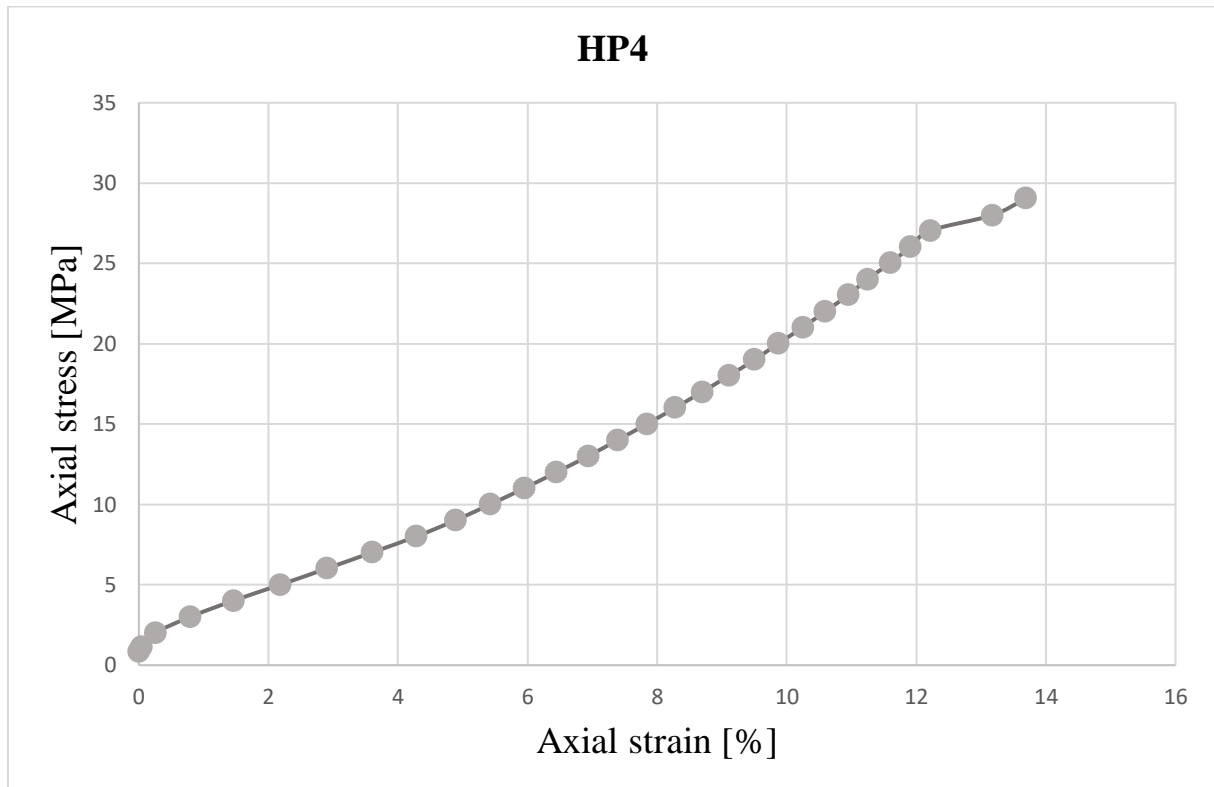


Figure 4.1. 8: Axial stress [MPa] as a function of axial strain [%] for HP4.

The creep phase lasted for 4 days (figure 4.1.9). The core was flooded with brine for 2.7 days and DW for 1.3 days. Toward the end of the transient creep phase, the axial creep strain was 6.4%. When starting to flood with DW, the core had an axial creep strain of 8.3%, and the total axial creep strain was 9.0%. There is a downward trend for the permeability, it fluctuates for the entire durations. Again, it could be due to the fact that the material is unconsolidated.

Table 4.1. 7: Values for HP4

	Total creep time [days]	Flooding brine [days]	Flooding DW [days]	Axial creep strain brine [%]	Total axial creep strain [%]
HP4	4	2.7	1.3	8.3	9.0

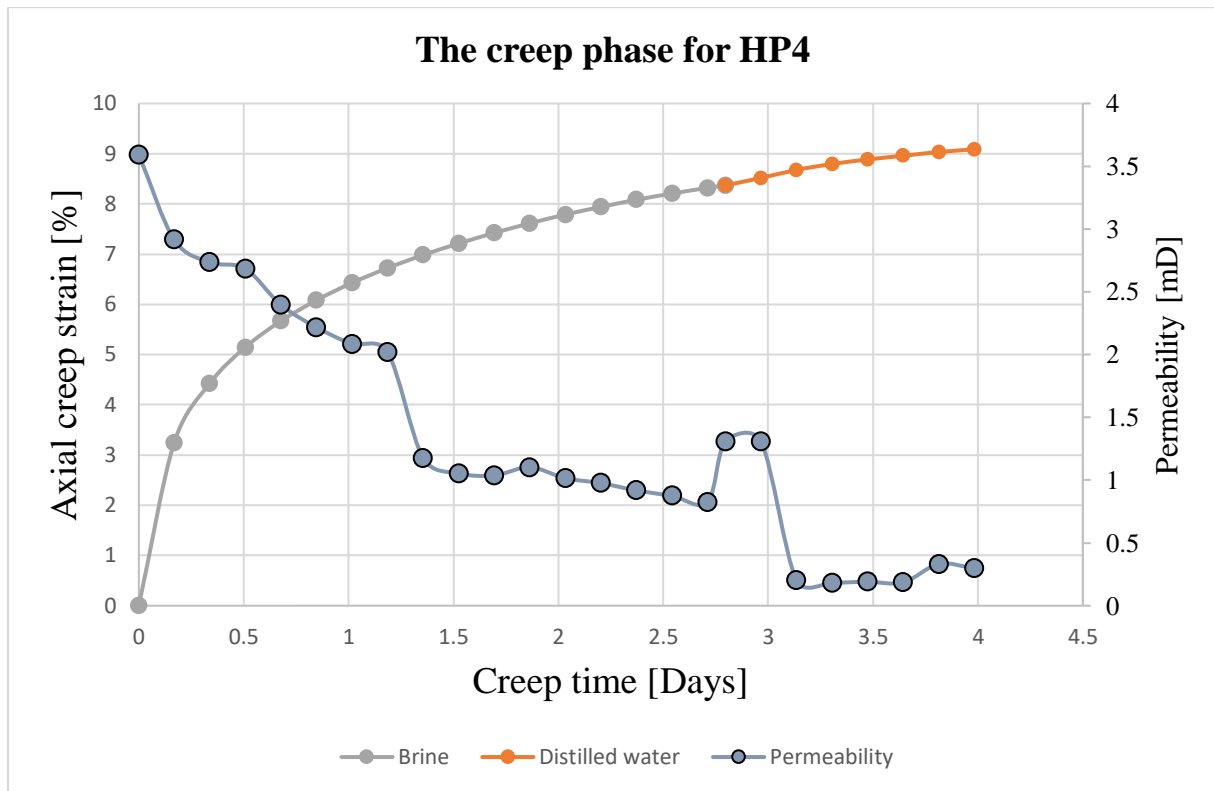


Figure 4.1. 9: Axial creep strain [%] and permeability as a function of creep time [Days] for HP4.

As seen in table 4.1.3, the total axial creep strains for HP1, HP2, HP3 and HP4 were 10.0%, 12.0%, 9.8% and 9.0%, respectively. HP2 had the highest compaction. The porosity reductions were 22.1% and 19.7% for HP1 and HP2, there has been a significant reduction of the void spaces in the cores. In the table, it can be seen that the porosity reduction for HP4 was 25.4%. This cannot be compared to the values for HP1 and HP2, as the porosity calculated after the testing was calculated with a core that had lost powder due to the absence of filters when first starting and having to re-start the test.

4.1.3. Experiment with organic additive and axial stress of 30 MPa

HPA7 used a brine that contained a small amount of oxalic acid. The brine used is described under section 3.3.2. *Brine preparation with additive (oxalic acid – HOCCOOH)*. This test was performed with an axial stress of 30 MPa for the creep phase, just like HP1, HP2, HP3 and HP4.

Table 4.1. 8: Overview of HPA7

	Original length [mm]	New length [mm]	Original mass weight [g]	Saturated mass weight [g]	New dry weight [g]	Porosity before test [%]	Porosity after test [%]	Total axial creep strain [%]
HP7	59.8	47.9	87.9	99.0	86.7	49.0	32.1	8.2

The total axial creep strain was 8.2%, meaning the core experienced the lowest compaction compared to HP1, HP2, HP3 and HP4, as presented above in table 4.1.3. The porosity has also been reduced by 16.9%, there has been a significant reduction of the void spaces in the core.

HPA7

Uniaxial strain loading and creep

HP7 lasted a total of 13 days. In the uniaxial strain loading phase, the axial strain reached 15.5% and the axial stress reached 29.0 MPa (figure 4.1.10).

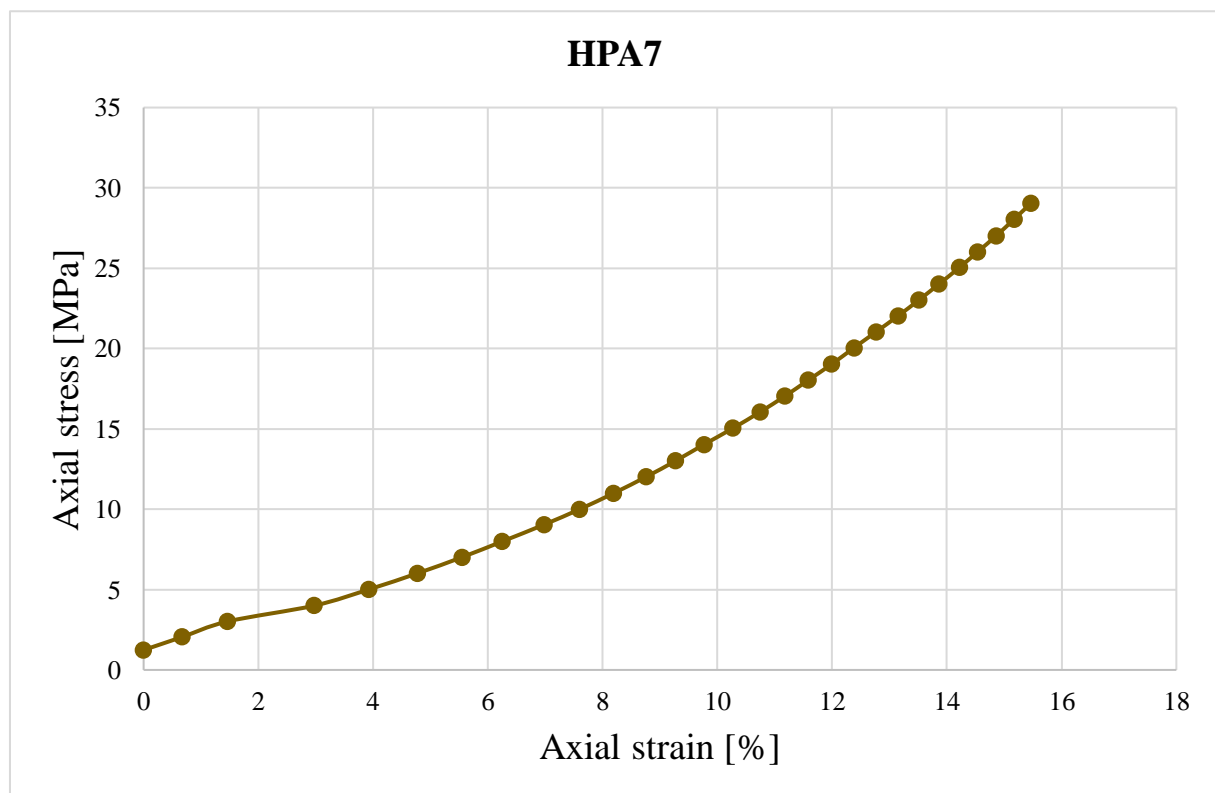


Figure 4.1. 10: Axial stress [MPa] as a function of Axial strain [%] for HP7.

The creep phase for HP7 lasted approximately 9.5 days, see figure 4.1.11. The core was flooded with the brine containing oxalic acid for 6.5 days, before being flooded with DW the remaining

days. In the transient creep phase, the axial creep strain reached approximately 7.2%. The axial creep strain in the steady state phase reached 8.0 % towards the end of flooding with the brine. The total axial creep strain was 8.2%. Also here, as for HP2, the change of the fluid flooding the core did not impact the creep graph, the line kept stable and steady. The permeability has a downward trend with few fluctuations.

Table 4.1. 9: Values for HPA7

	Total creep time [days]	Flooding brine [days]	Flooding DW [days]	Axial creep strain brine [%]	Total axial creep strain [%]
HP7	9.5	6.5	3	8.0	8.2

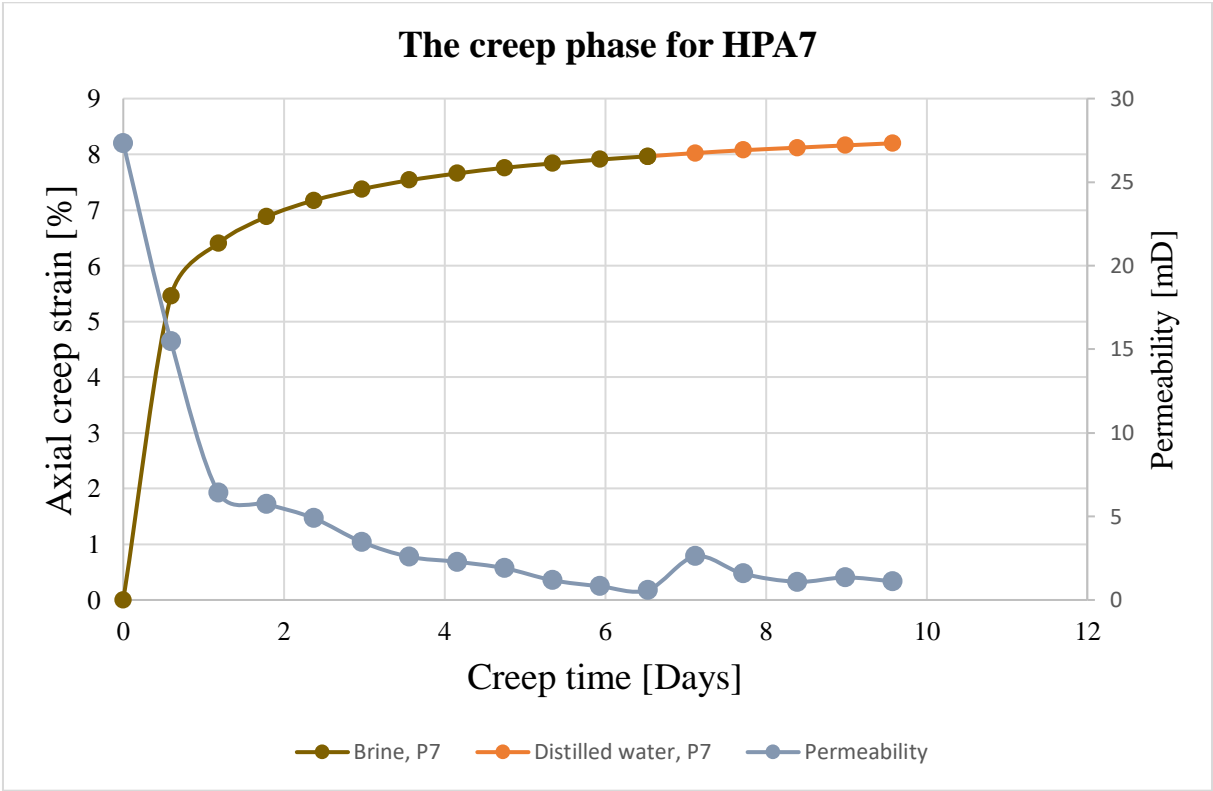


Figure 4.1. 11: Axial creep strain [%] and permeability as a function of creep time (days).

4.1.4. Experiments with oil leakage

Two of the tests performed, HPA6 and LP9, had oil leakages. When disassembling the tests and drying the cores up in a heating cabinet, they both had a brown looking color, in contrary to the other tests that were all white and clean. HPA6 was performed the same way as HPA7, with organic additive and with high stress. LP9 was performed the same way as LP5, without organic additive, and low stress.

Table 4.1. 10: Overview of HPA6 and LP9

	Original length [mm]	New length [mm]	Original mass weight [g]	Saturated mass weight [g]	New dry weight [g]	Porosity before test [%]	Porosity after test [%]	Total axial creep strain [%]
HPA6	58.6	43.0	87.4	98.1	89.1	48.3	26.5	11.0
LP9	58.2	56.0	87.1	110.6	92.3	48.6	40.6	0.004

HPA6

Uniaxial strain loading and creep

HPA6 lasted a total of 15 days. The axial strain reached 12.8% at an axial stress of 29.0 MPa, see figure 4.1.12.

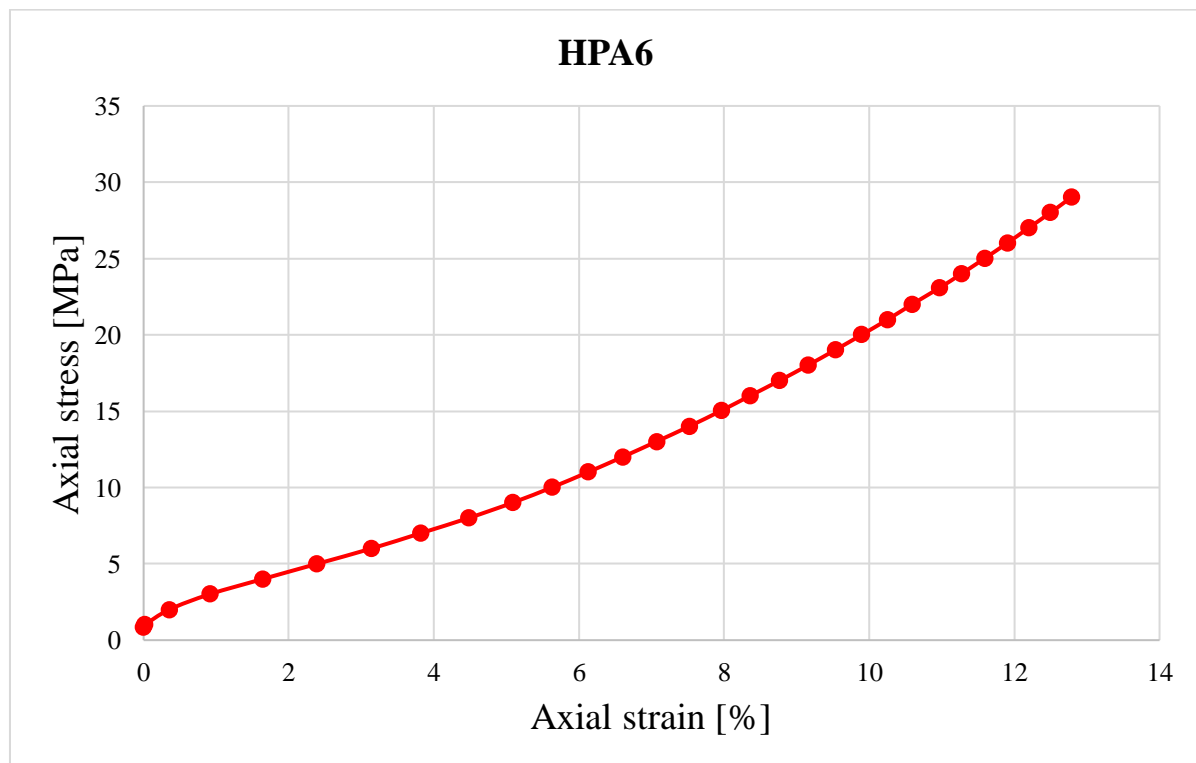


Figure 4.1. 12: Axial stress [MPa] as a function of Axial strain [%] for HPA6.

The creep period lasted approximately 12.7 days. The core was flooded with brine containing oxalic acid for the first 11.7 days before being flooded with DW the last day (figure 4.1.13). The axial creep strain reached approximately 8.3% in the transient creep phase, and it reached 10.4% when changing the flood fluid. The total axial creep strain was 11.0 %. In the graph, there is a rise towards the end of the creep period when the core is being flooded with DW. The permeability has a downward, stable trend without fluctuations.

Table 4.1. 11: Values for HPA6

	Total creep time [days]	Flooding brine [days]	Flooding DW [days]	Axial creep strain brine [%]	Total axial creep strain [%]
HPA6	12.7	11.7	1	10.4	11.0

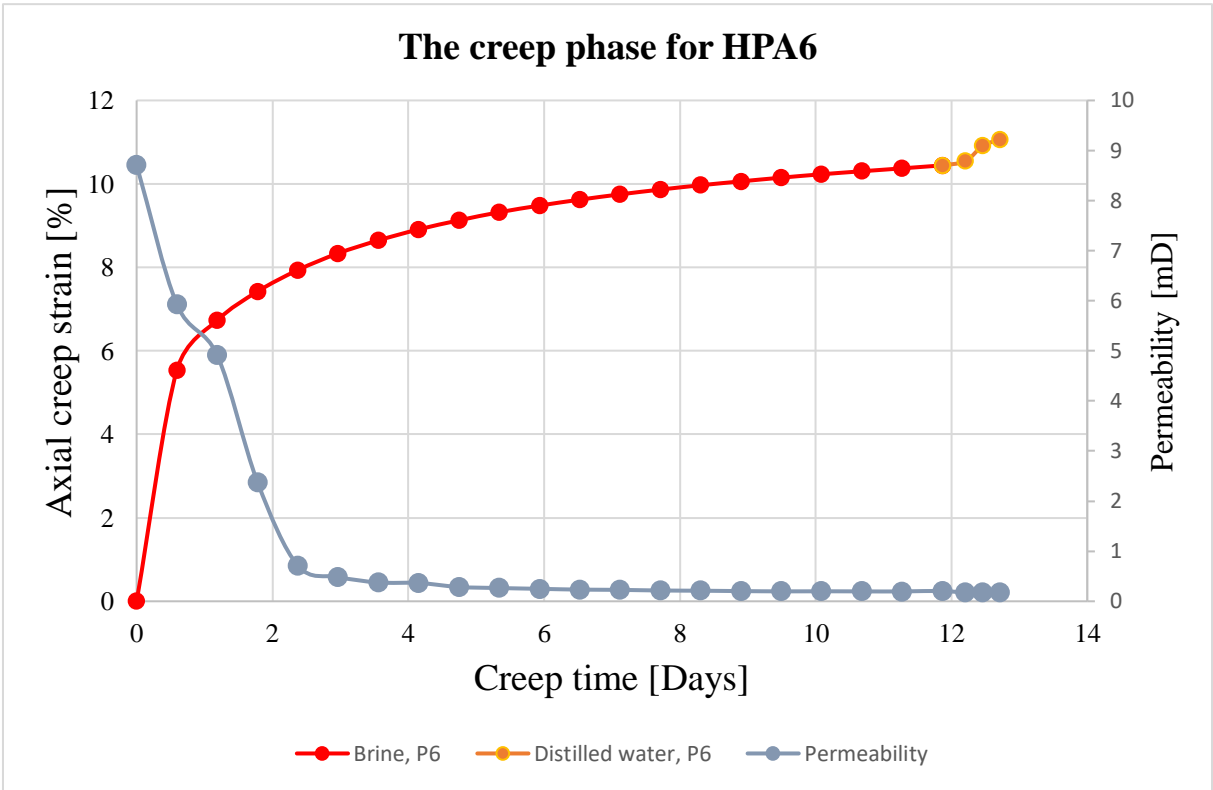


Figure 4.1. 13: Axial creep strain [%] and permeability as a function of creep time [Days] for HPA6.

LP9

Uniaxial strain loading and creep

Figure 4.1.14 does not look like any of the other creep graphs presented. This test did not creep, there was no compaction of the core. The permeability does not have the same trend as observed from the other tests; it has a straighter trend up until approximately creep day 12. It does follow the creep, except towards the end and it has many fluctuations. The creep period lasted 13.8 days, and the change in flooding fluid to DW did not influence the creep.

Table 4.1. 12: Values for LP9

	Total creep time [days]	Flooding brine [days]	Flooding DW [days]	Axial creep strain brine [%]	Total axial creep strain [%]
LP9	13.8	11.2	2.6	0.018	0.004

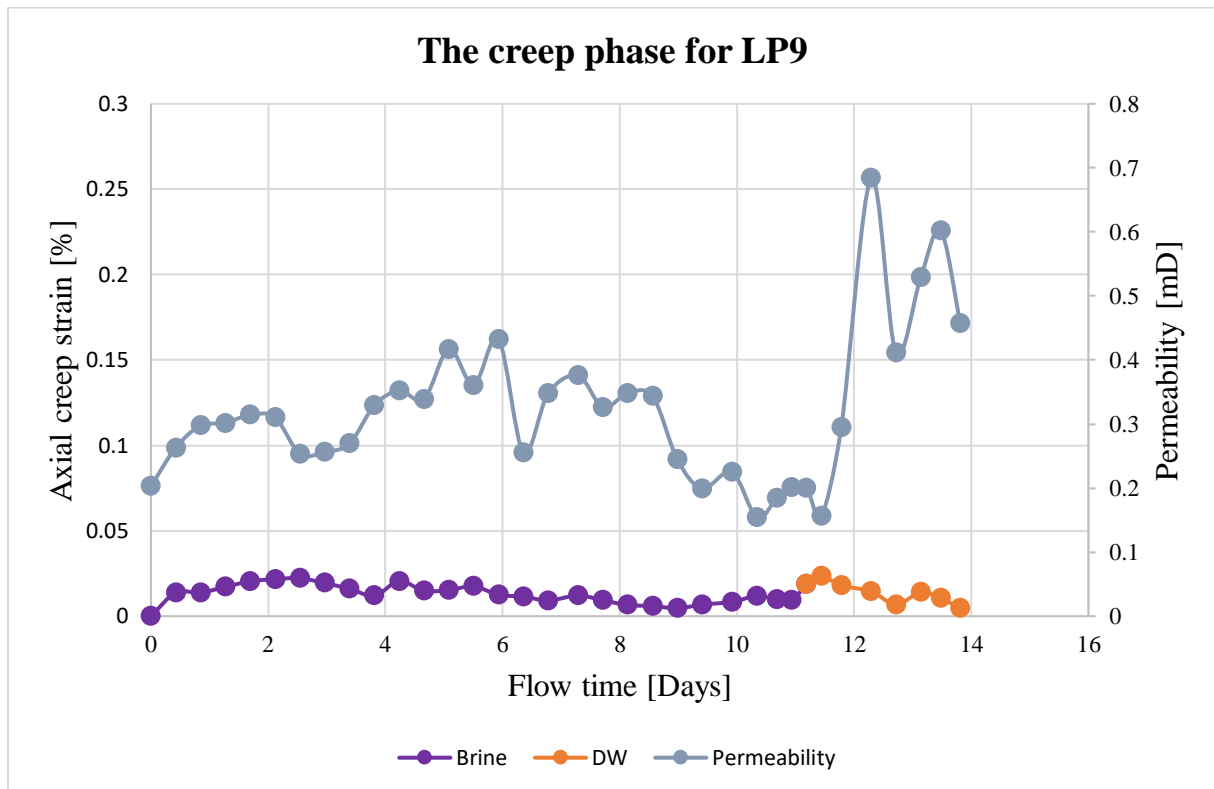


Figure 4.1. 14: Axial creep strain [%] and permeability as a function of creep time [Days] for LP9.

Looking at table 4.1.10, these are the only two tests that weighted more after the tests were finished compared to the original mass weight. This had to do with the oil leakage into the cores, making them heavier. The porosity reductions were 21.8 % and 8.0 % for HPA6 and

LP9, meaning that HPA6 has a significantly higher reduction in the void spaces in the core. This is because of the difference in exposed stress. The total axial creep strains were 11.0% and 0.004% for HPA6 and LP9, respectively. The difference is significant, LP9 did not experience any compaction.

4.2. Chemical analysis

The chemical analysis with the ion concentrations and pH-values as a function of time are presented for all tests. The Ca^{2+} concentrations have been multiplied by 100. This was done so that all three ion concentrations could be presented on the same axis and then have the pH values presented on the secondary axis. The black lines in all the figures shows when the flooding fluid was changed to DW. There are no black lines for HP1 and HP3. HP1 was started being flooded with DW after the last effluent sample had been collected and the temperature was turned off and HP3 failed.

For all tests, it was observed that the Na^+ and Cl^- concentrations fluctuate around the originals, until the cores start being flooded with DW. Then the concentrations make a big drop in values. For some effluent samples prior to the cores being flooded with DW, the values were above the original, this is probably due to evaporation from the effluent sample or incorrect dilution prior to testing. Beforehand, it was not expected that neither the Na^+ or Cl^- concentrations would change much throughout the tests. The original values for Na^+ and Cl^- were 0.1052 M and 0.1003 M.

The Ca^{2+} concentrations for all tests fluctuate below the originals. This indicates that there have been some calcium losses throughout the test durations. It seems like the change in flooding fluid to DW does not affect the concentration of Ca^{2+} in the effluent. As can be seen in table 4.2.1, it seems like the ion concentrations are lower for the two cores flooded with organic additive, they experience a greater loss of Ca^{2+} . The original value for Ca^{2+} was 0.02 M after being multiplied by 100.

4.2.1. Experiment without organic additive and low stress

LP5

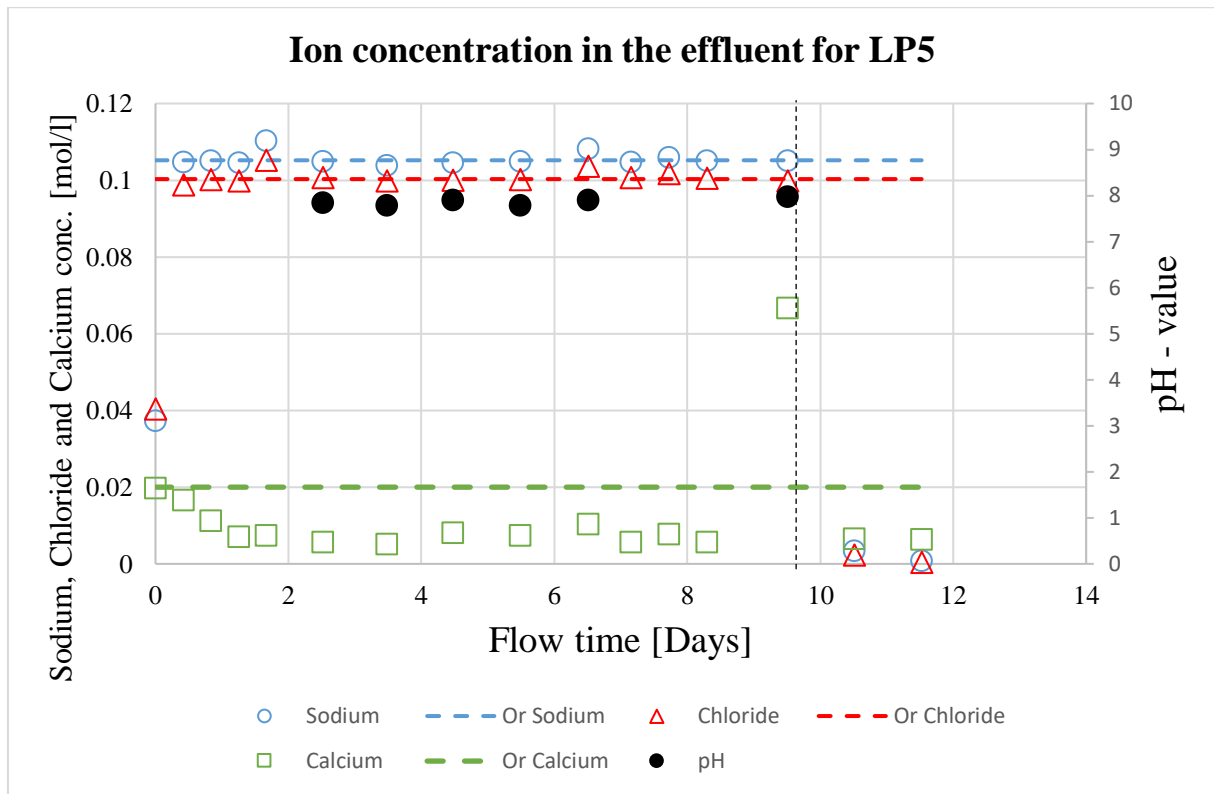
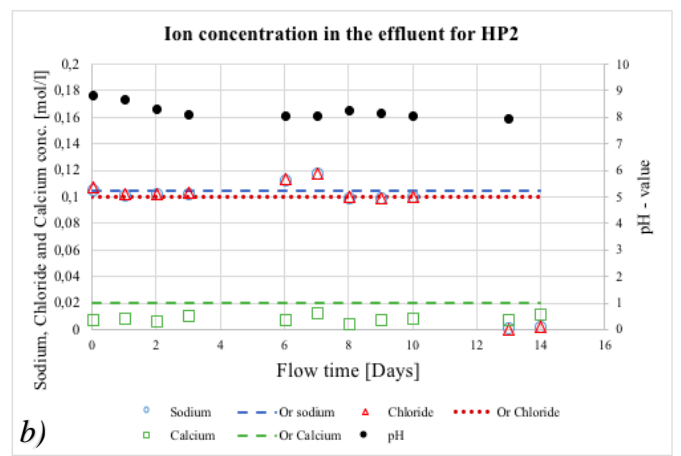
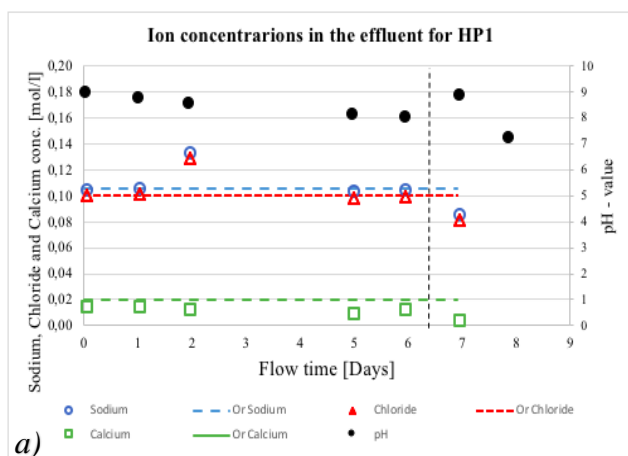


Figure 4.2. 1: Sodium, chloride and calcium concentrations [mol/l] as a function of flow time [days] for LP5

4.2.2. Experiments without organic additive, but with axial stress of 30 MPa

HP1, HP2, HP3 and HP4



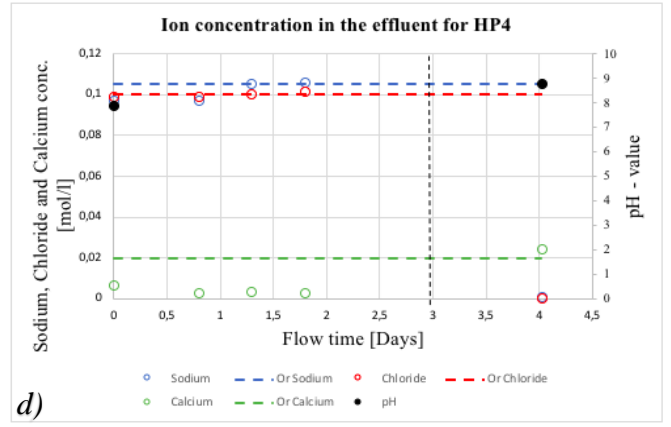
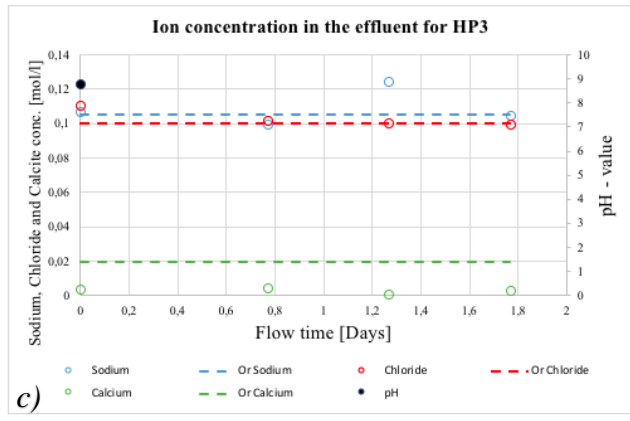


Figure 4.2. 2: Sodium, chloride and calcium concentrations [mol/l] as a function of flow time [days] for HP1 (a), HP2 (b), HP3 (c) and HP4 (d)

4.2.3. Experiment with organic additive and axial stress of 30 MPa

HPA7

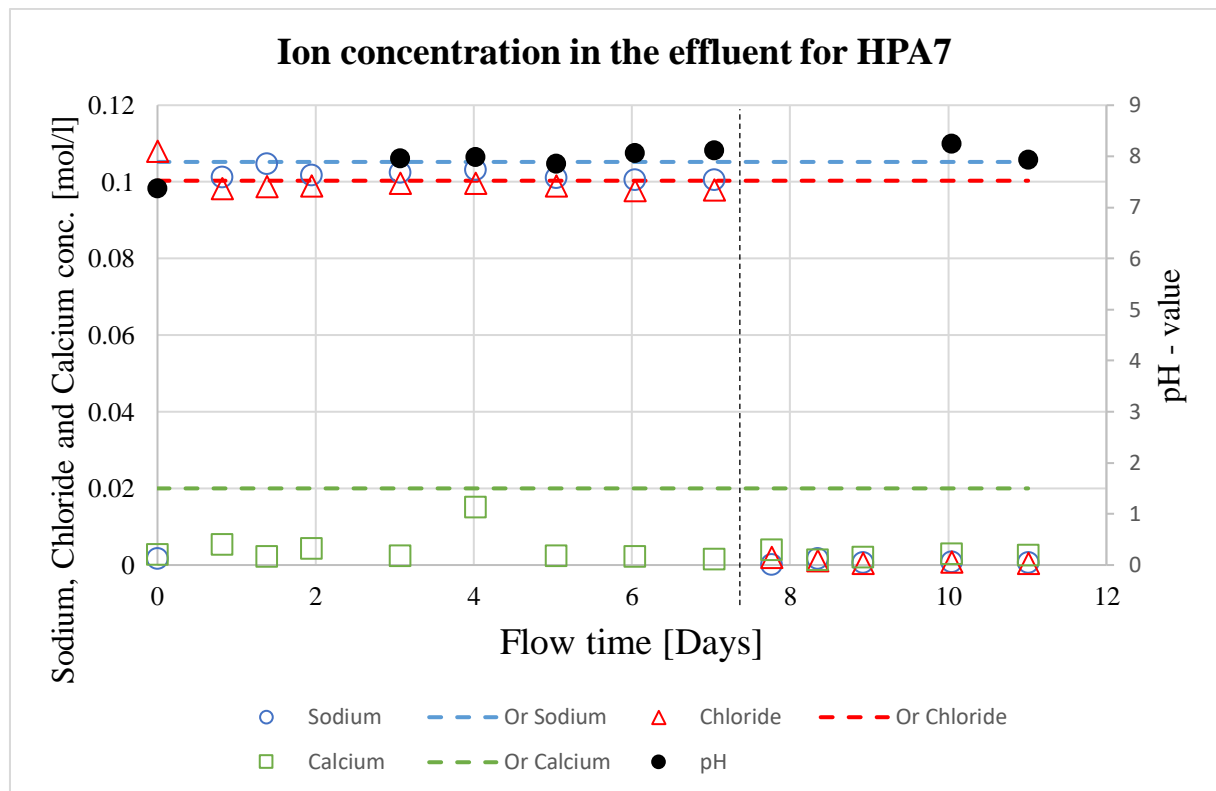


Figure 4.2. 3: Sodium, chloride and calcium concentrations [mol/l] as a function of flow time [days] for HPA7.

4.1.4. Experiments with oil leakage

HPA6 and LP9

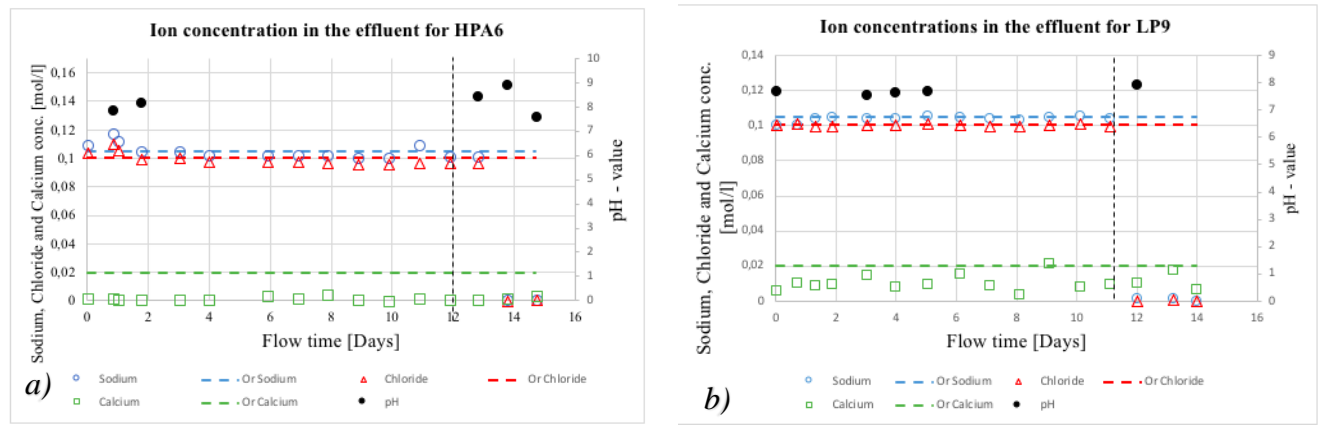


Figure 4.2. 4: Sodium, chloride and calcium concentrations [mol/l] as a function of flow time [days] for HPA6 (a) and LP9 (b).

4.2.5. pH - values

In table 4.2.1 below, there is an overview of the pH values that were sampled and measured for all the experiments. There is also an overview of the Ca^{2+} concentrations for all the samples. The pH values are marked in red, while the Ca^{2+} concentrations are marked in black. Where there is marked a *, it indicates that the cores are being flooded with DW. HPA6 and HPA7 are marked in a darker grey color compared to the rest. This has been done to easily separate the cores flooded with oxalic acid from the cores flooded without oxalic acid.

The reason for the days that does not have a value for the pH or the Ca^{2+} concentration is weekends and the Easter holiday.

Table 4.2. 1: A table showing the pH values for each test on different days in the test period. The values marked with * means that the tests are being flooded with DW. Note that the Ca²⁺ values seem to be lower for the test containing oxalic acid (HPA6 and HPA7, marked with a darker grey color) for all the different days compared to the rest.

Time [days]	HP1 pH Ca²⁺- cons [mol/l]	HP2 pH Ca²⁺- cons [mol/l]	HP3 pH Ca²⁺- cons [mol/l]	HP4 pH Ca²⁺- cons [mol/l]	LP5 pH Ca²⁺- cons [mol/l]	HPA6 pH Ca²⁺- cons [mol/l]	HPA7 pH Ca²⁺- cons [mol/l]	LP9 pH Ca²⁺- cons [mol/l]
0	9.06 1.677E-02	8.88 0.879E-02	8.79 0.406E-02	7.90 0.667E-02		7.87 0.219E-02	7.37 0.276E-02	7.72 0.690E-02
1	8.83 1.686E-02	8.70 0.738E-02				8.22 0.088E-02		
2	8.64 1.511E-02	8.37 0.0118E-02						
3		8.15			7.85 0.567E-02		7.95 0.225E-02	7.58 1.548E-02
4				8.81* 2.442E-02	7.78 0.519E-02		7.98 1.509E-02	7.69 0.848E-02
5	8.23 1.197E-02				7.90 0.808E-02		7.85 0.225E-02	7.72 1.063E-02
6	8.12 1.424E-02	8.09			7.98 0.736E-02		8.06 0.208E-02	
7	8.96* 0.672E-02	8.12 0.790E-02			7.90 1.026E-02		8.11 0.148E-02	
8	7.32*	8.29 1.367E-02						
9		8.19 0.494E-02						
10		8.08 0.847E-02			7.97 6.660E-02		8.24* 0.293E-02	
11							7.93* 0.250E-02	
12						8.47 0.095E-02	7.02*	7.96* 1.091E-02
13		7.98*				8.96* 0.241E-02		
14						7.65* 0.409E-02		

4.3. Calcite microstructure morphology - SEM

When taking SEM images, different enlargements were chosen. What was focused on was images with an enlargement of 10 μm and for each test the images were printed out. This was done in order for the grains to be counted. Different scales for the grains were decided beforehand, and they were approximately as follows:

- Tiny: $\sim \leq 1.5 \times 1.5 \text{ mm}$ ($0.87 \times 0.87 \mu\text{m}$)
- Very small: $1.5 \times 1.5 \text{ mm} - 3 \times 3 \text{ mm}$ ($0.87 \times 0.87 \mu\text{m} - 1.74 \times 1.74 \mu\text{m}$)
- Small: $3 \times 3 \text{ mm} - 5 \times 5 \text{ mm}$ ($1.74 \times 1.74 \mu\text{m} - 2.90 \times 2.90 \mu\text{m}$)
- Medium: $5 \times 5 \text{ mm} - 11 \times 11 \text{ mm}$ ($2.90 \times 2.90 \mu\text{m} - 6.38 \times 6.38 \mu\text{m}$)
- Large: $\geq 11 \times 11 \text{ mm}$ ($6.38 \times 6.38 \mu\text{m}$)

After counting the grains, frequency plots were made. They were plotted for inlet, middle, outlet and for some of the tests, the rim was also plotted. There are results from all the tests except for HPA6 and LP9 due to the oil leakages. The presence of oil in both cores meant that the cores could not be investigated in SEM.

For all samples, the grains were counted on one-fourth of the image. We assume that $\frac{1}{4}$ of the image is representative of the entire photo. This was done to make the counting manageable and not too time-consuming. The part of the photo that was counted are marked with a red square for HP1, shown further down in figures 4.3.2-4.3.5. The exception was for the image taken of the raw powder that the artificial cores were made out of. Here, the grains were counted on the entire photo (figure A.10. in Appendix). The images taken from the other cores are presented in the Appendix at the end of this thesis. They have been counted the same way as for HP1.

4.2.1. Experiment without organic additive, but with axial stress of 30 MPa

HP1

Below is a drawing (figure 4.3.1) of where the samples were collected from the core in HP1.

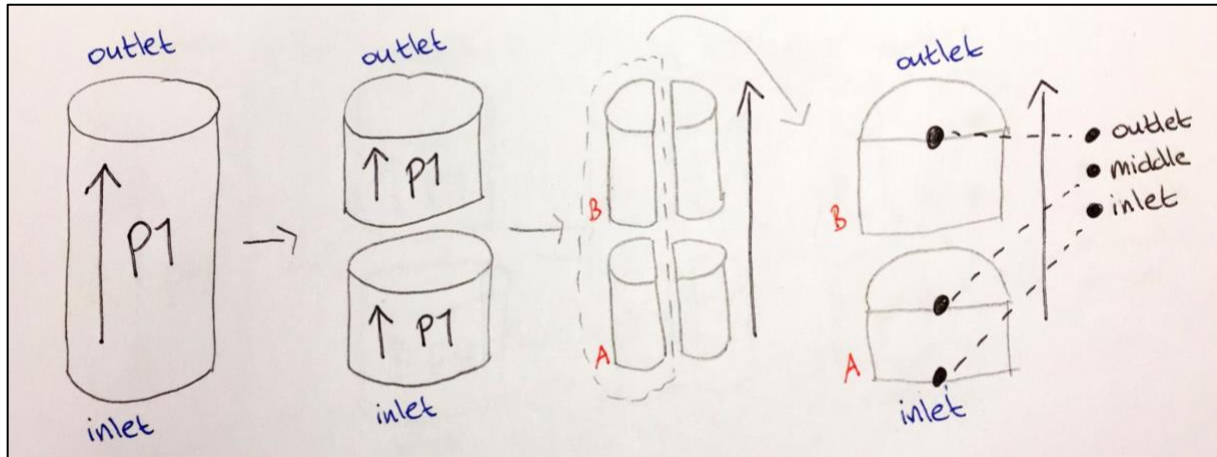


Figure 4.3. 1: The different locations the samples investigated in SEM are collected from for HP1.

Pictures were taken at two different places for each sample that was prepared. For the inlet sample, there was a clear difference in the amount of tiny grains in the two photos presented for HP1. For that reason, the grains were counted for both, and the average of each distribution was used. For the other sample-locations, the photos were equal so only one photo was counted. The results of counting the grains are presented in figure 4.3.6.

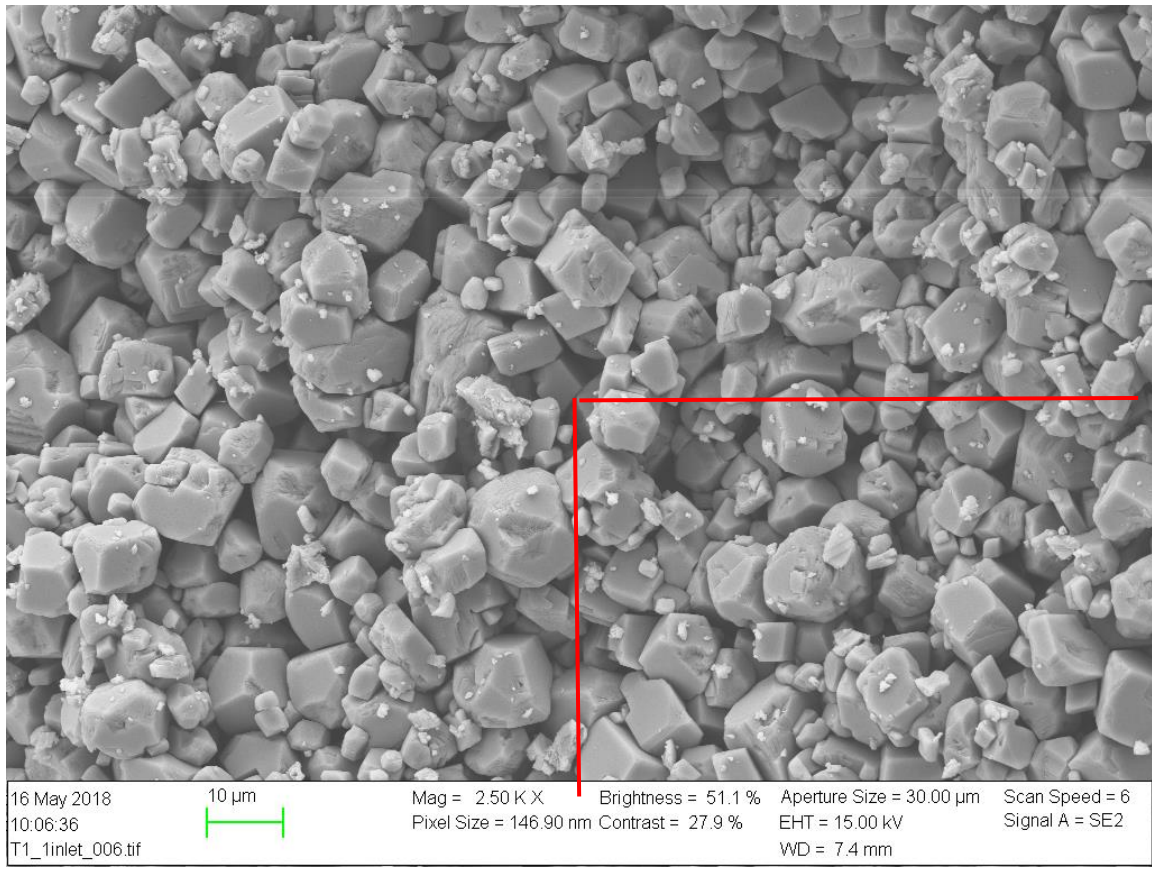


Figure 4.3. 2: SEM image of inlet for HP1.

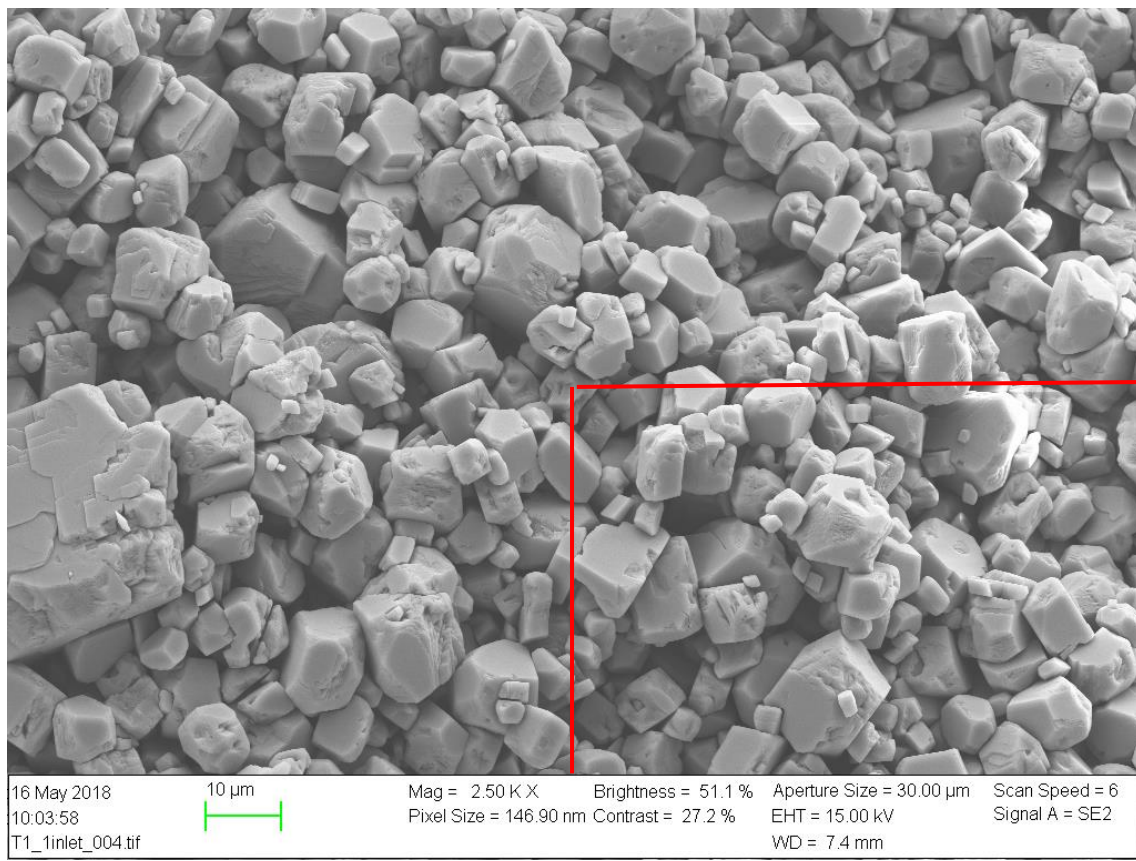


Figure 4.3. 3: SEM image of inlet for HP1.

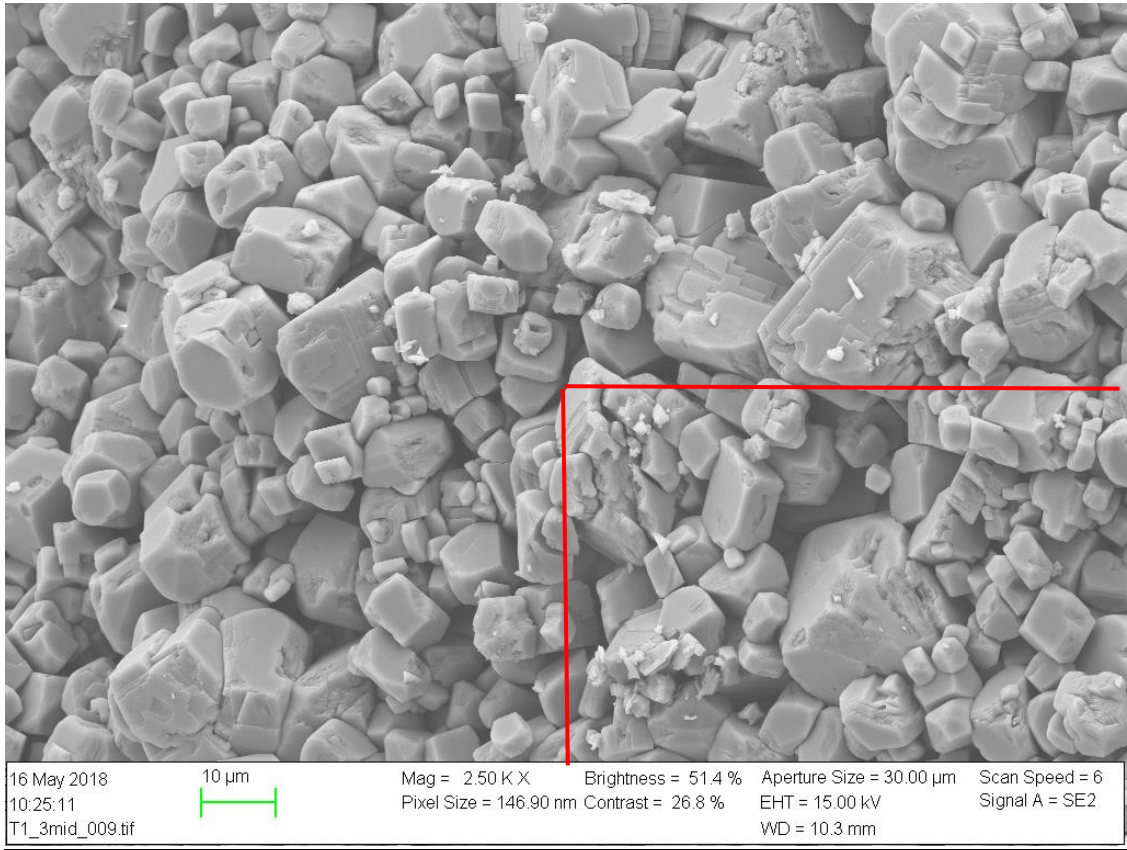


Figure 4.3. 4: SEM image of the middle location for HP1.

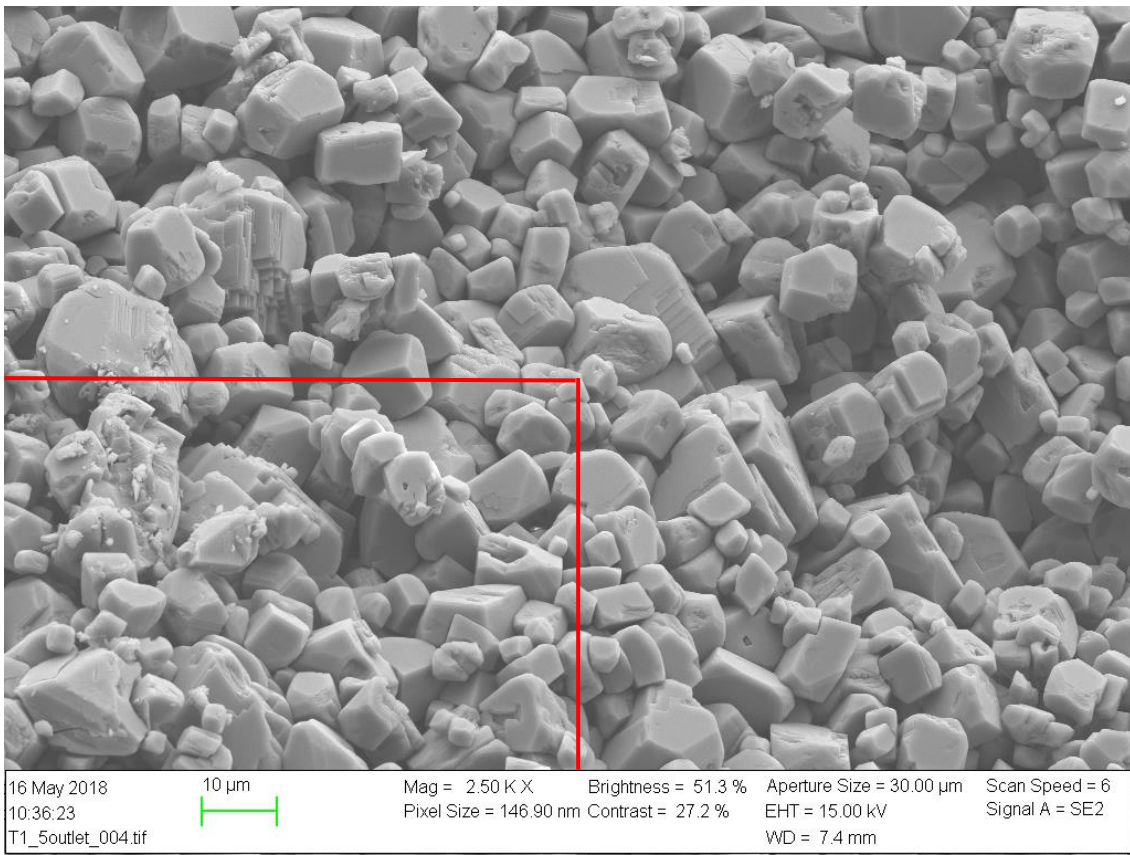


Figure 4.3. 5: SEM image of outlet for HP1.

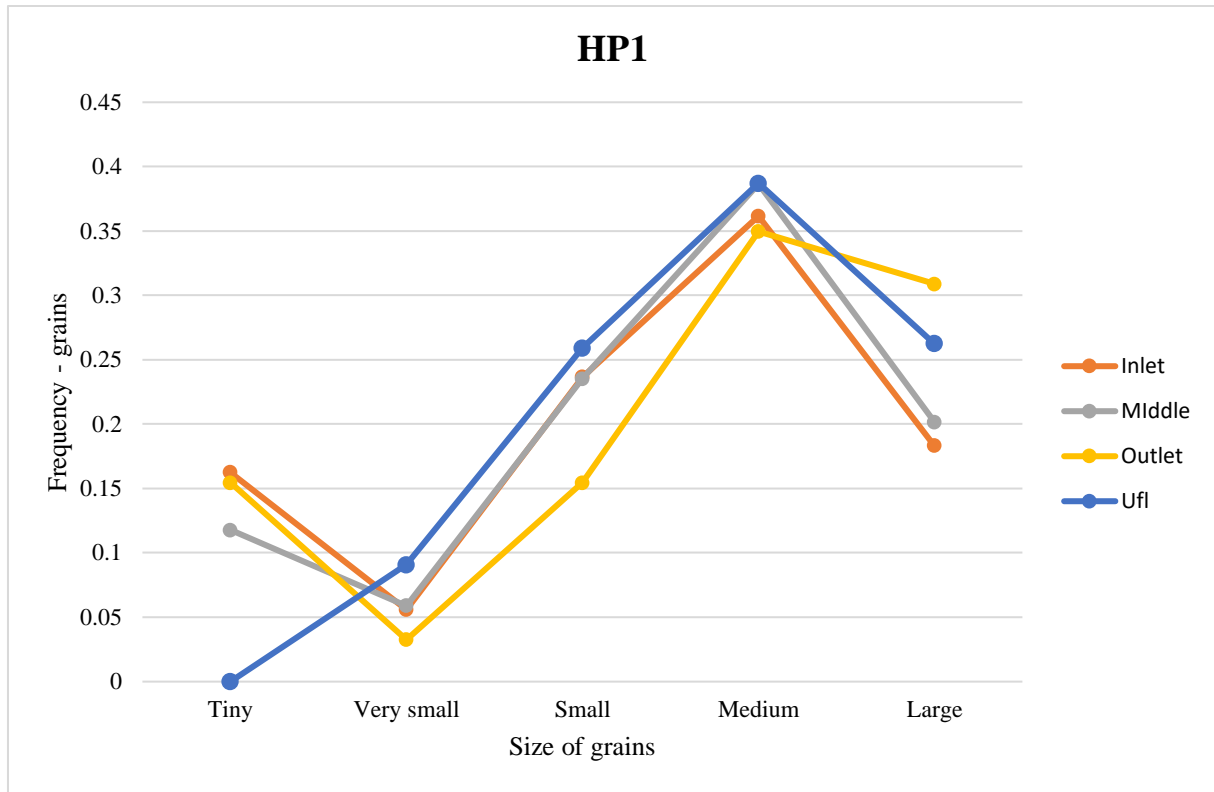


Figure 4.3. 6: The frequency of the grains as a function of different grain sizes for HP1. The ufl indicates the original and unflooded powder. (tiny: $0.87 \times 0.87 \mu\text{m}$, very small: $0.87 \times 0.87 - 1.74 \times 1.74 \mu\text{m}$, small: $1.74 \times 1.74 - 2.9 \times 2.9 \mu\text{m}$, medium: $2.9 \times 2.9 - 6.38 \times 6.38 \mu\text{m}$, large: $6.38 \times 6.38 \mu\text{m}$)

The frequency of grains in the sizes of *tiny*, *very small*, and *medium* follows approximately the same trend throughout the core for inlet, middle and outlet. For *small* there are more of that grain size in inlet and middle compared to outlet. For the biggest grain size, *large*, there seems to be a higher frequency of that size in outlet, compared to inlet and middle. Also, some raw powder was investigated. The blue line represents the results. *Tiny* grains were not present initially in the powder, and the size most frequently found was *medium*.

HP2

The locations for the sampling of the core (figure 4.3.7) and the distributions in a graph (figure 4.3.8) are presented here.

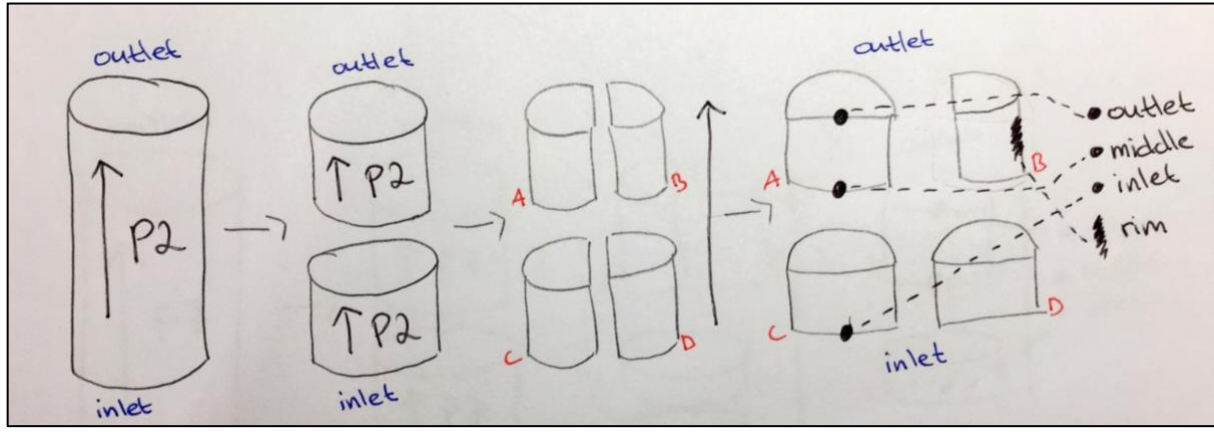


Figure 4.3. 7: The locations of where samples were collected from the core in HP2.

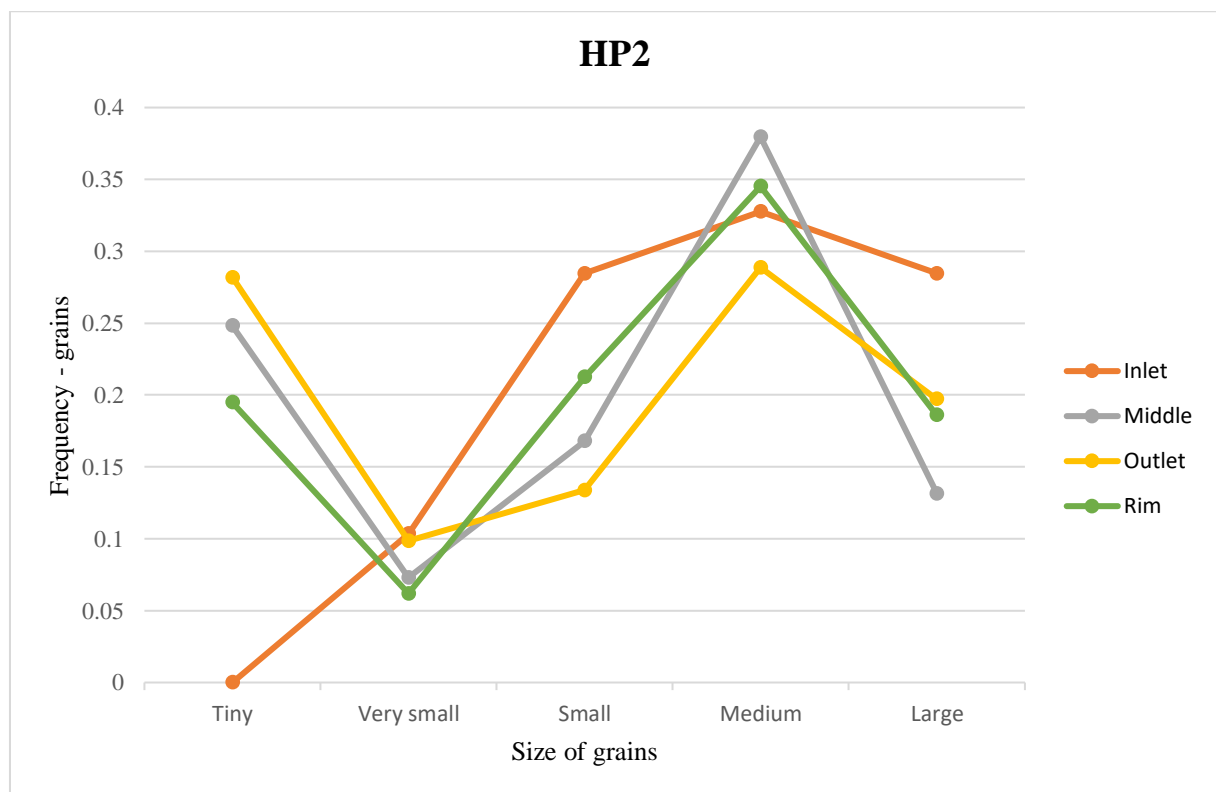


Figure 4.3. 8: The frequency of the grains as a function of different grain sizes for HP2. (tiny: $0.87 \times 0.87 \mu\text{m}$, very small: $0.87 \times 0.87 - 1.74 \times 1.74 \mu\text{m}$, small: $1.74 \times 1.74 - 2.9 \times 2.9 \mu\text{m}$, medium: $2.9 \times 2.9 - 6.38 \times 6.38 \mu\text{m}$, large: $6.38 \times 6.38 \mu\text{m}$)

For the *tiny* grain size, it is clear that there were no tiny grains at inlet, but that the amount increases as you move further into the core to middle and outlet. There are also some *tiny* grains found at the rim. Looking at the *very small* grains, there is not much of a difference throughout the core. The *small* grain size occurs most frequently at inlet, then on the rim, middle and the least amount is found at outlet. For *medium*, they are most frequently found in the middle of the core, followed by the rim and inlet. The least amount of the middle grain size is found in the outlet. For the larger grains there are a lot of them in inlet and the least of them in the middle.

HP4

The locations for the sampling of the core in HP4 (figure 4.3.9) and the distributions in a graph (figure 4.3.10) are shown below.

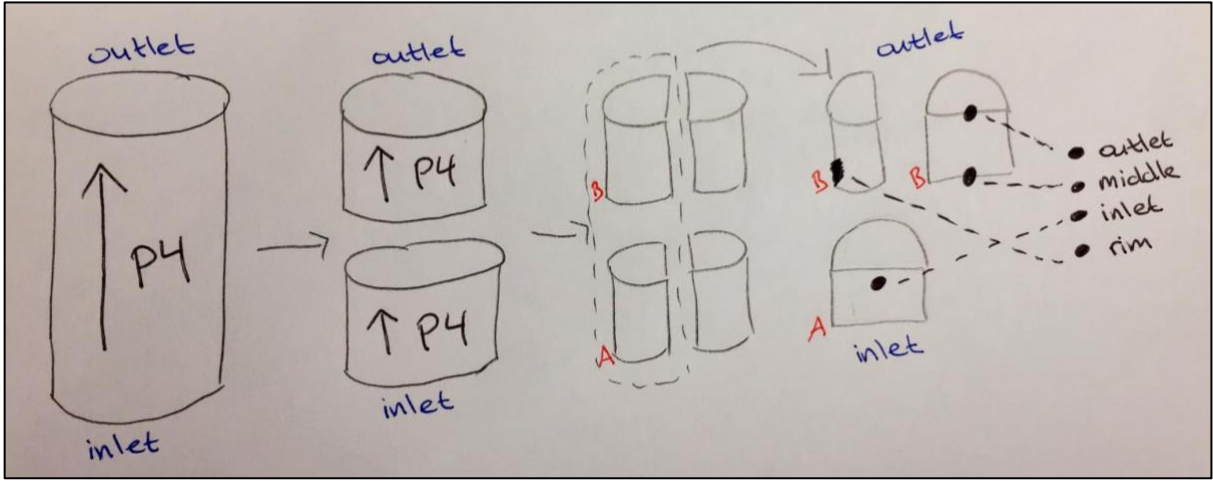


Figure 4.3. 9: The locations of where samples were collected from the core in HP4.



Figure 4.3. 10: The frequency of the grains as a function of different grain sizes for HP4. (tiny: $0.87 \times 0.87 \mu\text{m}$, very small: $0.87 \times 0.87 - 1.74 \times 1.74 \mu\text{m}$, small: $1.74 \times 1.74 - 2.9 \times 2.9 \mu\text{m}$, medium: $2.9 \times 2.9 - 6.38 \times 6.38 \mu\text{m}$, large: $6.38 \times 6.38 \mu\text{m}$)

There is a significant difference in the frequency of *tiny* grains in inlet, middle and outlet of the core. It increases as one moves further into the core, the content of *tiny* grains is higher in outlet compared to inlet. It is more even for *very small* grains. Looking at *small* grains, they are most frequently found at the middle, then inlet and the least amount at outlet. For medium, it is even for inlet and outlet, and a smaller amount in the middle. The situation is the same for large. Finally, looking at the rim. The content of the different grains sizes follows approximately the same trend as the inlet line, some sizes being over and some under the line.

4.3.2. Experiments without organic additive and low stress

LP5

The locations for the sampling of the core (figure 4.3.11) and the distributions in a graph (figure 4.3.12) are presented.

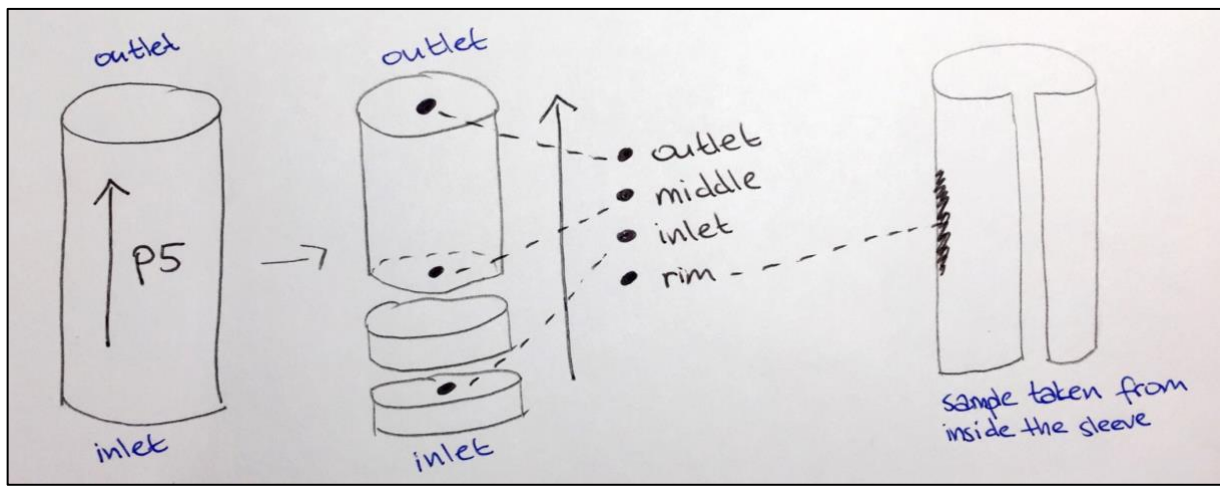


Figure 4.3. 11: The locations of where samples were collected from the core in LP5.

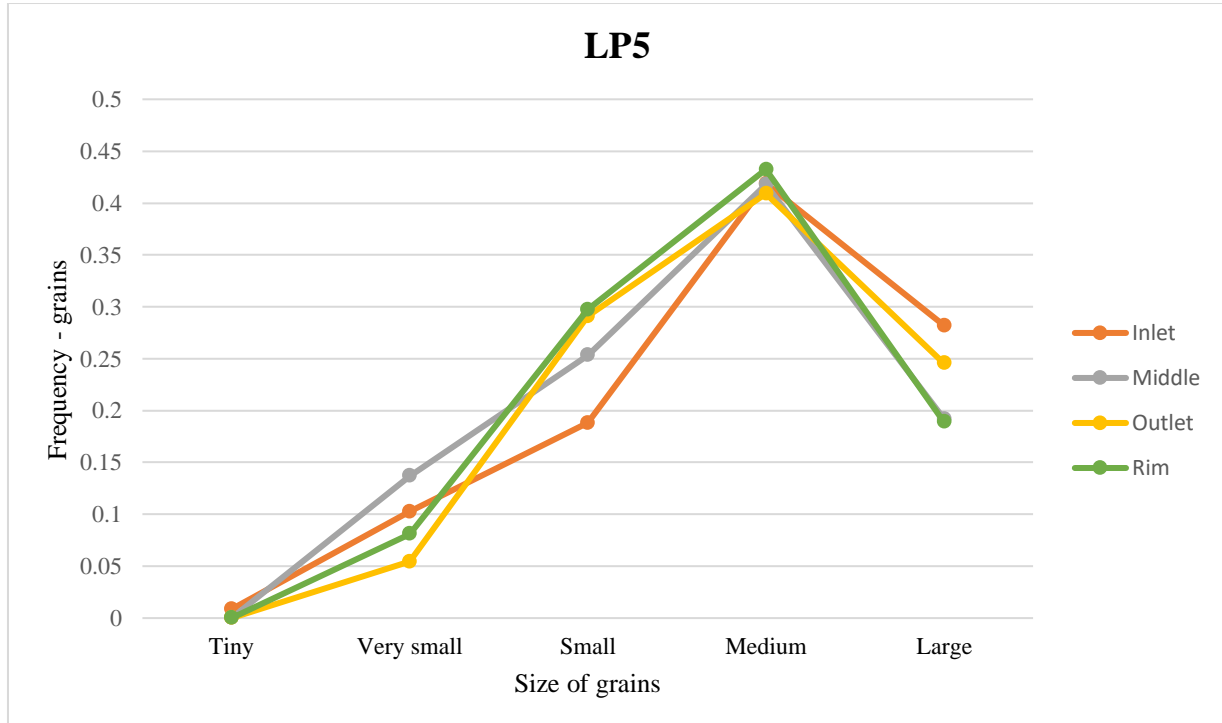


Figure 4.3. 12: The frequency of the grains as a function of different grain sizes for LP5. (tiny: $0.87 \times 0.87 \mu\text{m}$, very small: $0.87 \times 0.87 - 1.74 \times 1.74 \mu\text{m}$, small: $1.74 \times 1.74 - 2.9 \times 2.9 \mu\text{m}$, medium: $2.9 \times 2.9 - 6.38 \times 6.38 \mu\text{m}$, large: $6.38 \times 6.38 \mu\text{m}$)

It is clear that all the lines for all the samples taken follows roughly the same trend. There is not a significant difference in the distribution of the various grain sizes for the different placements on the core. The grain size most frequently found was *medium*, and there were no *tiny* grains found. The other sizes lie in between.

4.3.3. Experiments with organic additive and axial stress of 30 MPa

HPA7

The locations for the sampling for the core (figure 4.3.13) and the distributions in a graph (figure 4.3.14) are presented here.

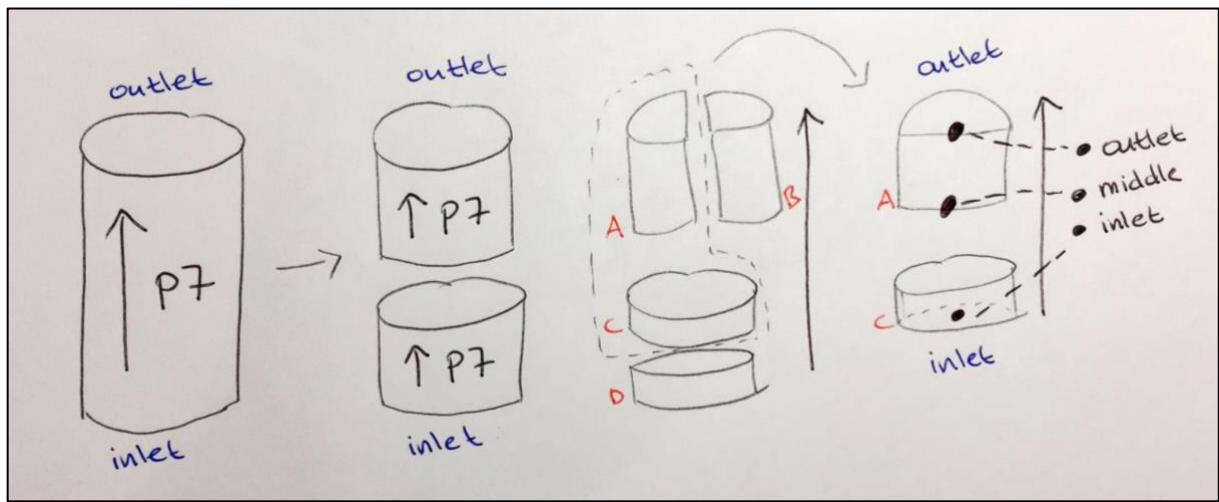


Figure 4.3. 13: The locations of where samples were collected from the core in HPA7.

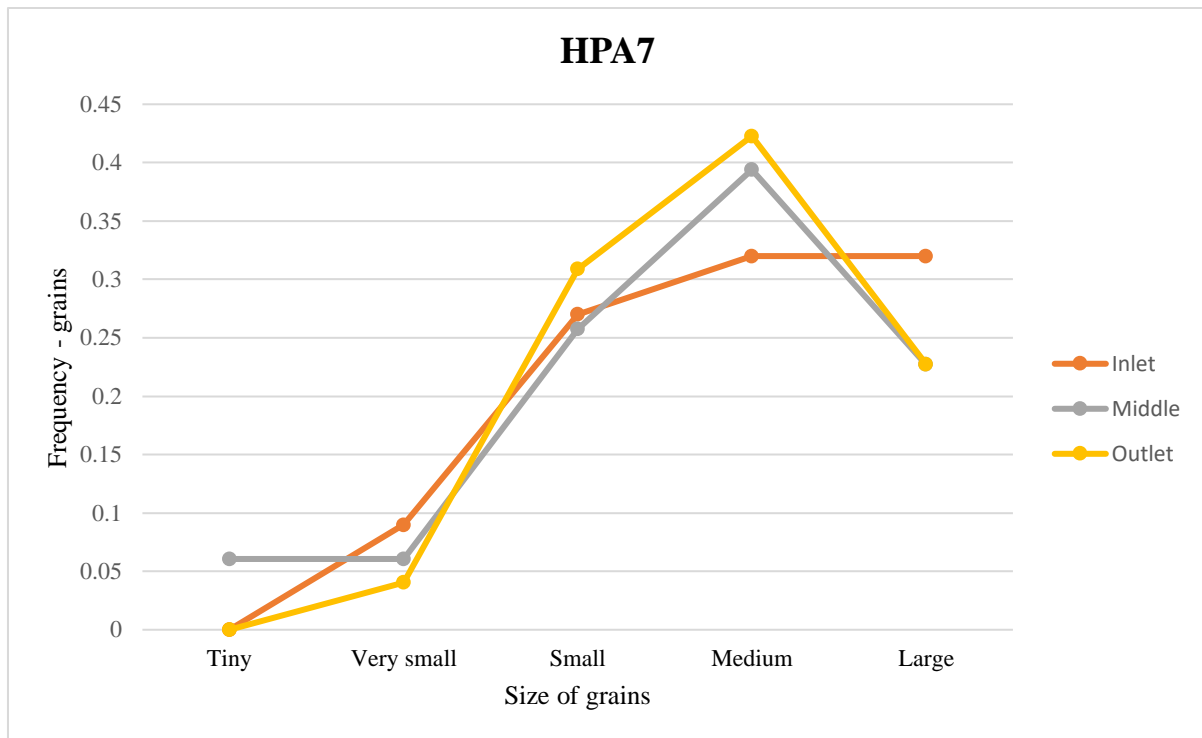


Figure 4.3. 14: The frequency of the grains as a function of different grain sizes for HPA7. (tiny: $0.87 \times 0.87 \mu\text{m}$, very small: $0.87 \times 0.87 - 1.74 \times 1.74 \mu\text{m}$, small: $1.74 \times 1.74 - 2.9 \times 2.9 \mu\text{m}$, medium: $2.9 \times 2.9 - 6.38 \times 6.38 \mu\text{m}$, large: $6.38 \times 6.38 \mu\text{m}$)

For middle and outlet, the lines follow each other with a small difference for the *tiny* grain size and the *small* grain size. There are not found any *tiny* grains for outlet, while there are some observed in the middle of the core. For the *small* grain size, there are more grains present in outlet compared to middle. For inlet, there are no *tiny* grains found. There are less *medium* grains and more *large* grains present compared to the other two locations. This is the only core flooded with organic acid where pictures were taken.

5. Discussion

5.1. Uniaxial strain loading

All the artificial cores were made from the same batch of powder to have the same basis for comparison. They were all flooded with either a brine containing organic additive or without. The porosity reductions can be found in table 5.1. The difference in porosity before and after the tests are significant, which was expected due to the fact that the cores were made out of powder and loaded up to an overburden stress of 30 MPa before they were left to creep. Prior to the start-up of the tests, the powder was compressed manually. This is in contrary to the stress applied in the Triaxial cell, making the powder in the cores a lot more compressed after the tests. The exceptions are for LP5 and LP9 where the porosity changes are minor compared to the others. This was expected beforehand since they were exposed low stress. It was also expected beforehand that LP5 and LP9 would have a significantly smaller reduction in lengths compared to the high pressure tests.

Table 5. 1: Overview of different values for all tests performed

	Brine [Without or without acid]	Axial stress of 30 MPa	Length before test [mm]	Reduction in length [mm]	Porosity before tests [%]	Porosity reduction [%]	Total axial strain after uniaxial strain loading [%]
HP1	Without	Yes	68.6	19.6	49.5	22.1	14.3
HP2	Without	Yes	58.0	14.4	45.5	19.7	12.7
HP3	Without	Yes	57.2	-	47.8	-	14.4
HP4	Without	Yes	58.9	19.0	48.3	25.4	13.7
LP5	Without	No	58.1	2.1	48.2	3.6	-
HPA6	With	Yes	58.6	15.6	48.3	21.8	12.8
HPA7	With	Yes	59.8	11.9	48.7	16.9	15.5
LP9	Without	No	58.2	2.2	48.3	8.0	-

The porosity reduction column is the calculated porosity value before starting each test minus the calculated porosity value after each test had finished. The same goes for the reductions in lengths. These values can be found in tables 4.1.1, 4.1.3, 4.1.8 and 4.1.10.

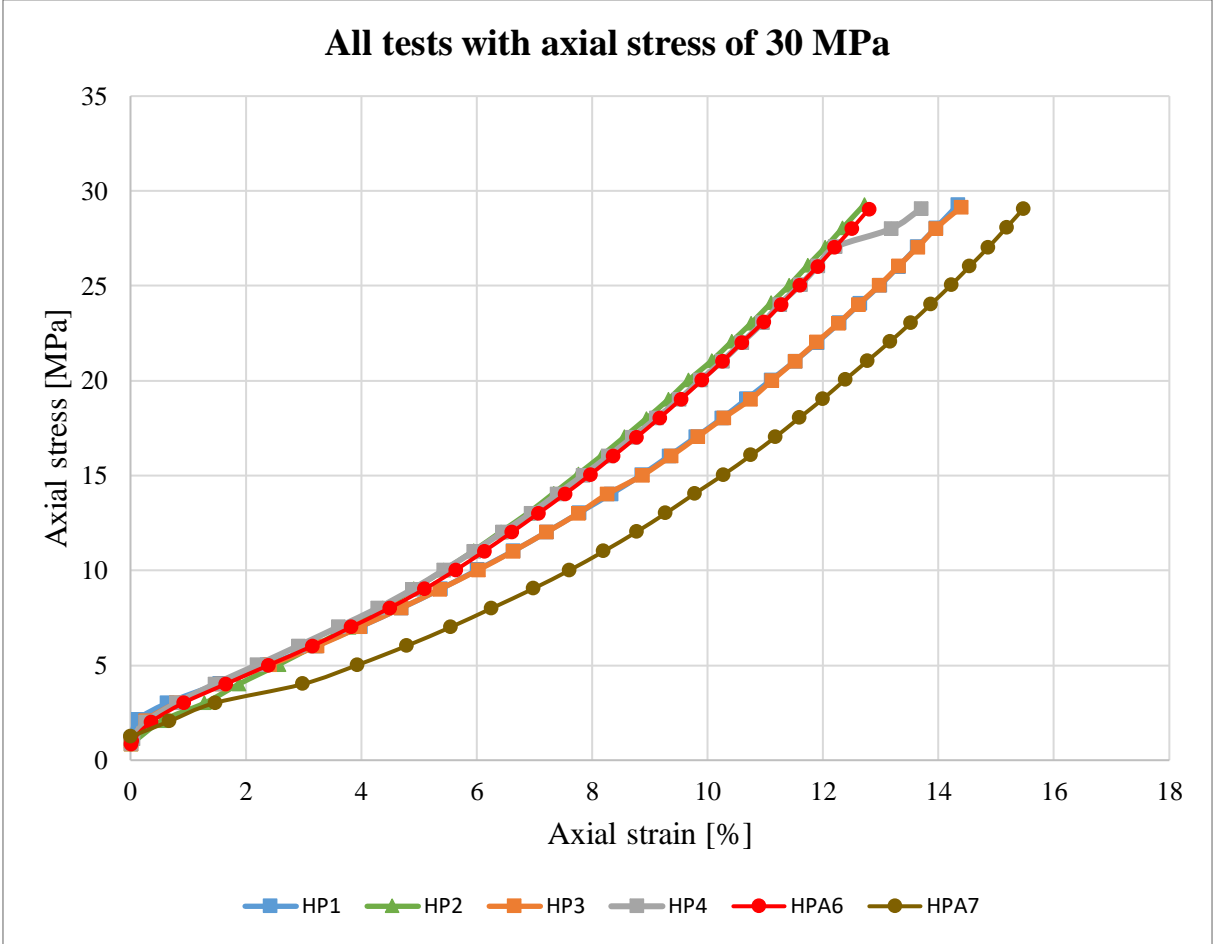


Figure 5.1. 1: An overview of all the tests plotted for axial stress [MPa] as a function of axial strain [%].

As seen in figure 5.1.1, all tests have a somewhat similar behavior when it comes to the axial strain under the same amount of stress applied. The total axial strain reached was about the same for HP2 and HPA6 with values of 12.7% and 12.8%. It was also similar for HP1, and HP3, having the values of 14.3% and 14.4%. HP4 reached a value in between, 13,7%. HPA7 is the test that reached the highest axial strain with a value of 15.5%.

They all show the strain hardening region, and the yield points are not visible for any of the tests. All the lines get steeper toward the end and this indicates that all the cores became stiffer compared to how they were at the test start-ups.

As seen, the total axial strains lie between 12.7-15.5%. Even though they are all very similar, the small differences could be explained by how the powder and the grains were compacted beforehand when making the artificial cores and the movements between them when the uniaxial strain loading phase started and evolved. The difference in brine content did not influence the stress-strain curves, both HPA6 and HPA7 have similar behavior to the other tests. There were no clear differences in the chemical analysis for all the tests in this phase, supporting the similar behavior.

5.2. Creep phase

High pressure tests without organic additive

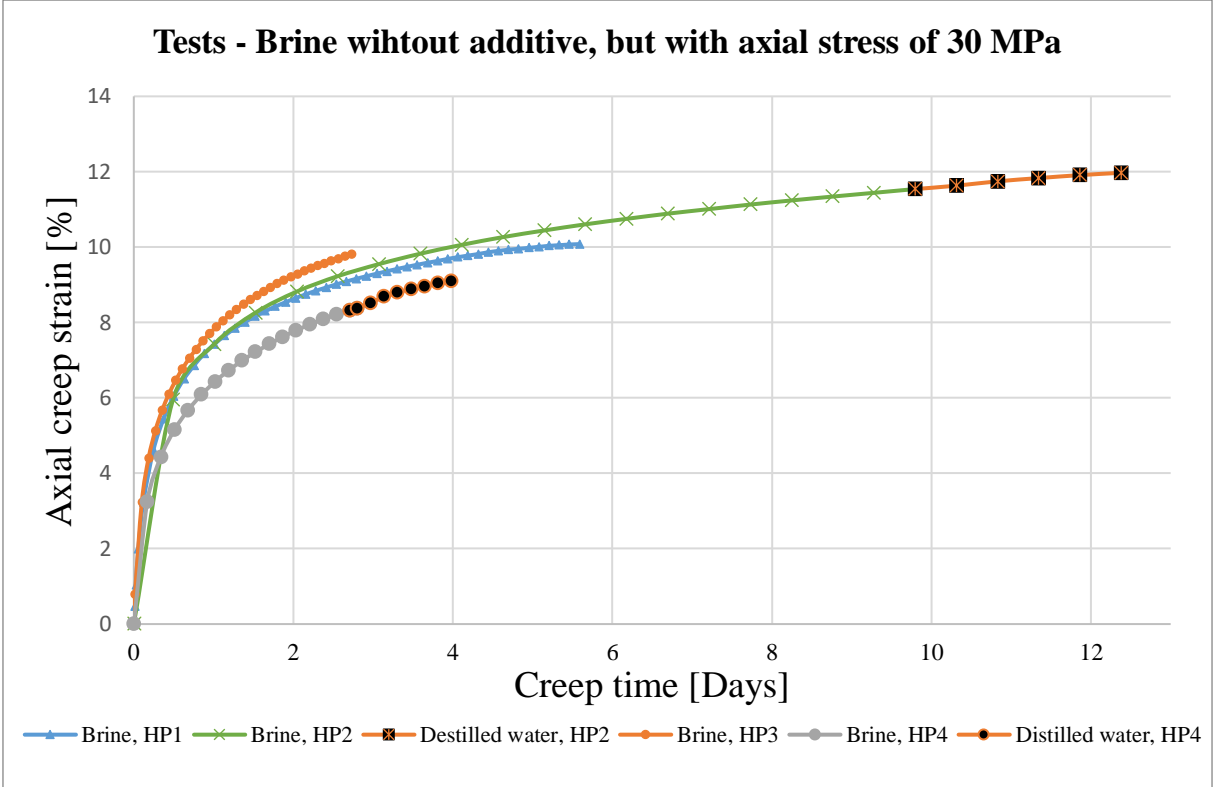


Figure 5.2. 1: Axial creep strain [%] as a function of creep time [Days] for all the high-pressure tests without organic additive. The black dots indicate DW.

Figure 5.2.1 shows the creep curve for HP1, HP2, HP3 and HP4. The creep curves only show small difference in the trends. They all have similar behavior prior to the transient phase. They follow approximately the same rate of deformation and creep. Looking at the creep durations, HP2 were left to creep a lot longer compared to the other three. The creep time for HP1, HP2,

HP3 and HP4 were 5.6 days, 12.4 days, 2.7 days and 4.0 days, respectively. So, the difference is significant. HP2 had the highest total axial creep strain of 12.0%. Had the other tests lasted longer than they did, some of them would might reach a strain value closer to HP2 or even higher than HP2. It looks as though HP3 could have reached a higher value than HP2, if graph was extrapolated. The axial creep strain values for HP1, HP3 and HP4 were 10.0%, 9.8% and 9.0%, respectively. HP1 had the most creep strain out of these three because the test lasted longer than HP3 and HP4. If we compare at the same time (about 3 days), HP3 had the most strain.

Comparing this to the grain size distributions for HP1, HP2 and HP4 (figures 5.4.2-5.4.4), they have some similarities. Throughout the cores, it has been found all grain sizes for all locations, except for *tiny* at inlet for HP2, but the cores are quite even. There were some differences in the amount of each grain size at different locations, but all could be found throughout the cores. This is compatible with the fact that these three creep curves show similar behavior. And as mentioned under 4.3. *Chemical analysis*, the different graphs showed that there were no ion concentration changes throughout the tests compared to the original for Na⁺ and Cl⁻. There were no chemical reactions, again supporting the similar behavior. For Ca²⁺, the concentrations were lower than the original, for all tests.

HP1 was the longest core made and the creep curve for the test is placed in between the other tests in figure 5.2.1. So, the difference in lengths had no effect. It is a good sign that all the tests are giving equal results in uniaxial loading phase and creep phase. It shows that we have reproducible tests, and that we have reliable results.

Only HP2 and HP4 were flooded with DW toward the end of the creep phase, and as can be seen from figure 5.2.1, the creep strain was not influenced by the change in flooding fluid. For HP1, the core was not flooded with water before after the temperature was turned off and HP3 failed.

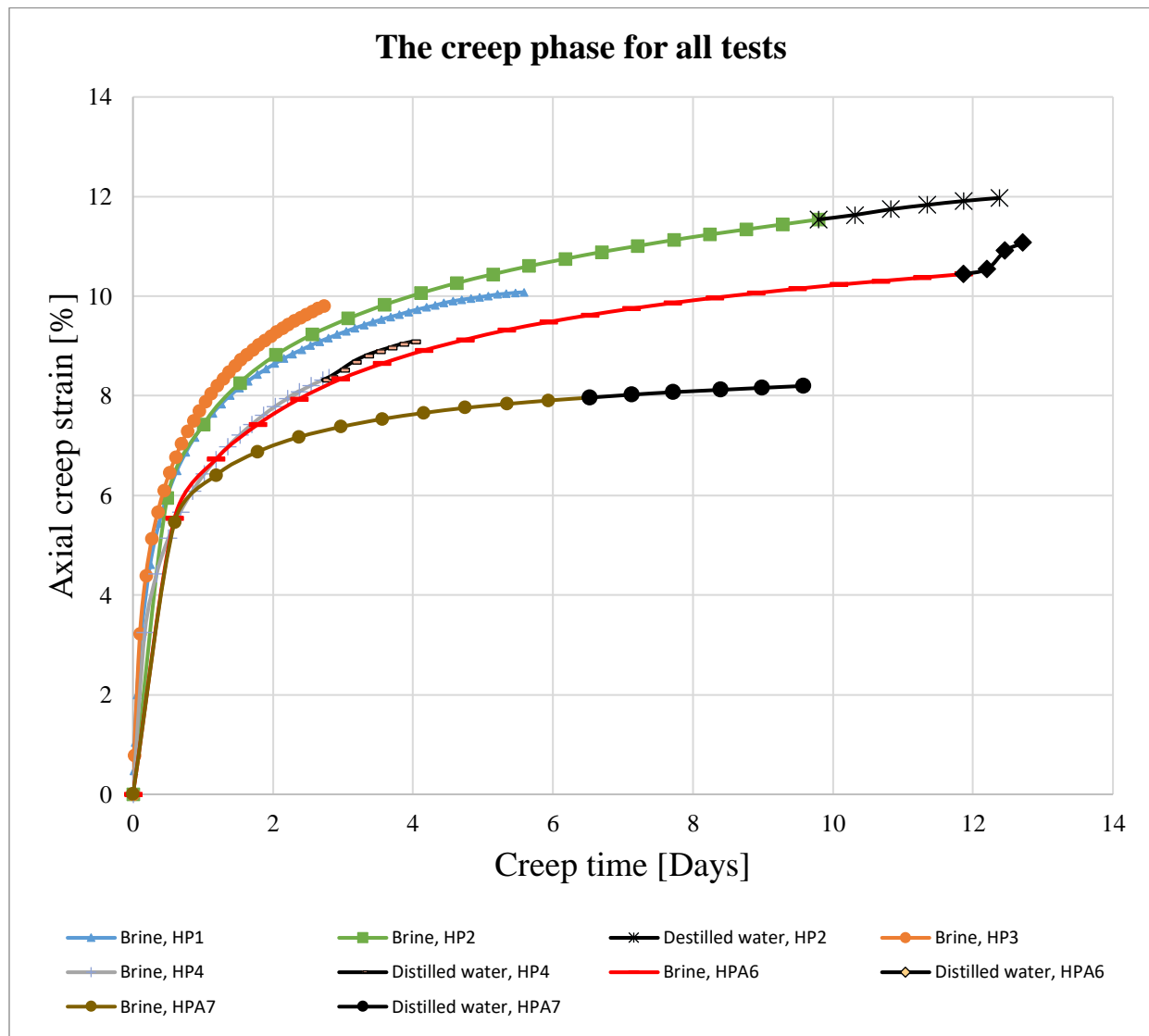


Figure 5.2. 2: Axial creep strain [%] as a function of creep time [Days] for all the high-pressure tests. The black color indicated flooding with DW.

In figure 5.2.2 the creep curve of all the tests are shown. Prior to the transient phase, the cores showed similar behavior. As the axial creep strain for all the cores started to reduce with time and the transient phase began, some differences occurred. The test that first started to decrease with time was PHA7, and this along with HPA6 (oil leakage) had the lowest creep on the graph, which was the two tests with organic additive. This could imply that the oxalic acid had an influence on the creep for the cores, making the cores stronger compared to the others. HPA6 (o.l.) had a higher deformation than HPA7 and reached a higher total axial creep strain. The total axial creep strains were 11.0% and 8.2%, respectively. Also, when HPA6 (o.l.) started

being flooded with DW, the line accelerated, and looking like the beginning of the tertiary creep phase. Here, the deformation increases with time. The reason for HPA6 (o.l.) having a higher axial creep strain could have something to do with the oil leakage along with the grain size distribution making it less strong compared to HPA7. With the absence of oil, the creep behavior would be expected to be closer to the creep behavior of HPA7.

Comparing the total axial creep strain of HPA7 to not only HPA6 (o.l.) but the others as well, HPA7 reached the lowest axial creep strain. HP1, HP2, HP3 and HP4 were 10.0%, 12.0%, 9.8% and 9.0%, respectively. So, HPA7 with 8.2% is clearly lowest while HPA6 lies in between these values. Looking at the graph after three days, HPA6 has the second lowest value and if the durations for HP1, HP3 and HP4 were longer, it could have ended up being the second lowest value towards the end of all testing. The graph gives an indication of that, again seeing that the creep is influenced by oxalic acid and making those cores the strongest, even with the presence of some oil. As written in the introduction, the presence of organic molecules makes the characteristics and condition differ compared to if they were not present. It will often make the material stronger with a more resilient structures and textures, and it is very interesting that this has been observed here.

Since the grain size distributions for HPA7 and LP5 were very similar, especially for middle and outlet (see figure 5.4.3 and 5.4.4.), it could imply that the oxalic acid does influence the grains, keeping them more intact and even throughout the cores as they were in low-pressure tests. While oil could then have an opposite impact on the grains and hence the creep deformation. It is quite possible that HPA6 had more of the *tiny* and *very small* grains in its distribution. Unfortunately, since it was not possible to look at the grain distribution for HPA6 it is difficult to have an indication of the different grain distributions in the core. Had the distribution been approximately the same, it would mean that when there is an oil leakage along with oxalic acid, it will make the creep rate reduce less compared to if the oil was not present. Unfortunately, there is only one successful test with oxalic acid that did not experience oil leakage.

Taking into account the grain size distributions for HP1, HP2 and HP4 and comparing them to HPA7, this adds up. All these tests had their creep lines reduce at a higher rate than PHA7 and reached a higher total axial strain. All of them had more of the *tiny* grains in the cores compared to HPA7. For *very small*, the distribution was more even. The same goes for *small*, *medium* and

large grain sizes (this is shown further down in 5.4 – *SEM Scanning electron microscope*). This, again indicates that there most likely were some *tiny* and *very small* grain sizes present in HPA6 along with the oil.

In all the creep graphs presented in the subchapter 4.1 – *Uniaxial strain tests*, the permeability seemed to be the higher for HP1 compared to the rest of the tests. The reasons may be differences in grain sizes, clogged filters or that the flooding fluid for some of the tests flowed along the wall of the shrinking sleeve. What is important is that one gets control of the permeability, because then equation 2.10 can be used and one can get information about pore sizes that can be compared to SEM results, and useful information about the inside of the cores can be achieved.

Low-pressure tests

Figure 5.2.3 and 5.2.4 show the two low-pressure tests. The first graph is the axial creep strain [%] as a function of creep time [days] and the second is the radial creep strain [%] as a function of creep time [days]. LP5 had a higher total axial creep strain compared to LP9 (o.l.). It was approximately 0.56%. The core was flooded with DW towards the end, but that has not influenced the creep. The creep for LP9 (o.l.) was almost none existent. The total axial creep strain was 0.004% and also here, the change of flooding fluid to DW did not influence the creep. It was not expected that either of these two tests would have a high axial creep strain since they were exposed to low stress. But it was expected that LP9 (o.l.) would have a higher creep than it got. The oil leakage has most likely influenced the creep. All the water samples collected from LP9 (o.l.) throughout the test duration had a thick layer of oil on top of the sample. This gave an indication that the amount of oil in this core was higher compared to HPA6, which had less oil in the water samples.

Looking at the second graph (figure 5.2.4) and the radial creep strain for LP9, there is no creep. This shows consistency between the axial- and radial creep strain, again suggesting that the oil had a big impact. For LP5, there was some radial creep strain showing consistency with the axial creep strain.

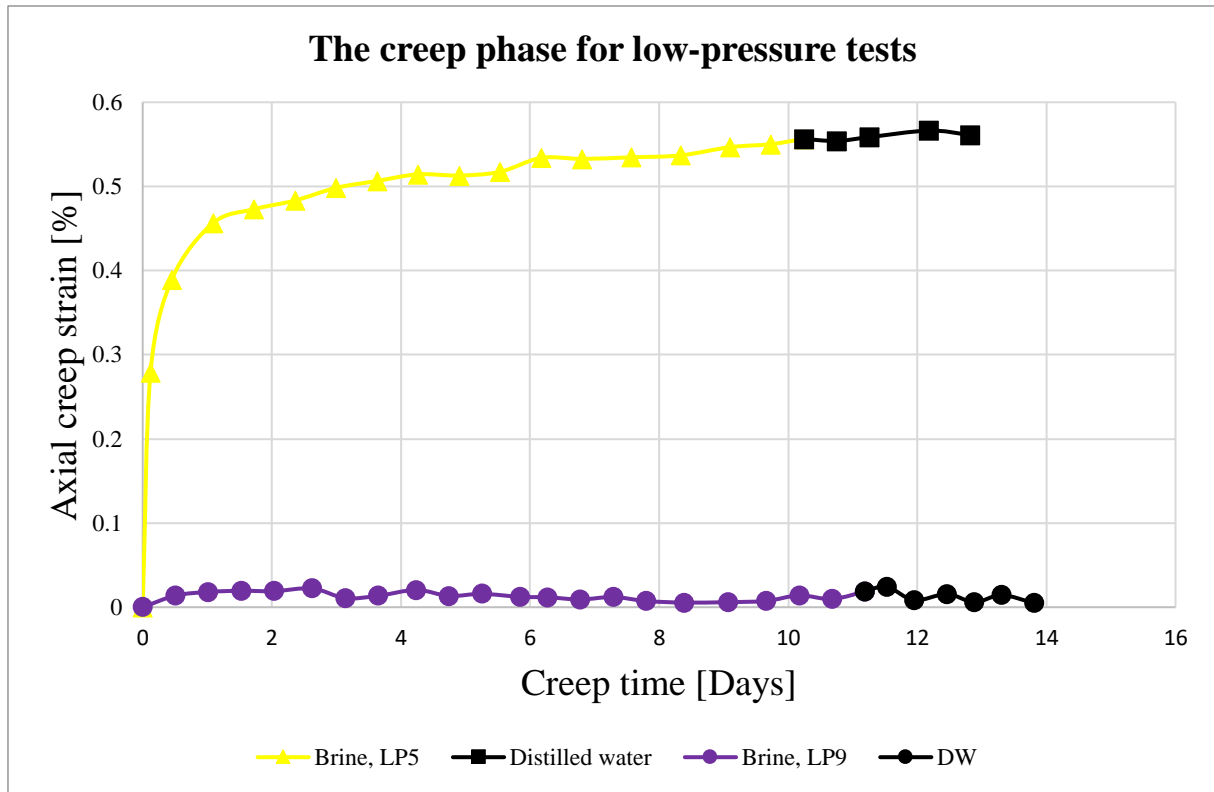


Figure 5.2. 3: Axial creep strain [%] as a function of creep time [Days] for low-pressure tests

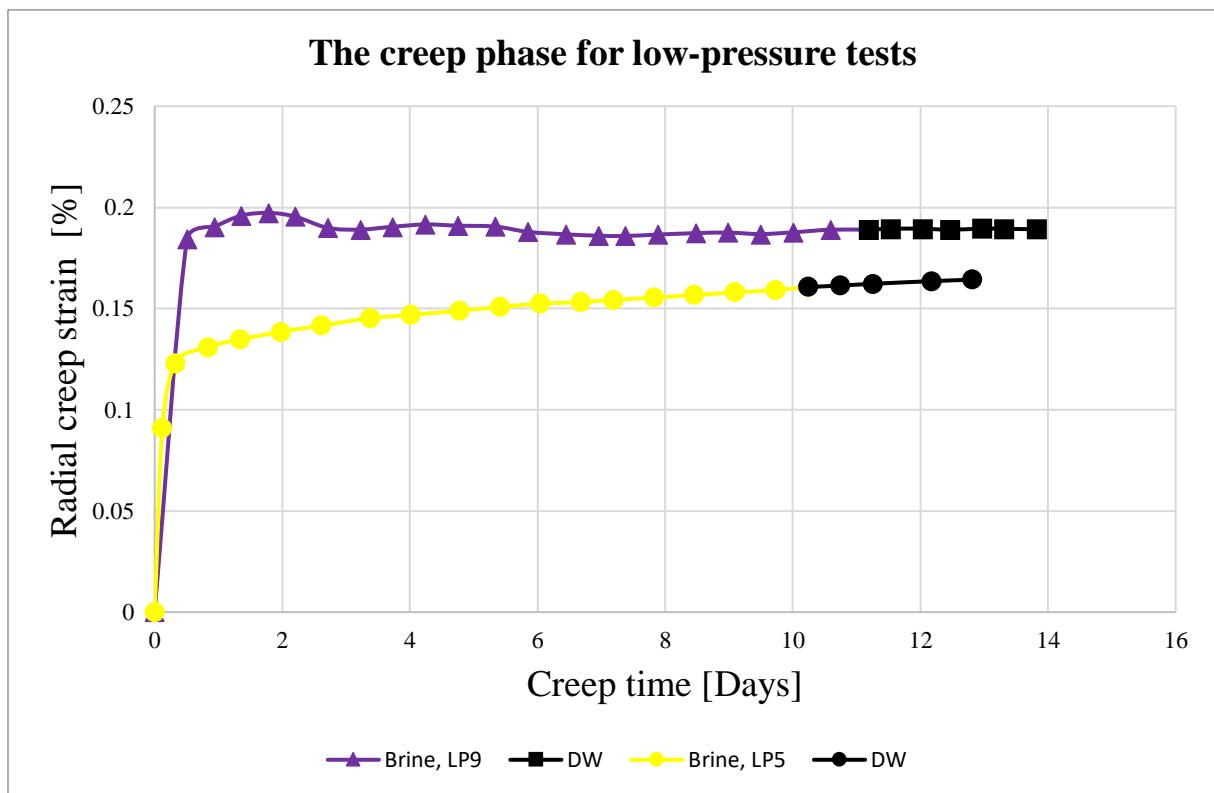


Figure 5.2. 4: Radial creep strain [%] as a function of creep time [Days] for low-pressure tests

5.3. Chemical analysis

As came clear looking all the ion concentrations for all the tests performed, there were not much difference between them. The amounts on Na^+ and Cl^- did not change during the tests, neither with or without organic additive. In other words, there were no chemical reactions happening for either concentrations. A few samples here and there had a value that stood out from the rest, most likely due to evaporation or other experimental errors. For Ca^{2+} , the concentration stayed below the original for all tests performed. There has been Ca^{2+} losses throughout the test durations, and from the table 4.2.1, the loss seems to be bigger for the tests containing oxalic acid.

5.4. SEM - Scanning Electron Microscope

Having done eight uniaxial strain tests with some minor performance differences as described, next step was SEM analysis. Prior to counting the grains, various scales had to be decided, as seen in subchapter 4.3. *Calcite microstructure morphology – SEM*. This provided the basis for counting the grains and the grains were counted with the naked eye for all the cores. No data program or other technologies were used. The reason was that one wanted the counting process to be as equal and even as possible for all the images and believing that this would be achieved in the best possible way by not using a data program. What was challenging, was that the grains came in not only different sizes, but also all sorts of different shapes. In addition, a few areas on some of the images were quite dark. It is possible that in one of these dark areas, a data program would struggle a lot more in seeing the different sizes and telling grains apart, compared to a human using its eyesight.

Choosing images being in the scale of 10 μm when counting the grains, seemed to be the best choice in terms of having a good overview of the sample, clearly seeing the different sizes of the grains and being able to tell them apart. The images represented the entire sample in a good way, despite that the images were only a small part of the entire sample and placement of the core. Had 2 μm or 5 μm been chosen, it would have been too close to the grains and the overall overview of the core sample would not be represented in a good way. Also, choosing 20 μm or 100 μm would not be ideal. This would result in the grains being too small and seen from too

far of a distance, making it difficult telling the different sizes and grains apart. All the grains could easily end up in only one or two scales.

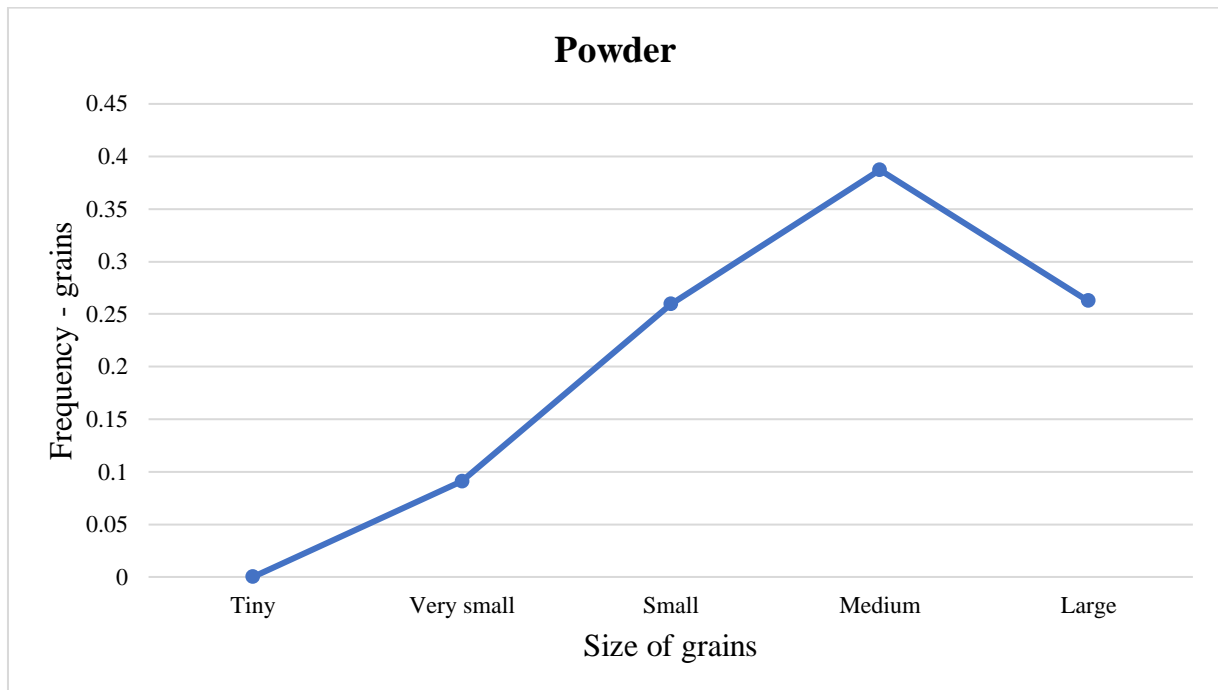


Figure 5.4. 1: the distribution for the unflooded powder. (tiny: $0.87 \times 0.87 \mu\text{m}$, very small: $0.87 \times 0.87 - 1.74 \times 1.74 \mu\text{m}$, small: $1.74 \times 1.74 - 2.9 \times 2.9 \mu\text{m}$, medium: $2.9 \times 2.9 - 6.38 \times 6.38 \mu\text{m}$, large: $6.38 \times 6.38 \mu\text{m}$)

Figure 5.4.1. is showing the distribution of the unflooded powder. There are no *tiny* grains present, but some *very small* grains are found. The amounts of *small* and *large* grains are approximately the same, while the *medium* grain size is most frequently found. Looking at LP5 from figure 4.3.12, the results ended up having a similar distribution as the unflooded powder and this was expected due to the low stress the test was exposed to. The grain size distributions only have minor differences throughout the core, the core was equal. It would have been interesting to investigate LP9 in SEM, to see if the distribution would follow approximately the same trend as LP5. There were no tiny grains in LP5, so this is likely a result of the core not being exposed to the same high axial stress.

The following three graphs presented in figure 5.4.2-5.4.4 show the different distributions of all the grain sizes for all the cores for inlet, middle and outlet. It was desirable to see if there were any visible differences in the cores flooded with and without organic additive, and differences in creep durations.

Inlet

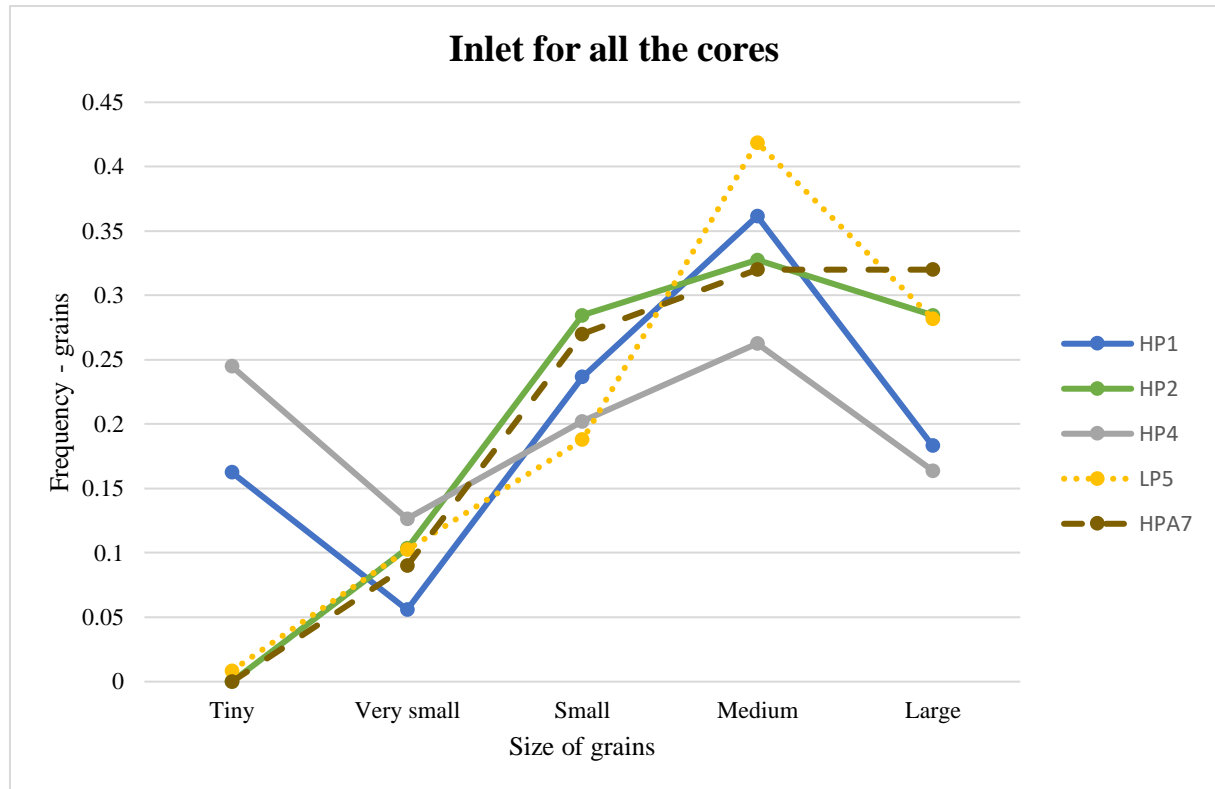


Figure 5.4. 2: Overview of the grain distributions for all the cores from the inlet samples. (tiny: $0.87 \times 0.87 \mu\text{m}$, very small: $0.87 \times 0.87 - 1.74 \times 1.74 \mu\text{m}$, small: $1.74 \times 1.74 - 2.9 \times 2.9 \mu\text{m}$, medium: $2.9 \times 2.9 - 6.38 \times 6.38 \mu\text{m}$, large: $6.38 \times 6.38 \mu\text{m}$)

Comparing only HP1 and HP4, since they had the most similar creep durations with 5.6 and 4 days, we see that HP1 and HP4 have all the different grain sizes present at inlet. There is a difference in *tiny* and *very small* grains, there are more of those sizes for HP4 compared to HP1, suggesting that the grains got more crushed at inlet for HP4. It is the opposite for the *small*, *medium* and *large* grain sizes, there are more for HP1 compared to HP4. Again, this indicates that HP4 got more crushed grains, hence having a smaller amount of the *small*, *medium* and *large* grains sizes compared to HP1. Even though HP4 seemed to experience the grains being more crushed, HP1 also experienced the grains being crushed, but in a smaller scale.

Then, doing the same comparison for HP2 and HPA7 which had creep duration of 12.4 and 9.5 days. Looking at the figure 5.4.1, the lines for the two cores follow each other closely for every grain size and neither had tiny grains present. This indicates that the two cores experienced the same changes for their grains. With the absence of *tiny* grains, the cores did not get as crushed at inlet, as HP1 and HP4 did. The fact that HP2 and HPA7 have more large grains compared to the other two, also gives this indication.

Middle

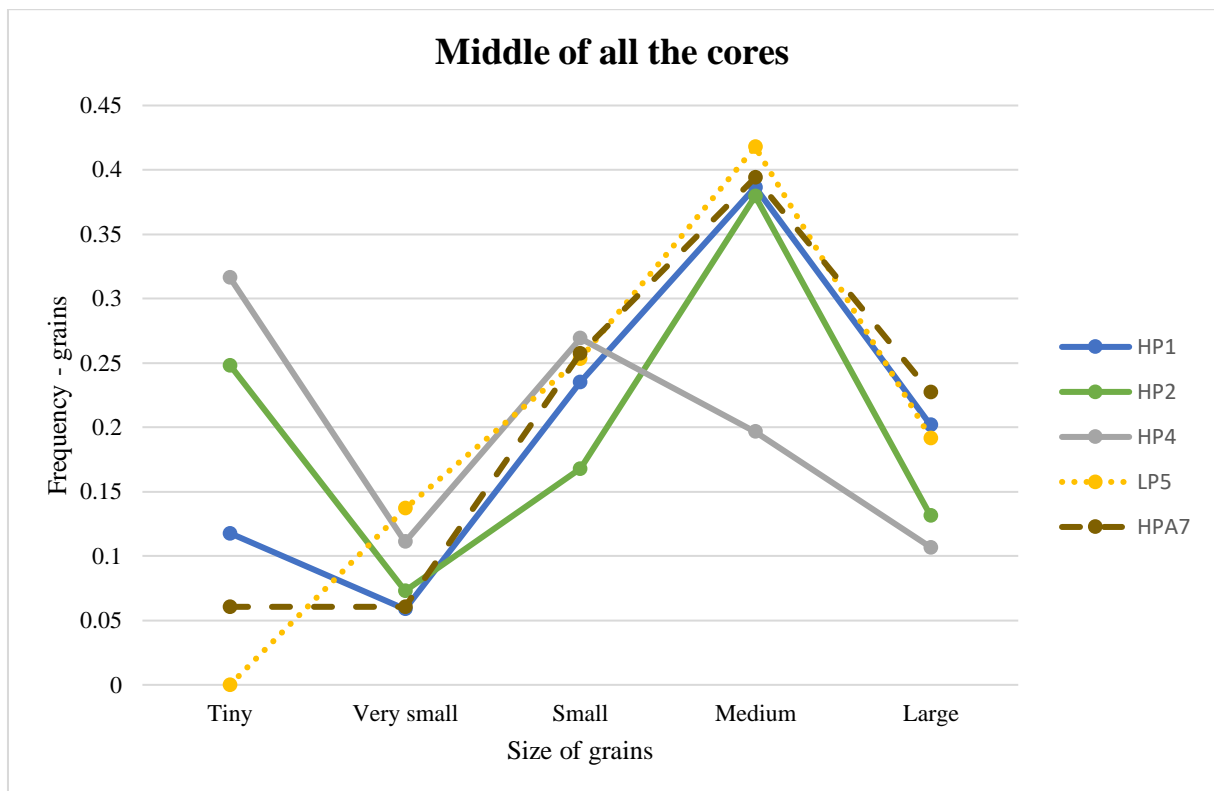


Figure 5.4. 3: Overview of the grain distributions for all the cores from the middle samples. (tiny: $0.87 \times 0.87 \mu\text{m}$, very small: $0.87 \times 0.87 - 1.74 \times 1.74 \mu\text{m}$, small: $1.74 \times 1.74 - 2.9 \times 2.9 \mu\text{m}$, medium: $2.9 \times 2.9 - 6.38 \times 6.38 \mu\text{m}$, large: $6.38 \times 6.38 \mu\text{m}$)

It is the same trend for the middle locations for HP1 and HP4 as seen for inlet. The grains for HP4 got more crushed compared to HP1 and therefore has a lot more of the *tiny* grains present. Also, there are more of the *very small* and *small* grain sizes for HP4. For the *medium* and *large* grains, there are more of those sizes present for HP1 compared to HP4. Since the differences in *tiny* grains and *large* grains between the two cores are bigger here, compared to at the inlet locations, it suggests that the grains were more crushed for HP4 at middle compared to inlet.

For HP2 and HPA7, there are some differences when moving into the two cores to the middle location. Here, there are a lot more of the *tiny* grains for HP2. For *very small*, it is even and the same goes for *medium*. For *small* and *large*, there are more grains of these sizes for HPA7, suggesting that the grains for HP2 got a lot more crushed at the middle location. For PHA7, it has not changed much from inlet, just a little more crushed, since there are some *tiny* grains present and a little less large grains (figure 5.4.3).

Outlet

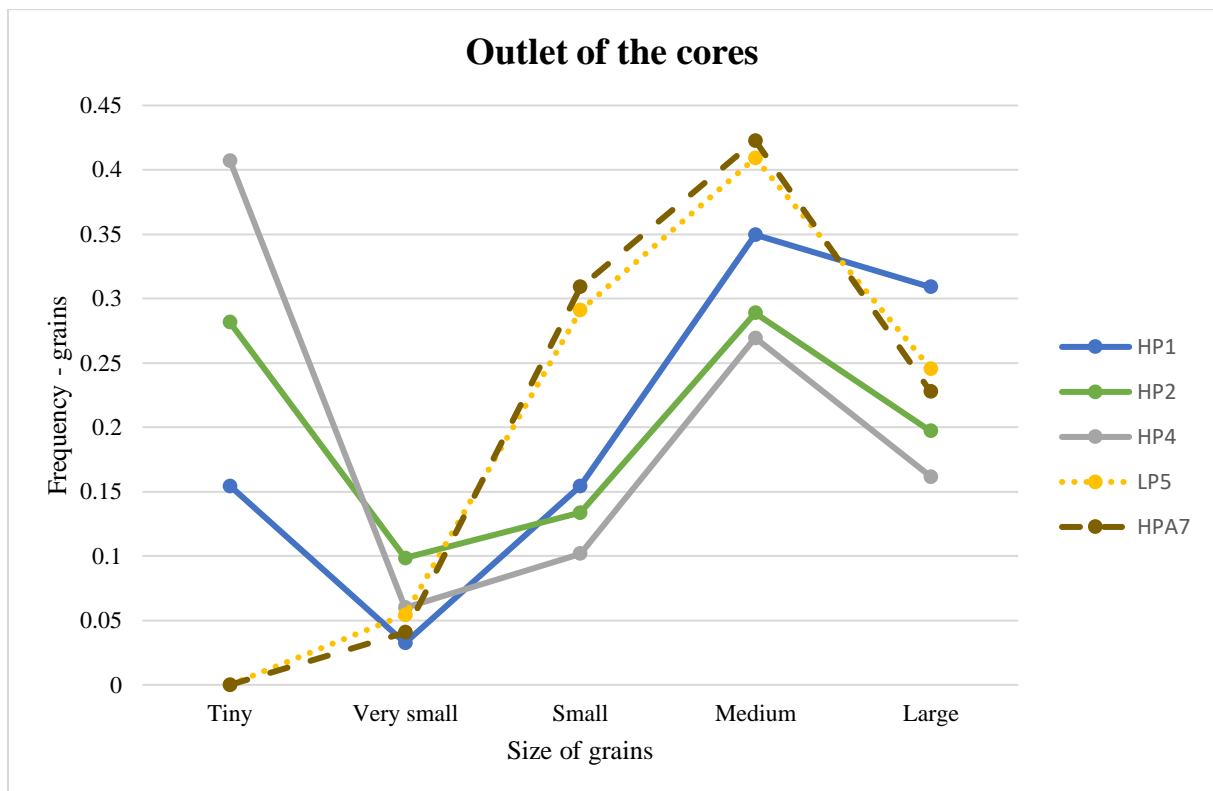


Figure 5.4. 4: Overview of the grain distributions for all the cores from the outlet samples. (tiny: $0.87 \times 0.87 \mu\text{m}$, very small: $0.87 \times 0.87 - 1.74 \times 1.74 \mu\text{m}$, small: $1.74 \times 1.74 - 2.9 \times 2.9 \mu\text{m}$, medium: $2.9 \times 2.9 - 6.38 \times 6.38 \mu\text{m}$, large: $6.38 \times 6.38 \mu\text{m}$)

Again, there are a lot more of the *tiny* grains for HP4 compared to HP1 and the opposite for *medium* and *large* grains (figure 5.4.4). It is more even for *very small* and *small*. In other words, throughout the two cores, the grains were more crushed for the core in HP4, resulting in having more *tiny* and *small* grains for the entire core compared to HP1. HP1 had more of the *medium* and *large* grains size, supporting this, but HP1 also experienced grains being crushed through the core but to a smaller extent.

For the outlet, it is quite similar as for the middle location for HP2 and HPA7. No *tiny* grains were found for HP7, while there is a frequency of 0,28 of *tiny* grains for HP2. For *very small* grains, there are more of them found at HP2. For *small*, *medium* and *large*, they are more frequently found for HPA7. This again supports the distributions at the middle locations. HP2 had its grains being more crushed compared to HPA7, hence having *tiny* grains and more of the *very small* grains in addition to having less of the larger grains throughout its core.

Looking at all four tests together, HPA7 was the only test that barely had any of the *tiny* grains present for any of the locations. It only had a frequency of 0,06 for the middle location and they were none existent for inlet and outlet. This could be due to the presence of oxalic acid. Unfortunately, since it was not possible to investigate HPA6 in SEM, there is not a basis of comparison to check with. It would have been interesting to see if the grain distribution for the *tiny* grain size for the entire core and all the distributions for outlet on HPA6 would have had a similar trend as HPA7.

In addition, HPA7 does stand out for the outlet location compared to the other high-pressure tests for some of the other grains sizes. The amount of *small* and *medium* at outlet are significantly higher. If this is a coincidence, or if it has something to do with the oxalic acid, as it most likely has to do with the *tiny* grains, is difficult to tell but it does give that indication. HPA7 seemed to be having the most stable distributions out of the cores and it is similar to LP5, indicating that the presence of oxalic acid made the grains not change much during the test.

No clear conclusion can be made from the SEM investigation, other than the fact that LP5 ended up being as expected and that the oxalic acid most likely has prevented HPA7 from having grains crushed to the smallest size, *tiny*.

One can question if the results would be more accurate and more reliable if instead of only counting the grains with eyesight, it was also used a data program. Since it was not used a data program, it would in that case be ideal to have another person or more counting the grains on the exact same images with the same sizes decided beforehand to see if the results were approximately the same. As described under 4.2.1. *Experiment without organic additive, but with axial stress of 30 MPa*, some cores had two images counted on for the same location in the same sample. The reason was that the grain distribution, and especially for the smallest grain size – *tiny*, was uneven for the two photos and the average grain sizes for the two photos had to be used. This will of course influence the results, making them more uncertain. Had pictures been taken at another location on each small sample in SEM, the results could have been different.

5.5. Sources of error

When performing numerous tests, it is inevitable to not have some differences between them all. From the lengths of the cores made and the amount of powder used, to small differences in brine contents and dilution errors in the ion analysis to mention some. Also, trouble with equipment could occur. A list of sources of errors that could and did occur, and that could have an impact on the results is presented:

- When measuring up the different ingredients when making the two brines, there will be small differences in the amounts. These differences are minor. Also, if some of the equipment used were not completely clean it could affect the results.
- When calculating the porosity, since the cores were made out of powder, the lengths and diameters measured both before the testing and after, could have some errors, making the porosity values to also have some errors.
- HP3, HP4 did not go according to plan. This is something that can happen when having an experimental thesis, and even though the experiments are planned it can sometimes be difficult to prevent things from happening.
- Oil leakages in cores. This happened in two tests, HPA6 and LP9.
- When diluting the effluent samples before putting them in the Dionex ICS 5000+ machine, there could be some dilution errors, air in the tubes, etc.
- When analyzing the IC measurements, some effluent samples could have experienced evaporation.
- Counting the grains in all the images taken of the different cores. Can be challenging to stay in between the different scales due to numerous shapes and forms of the grains.
- Differences in the grain distribution of photos taken at the same sample from the same location on the core. Some images presenting the same sample from the same location on a core show significant differences in the amount of *tiny* grains. This will of course influence the results in counting the grains.

6. Conclusion

The effects of flooding artificial cores made out of calcite powder with and without organic additive have been studied. All tests were loaded to an axial stress of 30 MPa, except for two, before they were left to creep. The two other tests were performed at a confining pressure of 1.2 MPa. During the execution of this thesis, I have learned the following:

- 1) Chemical and physical background for understanding fluid - rock interacting
- 2) How to perform rock and core mechanics laboratory testing
- 3) How to perform chemical laboratory measurement
- 4) How to analyze and interpret interdisciplinary experimental data
- 5) How to explicate coincidence between macroscopic and microscopic observations

The different conclusions made from the results presented in the thesis are:

Uniaxial strain loading:

- Not much of a difference in this phase, all the high-pressure tests independent of injection brine show similar behavior when looking at the axial stress against axial strain. This shows that the tests are reproducible and that the results are reliable. The oxalic acid did not have an impact in this phase.

Creep phase:

- Also, for the creep phase, the results are reproducible as the behavior in this phase for the high-pressure tests were similar, especially for the ones without organic additive in their flooding fluid. From the behavior of the two tests that were flooded with oxalic acid, they did have a similar behavior as the other tests, but it appeared that the oxalic acid made the cores a bit stronger. This could indicate that the presence of organic additive could make the material behave stronger. Adsorption of organic molecules might affect the friction between the grains.
- Unfortunately, one of the two tests with oxalic acid had an oil leakage in the core (HPA6). Still this test experienced a lower creep compared to the cores without oxalic acid, but more tests should be done to reach a firm conclusion regarding the effect of oxalic acid on the creep.

- High porosity reduction was observed, which was expected since the cores were made out of powder and not drilled from blocks. The porosity reductions were significantly higher for the high-pressure tests compared to the low-pressure tests.
- We were able to measure the permeability of the cores, and the permeability followed a time dependence that was consistent with the creep. However, there was some large variations between the cores, which should be understood. For future studies the permeability should be measured, then one could use e.g. equation 2.10 to tease out some information about pore sizes that can be compared to SEM results.

Chemical analysis:

- For the Na^+ and Cl^- ions, there were no or little chemical reactions happening for either tests. The concentrations out of the core was similar to the concentrations into the core. The presence of oxalic acid did not influence these concentrations.
- Loss of Ca^{2+} was observed in all tests, which might be due to precipitation. There are indications that the loss was greater in the presence of oxalic acid.

SEM:

- The purpose of this thesis was to get a deeper understanding of pressure solution and being able to verify pressure solution by SEM investigations. It was only possible to take SEM images in five out of eight cores. We were expecting to possibly observe dissolution in areas at high stress and precipitation in areas at low stress, but it was not possible to make any firm conclusions from the SEM images.
- For the low-pressure tests, the grain size distributions were as expected. Due to the exposure of only low stress throughout the test duration, the grain size distribution was the same for all locations of the core - inlet, middle and outlet, and it showed similarities to the unflooded powder. This is a very good result, because it also proves that the grain counting procedures can be trusted.
- The SEM images gave an indication that for the high-pressure tests, the presence of oxalic acid does prevent the grains from being crushed to the smallest size (tiny), making the cores stronger compared to HP1, HP2 and HP4. They had a significantly higher amount of tiny grains throughout their cores. This is in line with the observations in the creep phase, the presence of organic additive might make the cores stronger and more resilient in their structures.

6.1. Future recommendations

- Perform the same experiments (same powder, brines, temperature) but with a longer duration, it could be for months. Since creep is time dependent, it could then be possible to get clearer results from the testing with and without organic additive and also to be able to shed more light on pressure solution.
- Eventually, if the results got clearer with and without organic additive as flooding fluid, then the temperature could be adjusted to see how the values change. One could also eventually change other parameters like axial stress, material, brine content, etc.
- Permeability should be estimated for all the cores, the permeability measurements can be used as a tool to get information about changes in grain sizes (after the porosity change has been corrected for)

7. References

- Ben-Itzhak, L Laronne, J Erez, and E Aharonov. 2015. *Precipitation of CaCO₃ in pressure solution experiments: The importance of damage and stress*. Earth and Planetary Science Letters, 434 (2016) 30-41: <http://dx.doi.org/10.1016/j.epsl.2015.10.038>.
- Croize, Delphine, Francois Renard, Knut Bjørlykke, and Dag Kristian Dysthe. 2010. *Experimental calcite dissolution under stress: Evolution of grain contact microstructure during pressure solution creep*. J. Geophys. Res, 115, B09207: doi:10.1029/2010JB000869.
- Croizet, Delphine , Francois Renard, and Jean-Pierre Gratier. 2013. *Compaction and porosity reduction in carbonates: A review of observations, theory, and experiments*. HAL, 54, pp.181-238.: <10.1016/B978-0-12-380940-7.00003-2>. <insu-00799787>.
- Fjær, E, R. M. Holt, P. Horsrud, A.M. Raaen, and R. Risnes. 2008. *Petroleum related rock mechanics*. Elsevier.
- Hellmann, Roland, Patrick Gaviglio, Peter J.N. Renders, Jean-Pierre Gratier, Samir Békri, and Pierre Adler. 2002. "Experimental pressure solution compaction of chalk in aqueous solutions. Part 2. Deformation examined by SEM, porosimetry, synthetic permeability, and X-ray computerized tomography." The Geochemical Society, Special Publication No 7.
- Hellmann, Roland, Peter J.N. Renders, Jean-Pierre Gratier, and Robert Guiguet. 2002. "Experimental pressure solution compaction of chalk in aqueous solutions Part 1. Deformation behavior and chemistry." The Geochemical Society, Special publication No 7,2002.
- Jaeger, J.C., and N.G.W. Cook. 1976. *Fundamentals of rock mechanics*. Chapman and Hall.
- Kristiansen, Kai, Markus Valtiner, George W. Greene, James R. Boles, and N. Israelachvili. 2011. *Pressure solution - The importance of the electrochemical surface potentials*. Elsevier, Geochimica et Cosmochimica Acta, 27 (2011): doi: 10.1016/j.gca.2011.09.019.
- Stadtländer, C.T.K.-H. 2007. *Scanning Electron Microscopy and Transmission Electron Microscopy of Mollicutes: Challenges and opportunities*. Modern Research and Educational Topics in Microscopy.
- Tiab, Djebbar, and Erle D. Donaldson. 2004. *Petrophysics - Theory and practice of measuring reservoir rock and fluid transport properties*. Gulf Professional Publishing.

- Ursin, Jann-Rune, and Anatoly B. Zolotukhin. 2000. *Introduction to petroleum reservoir engineering*. Høyskoleforlaget.
- van den Eide, M.P.A, G Marketos, A.R Niemeijer, and C.J. Spiers. 2017. *Investigating Compaction by Intergranular Pressure Solution Using the Discrete Element Method*. Journal of Geophysical Research: Solid Earth, 123, 107–124.:
<https://doi.org/10.1002/2017JB014440>.
- Zhang, X., C.J. Spiers, and J. Peach. 2011. *Effects of pore fluid flow and chemistry on compaction creep of calcite by pressure solution at 150 C*. Geofluid, 11, 108-122: doi: 10.1111/j.1468-8123.2010.00323.x.
- Zhang, Xiangmin, Christopher J Spiers, and Colin J Peach. 2010. *Compaction creep of wet granular calcite by pressure solution at 28C to 150C*. Journal of Geophysical Research, VOL. 115, B09217: doi: 10.1029/2008JB005853.

Appendix

First, there are two pictures showing the cores for HP1 and HPA6. As mentioned in the thesis, HPA6 experienced oil leakage in the core and for that reason it turned out brown after the test was finished. The same happened for LP9. This was in contrary to the other cores that were white.

Further, there are images of the cores from HP1, HP2, HP4, LP5 and HPA7. It was on these images the grains were counted.

HP1

- Inlet, Inlet, Middle, Outlet, Powder – calcite

HP2

- Inlet, Middle, Outlet, Rim

HP4

- Inlet, Inlet, Middle, Outlet, Rim

LP5

- Inlet, Middle, Outlet, Rim

HPA7

- Inlet, Inlet, Middle, Outlet

Core from HP1 and core from HP6

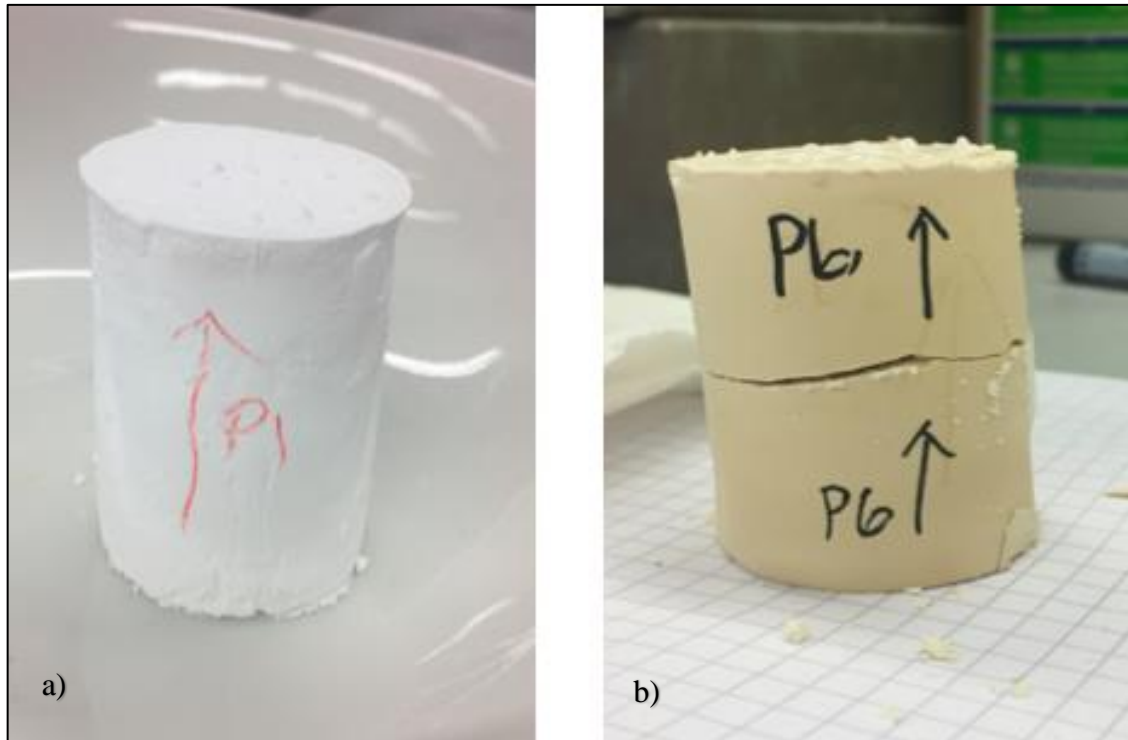


Figure A. 1: The HP1 core was clearly white (a), while P6 was brown in color (b).

SEM – images

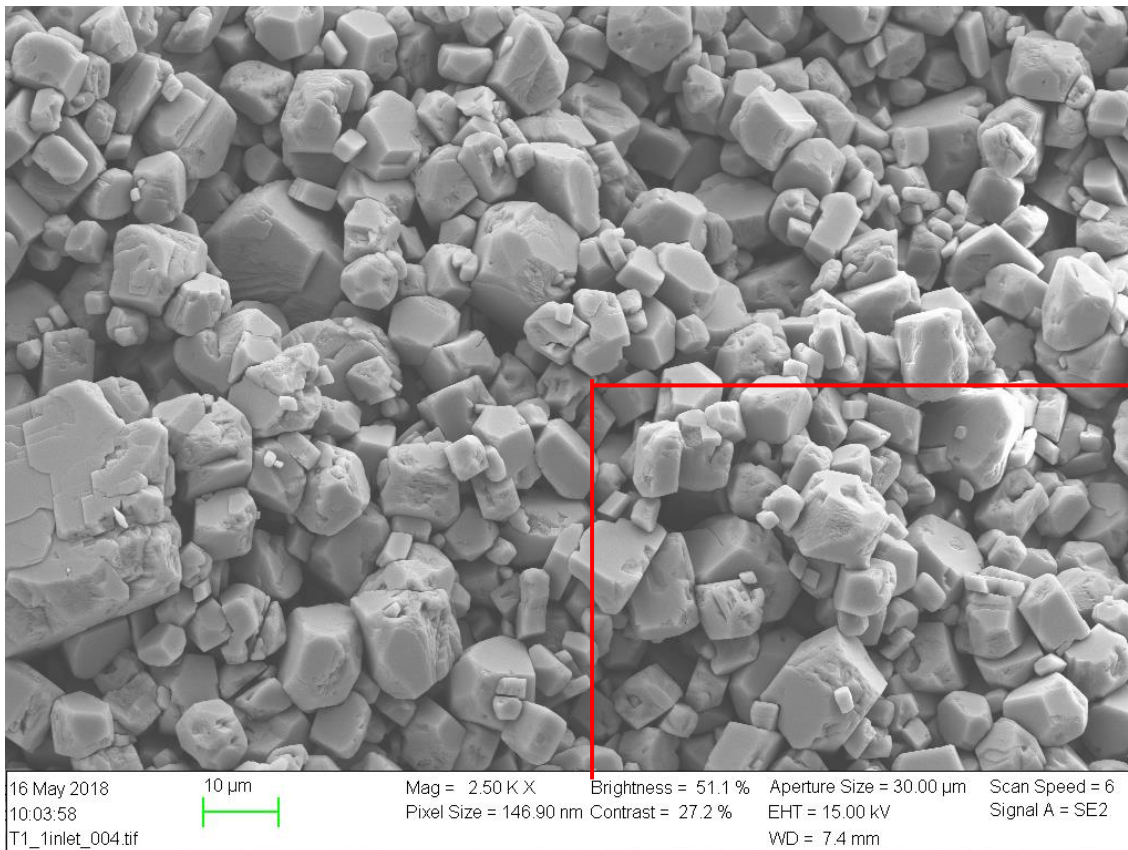


Figure A. 2: SEM image of inlet for HP1.

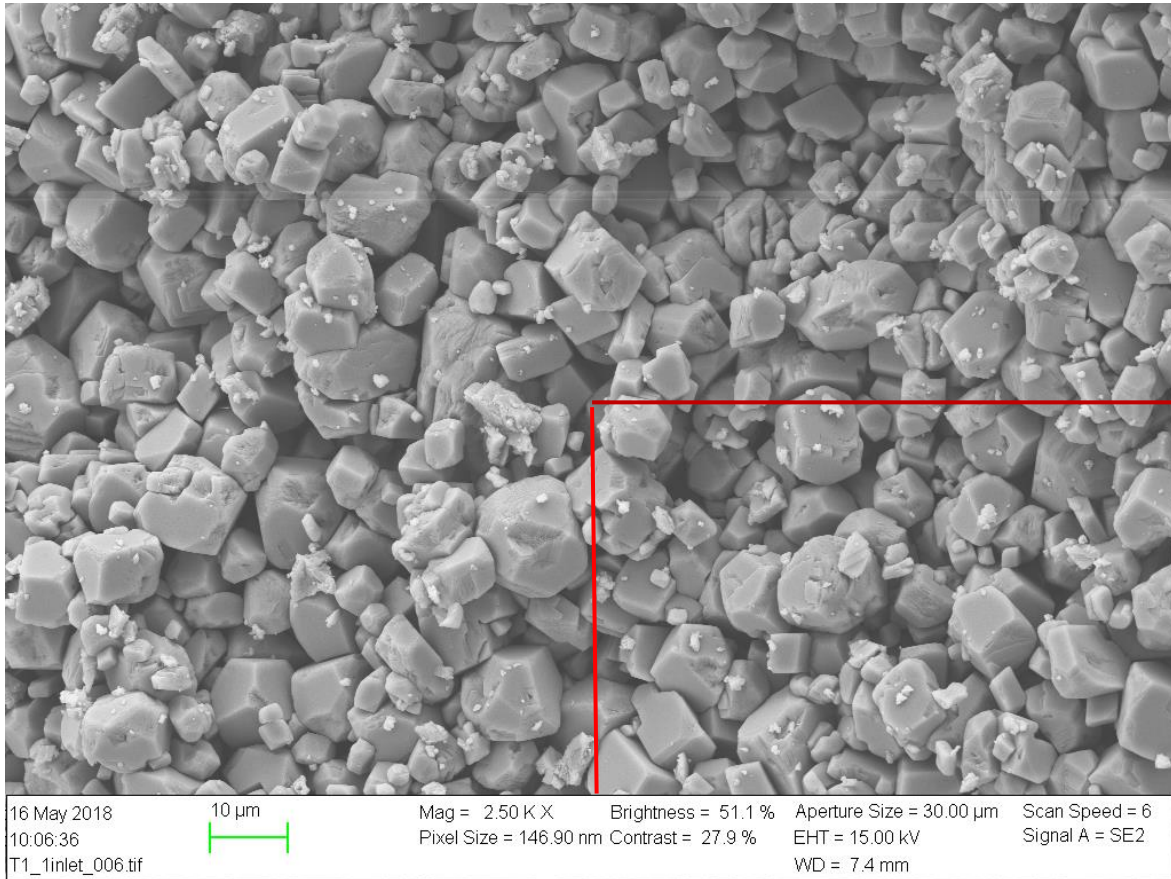


Figure A. 3: SEM image of inlet for HPI.

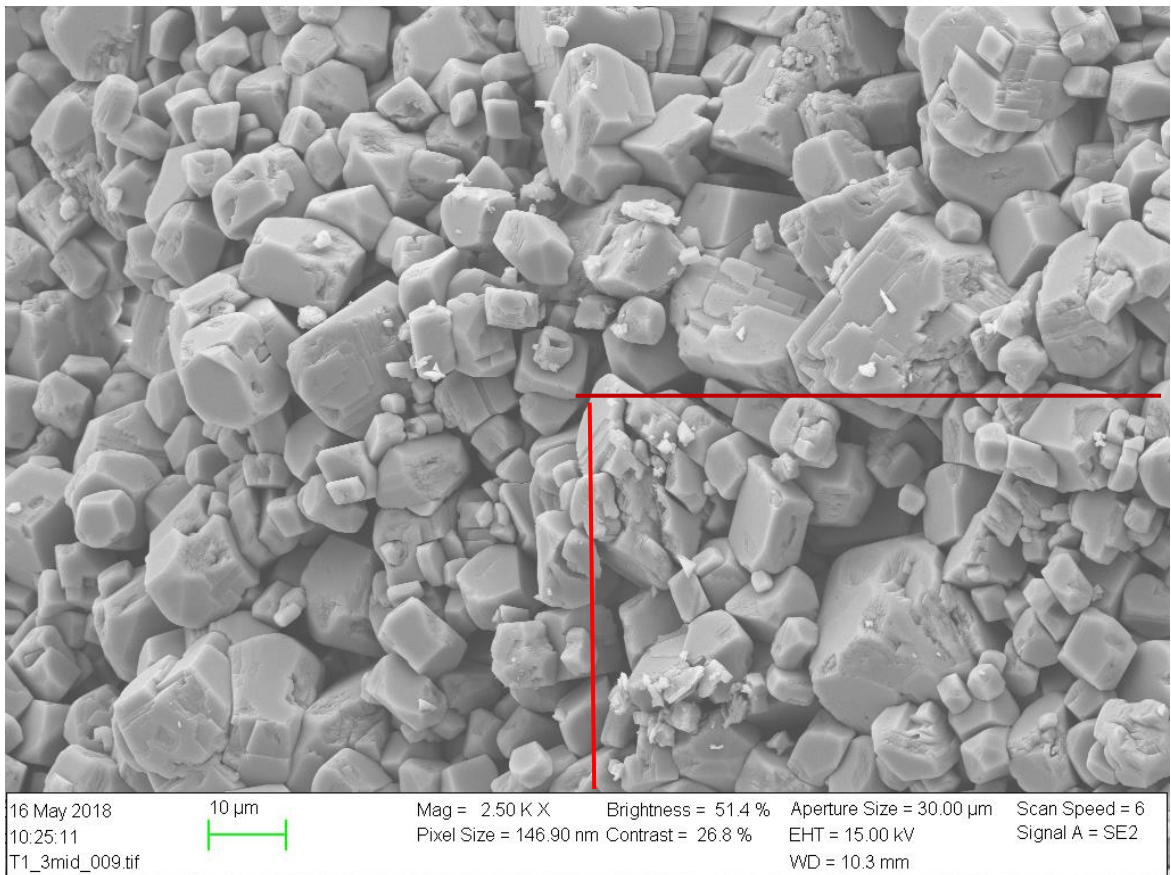


Figure A. 4: SEM image of the middle for HP1.

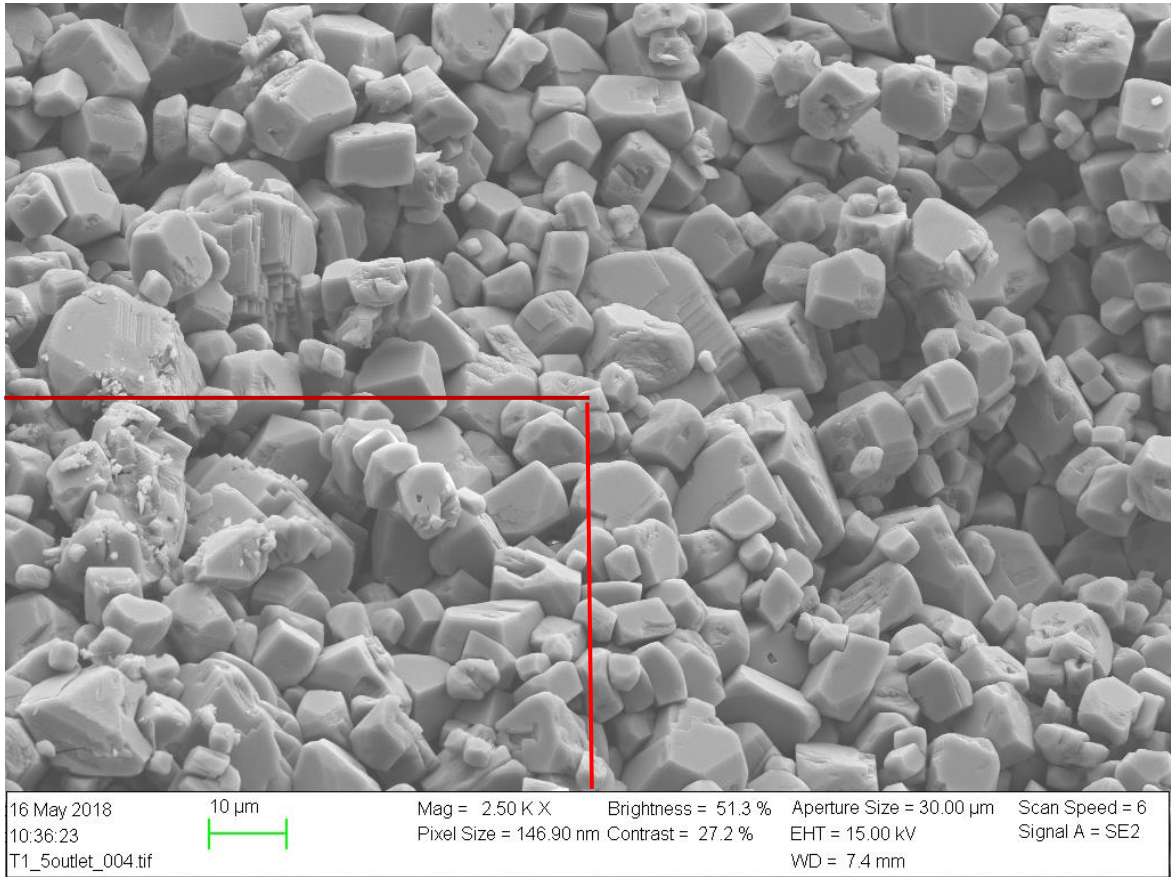


Figure A. 5: SEM image of outlet for HP1.

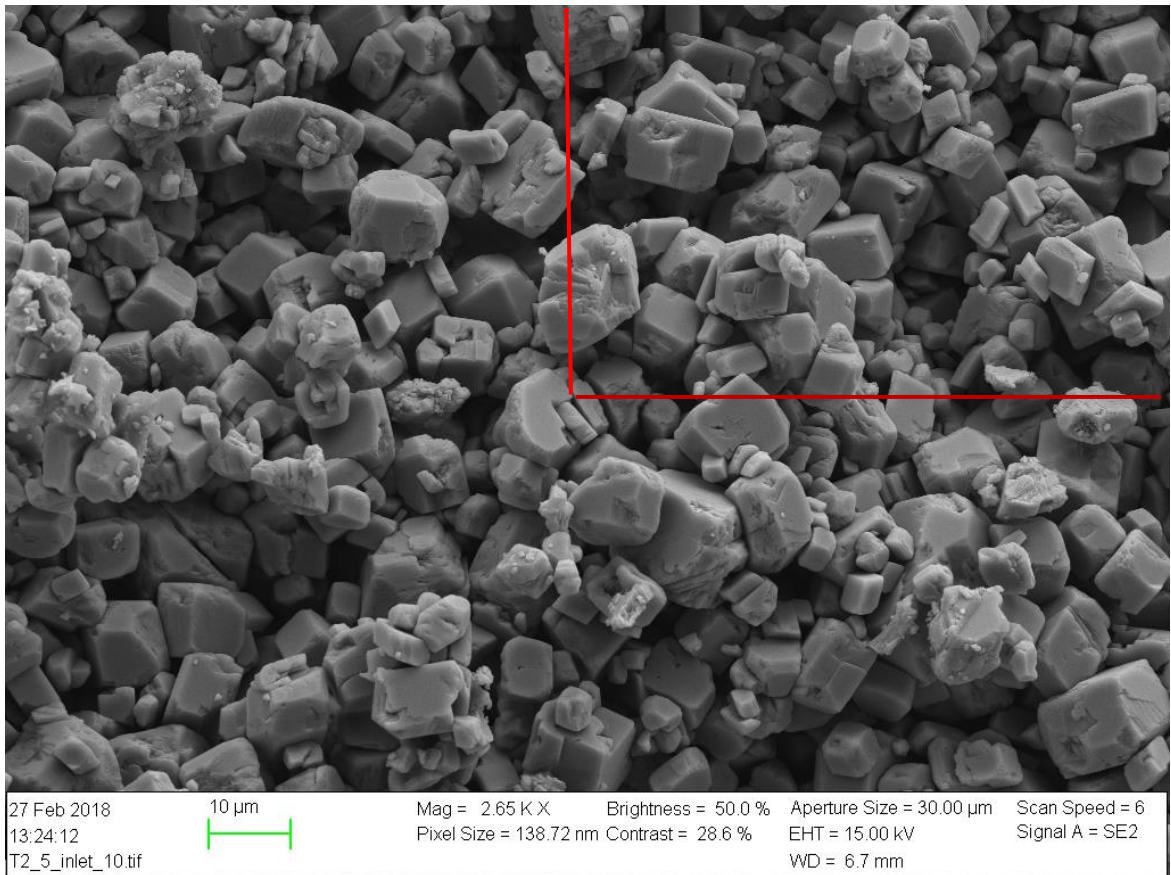


Figure A. 6: SEM image of inlet for HP2.

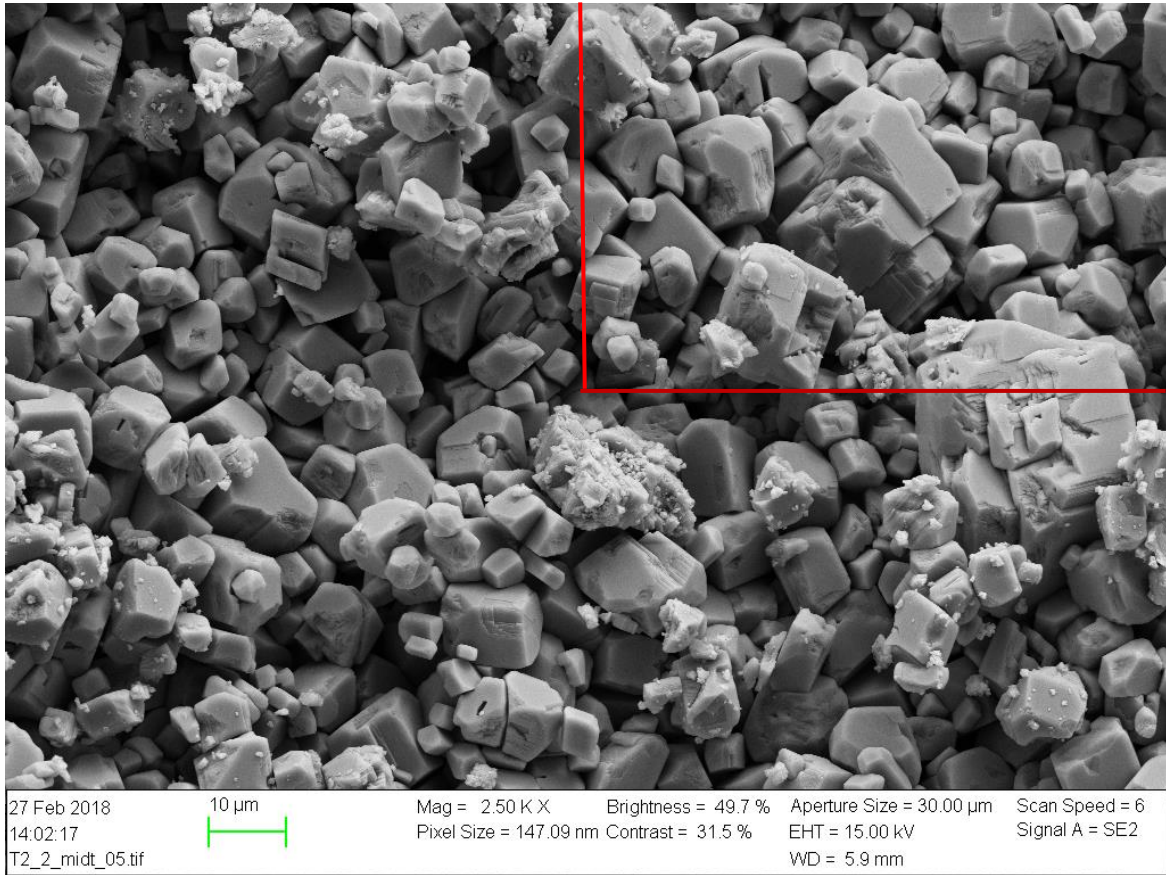


Figure A. 7: SEM image of the middle for HP2.

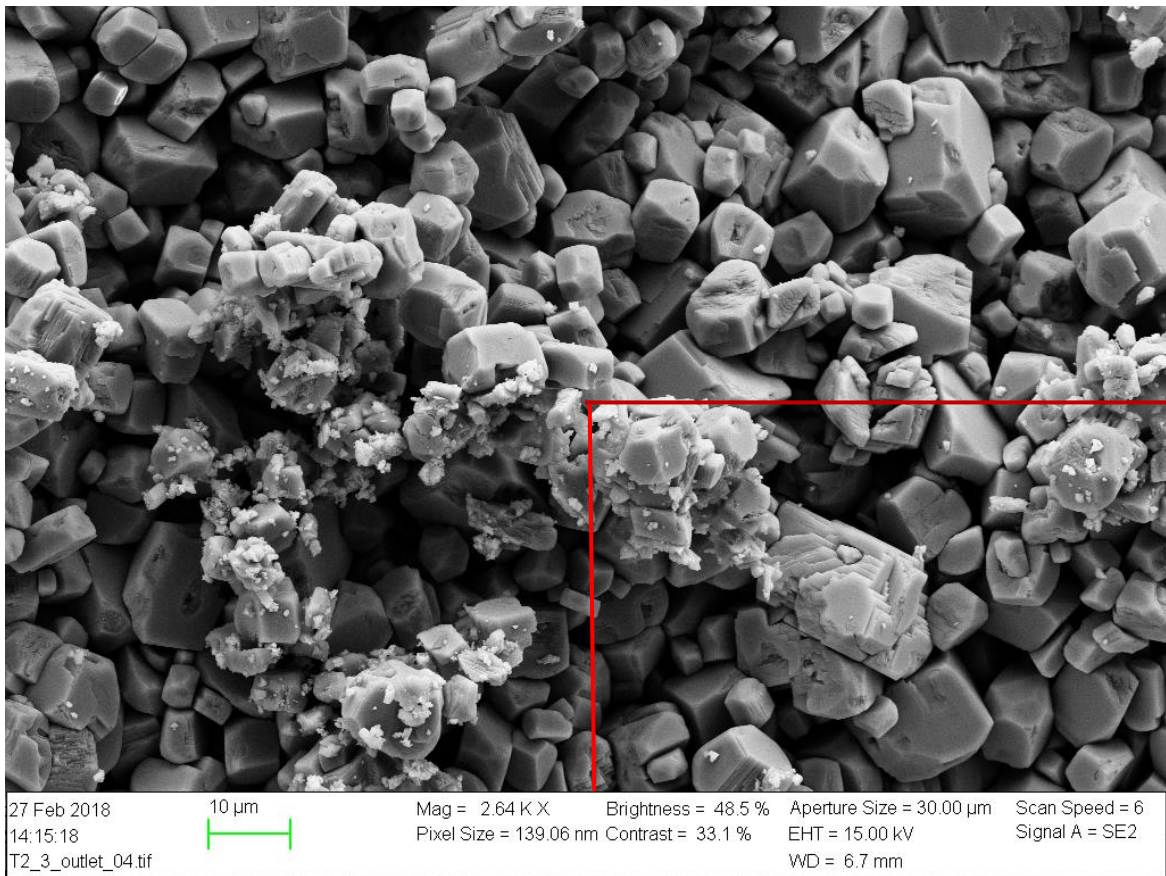


Figure A. 8: SEM image of outlet for HP2.

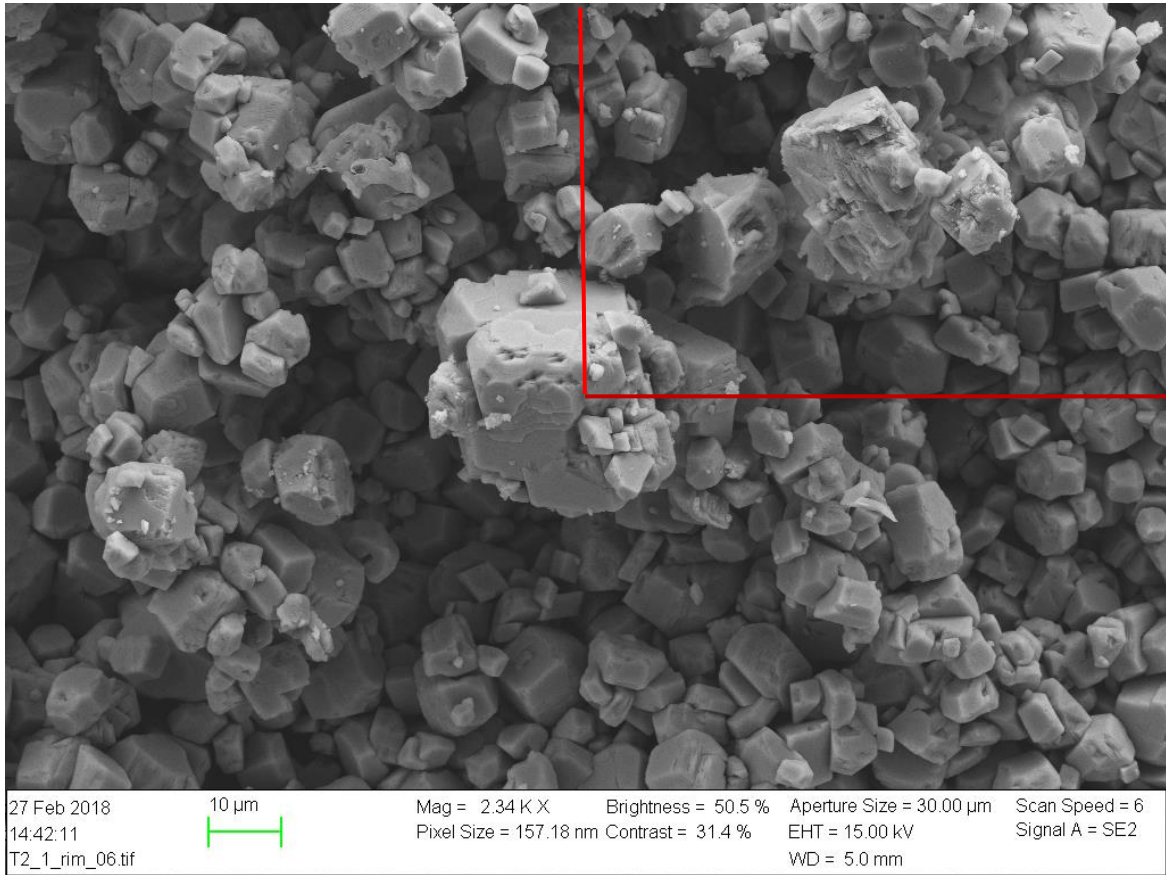


Figure A. 9: SEM image of rim for HP2.

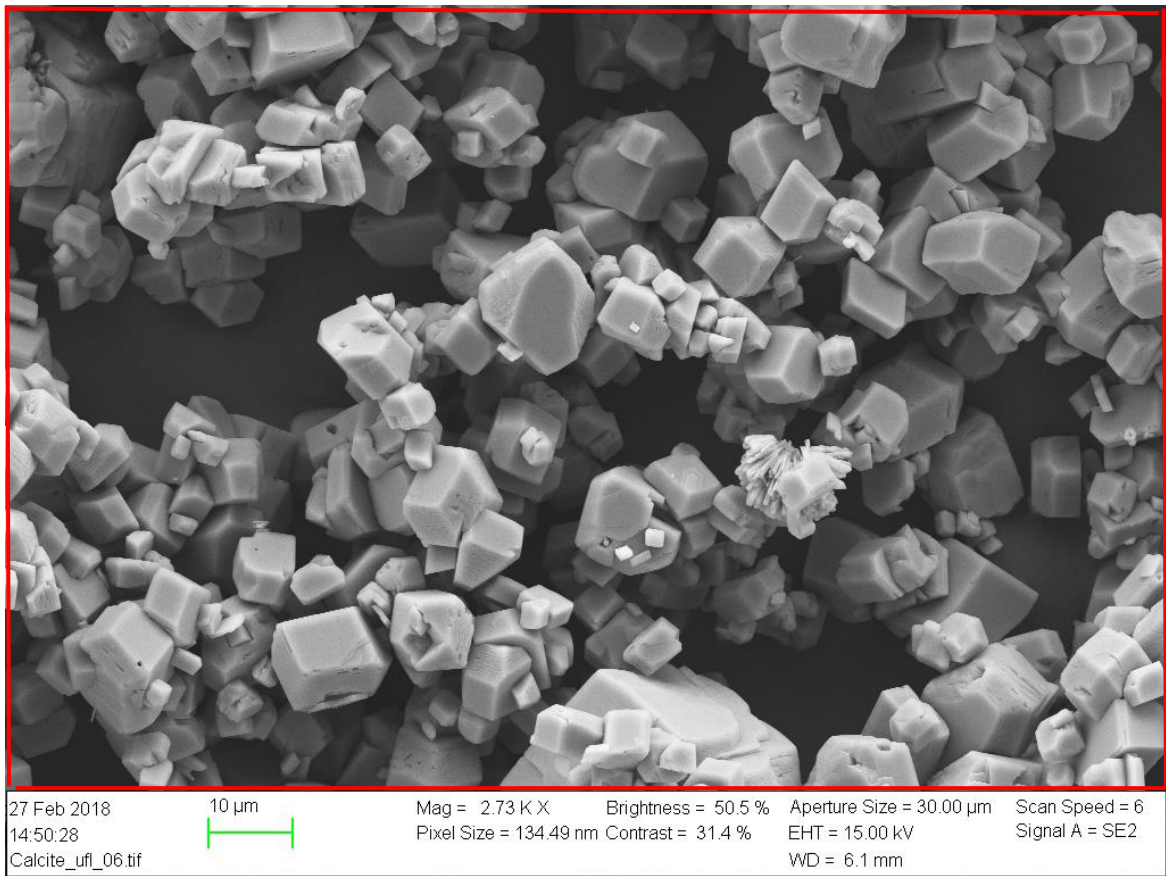


Figure A. 10: SEM image of the powder used to make the core.

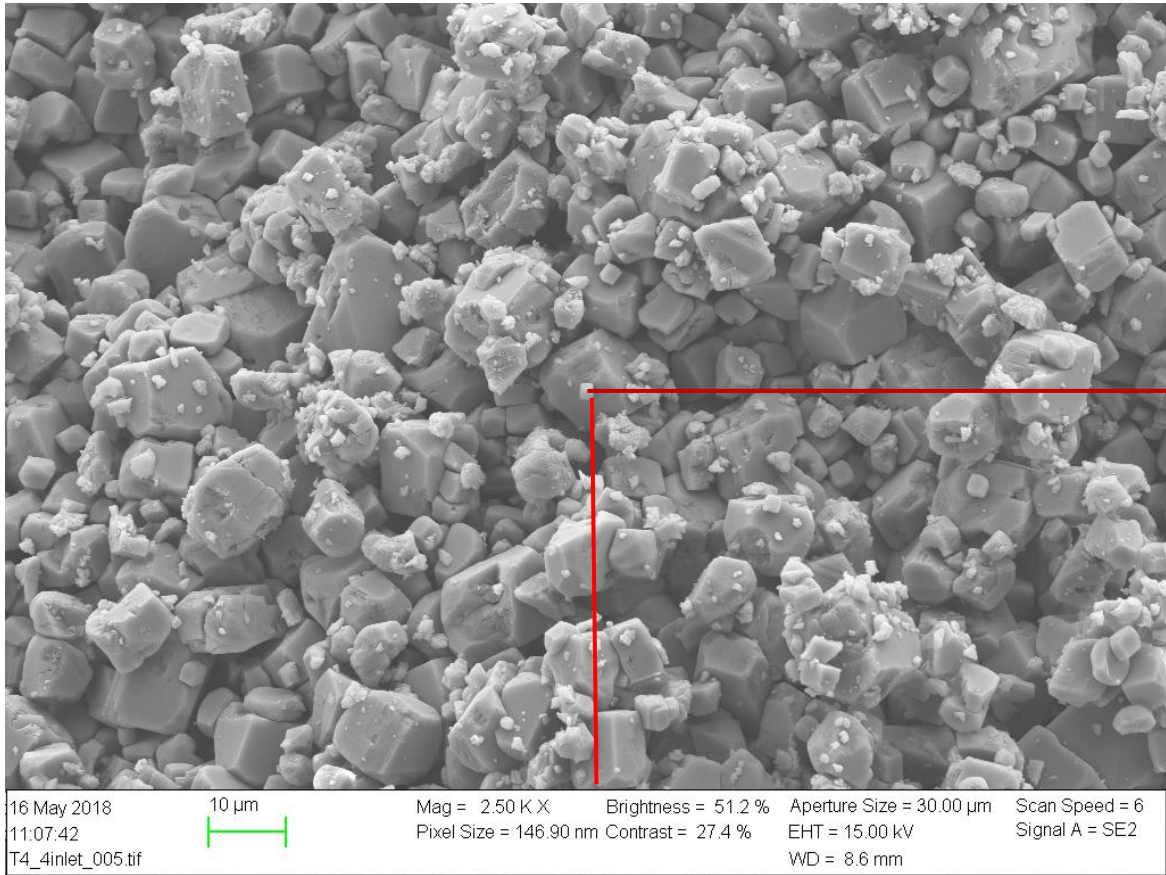


Figure A. 11: SEM image of inlet for HP4.

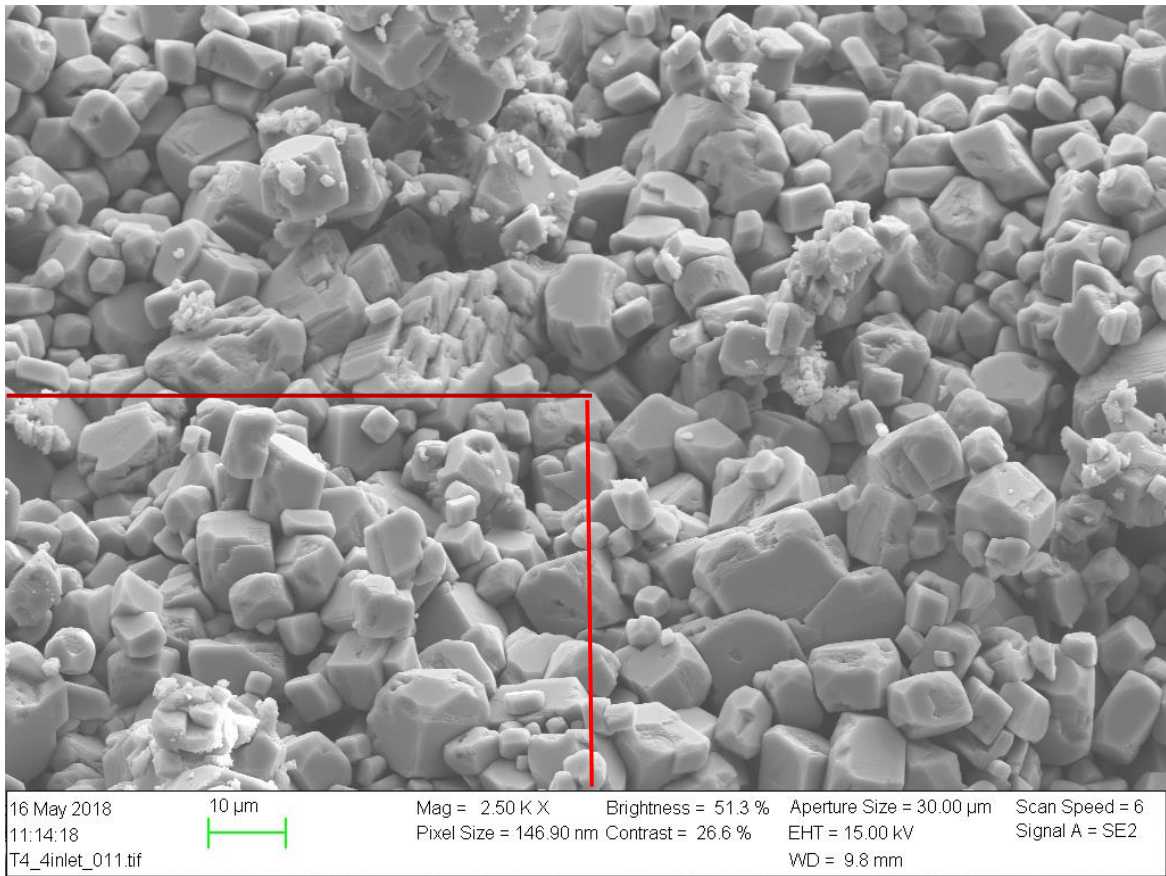


Figure A. 12: SEM image of inlet for HP4.

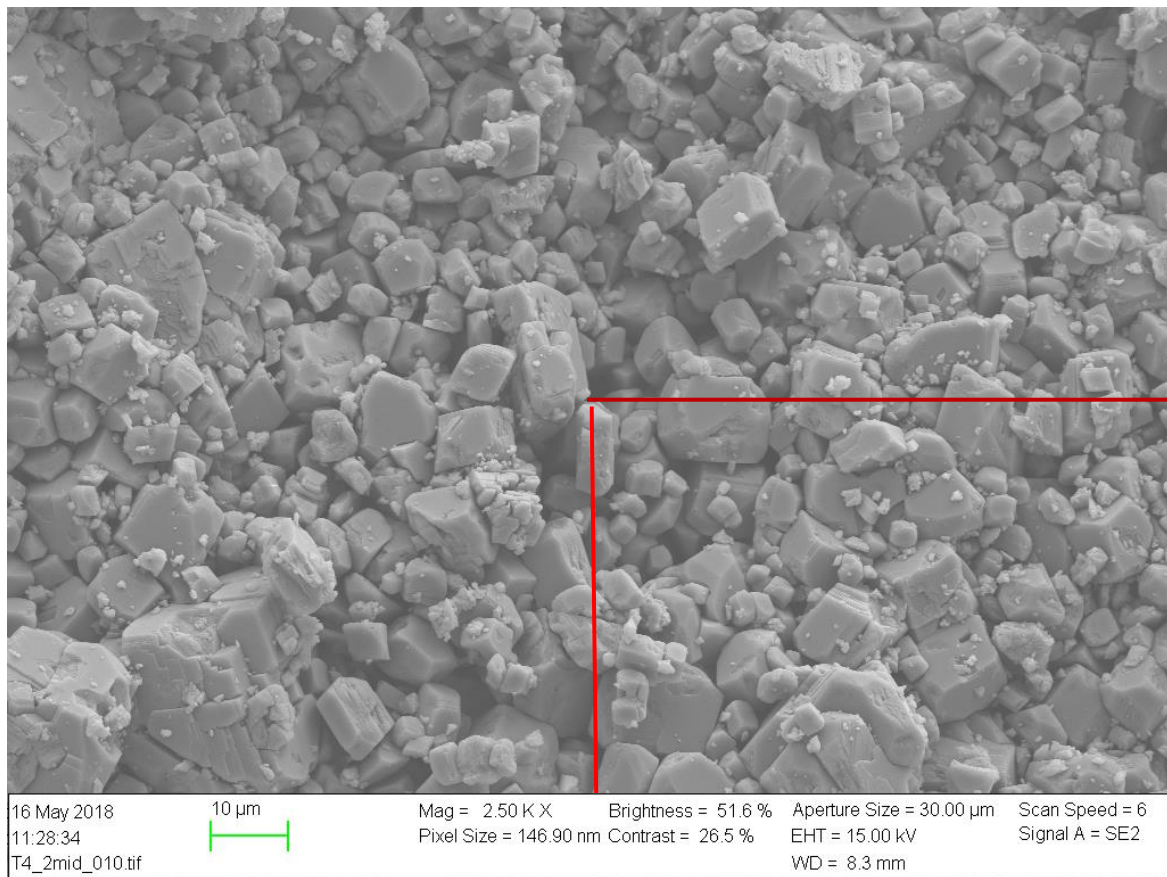


Figure A. 13: SEM image of the middle for HP4.

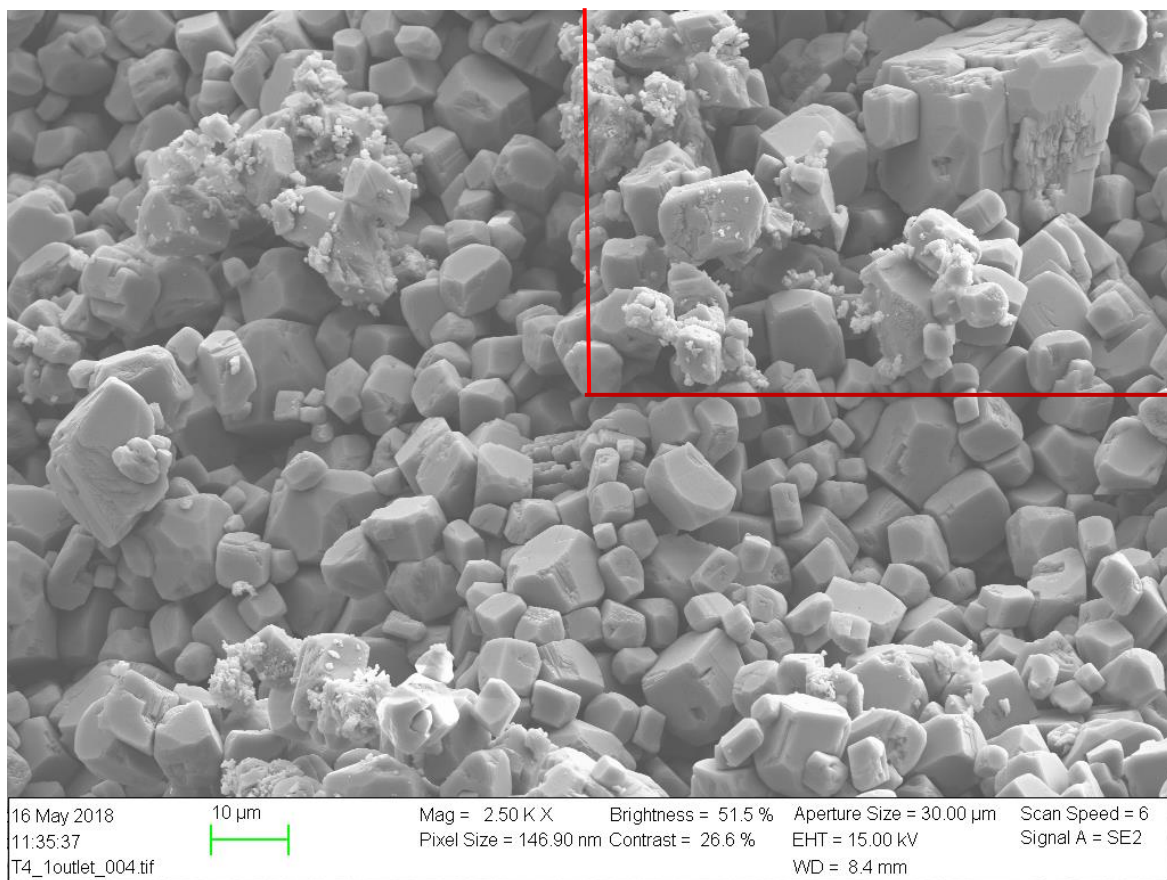


Figure A. 14: SEM image of outlet for HP4.

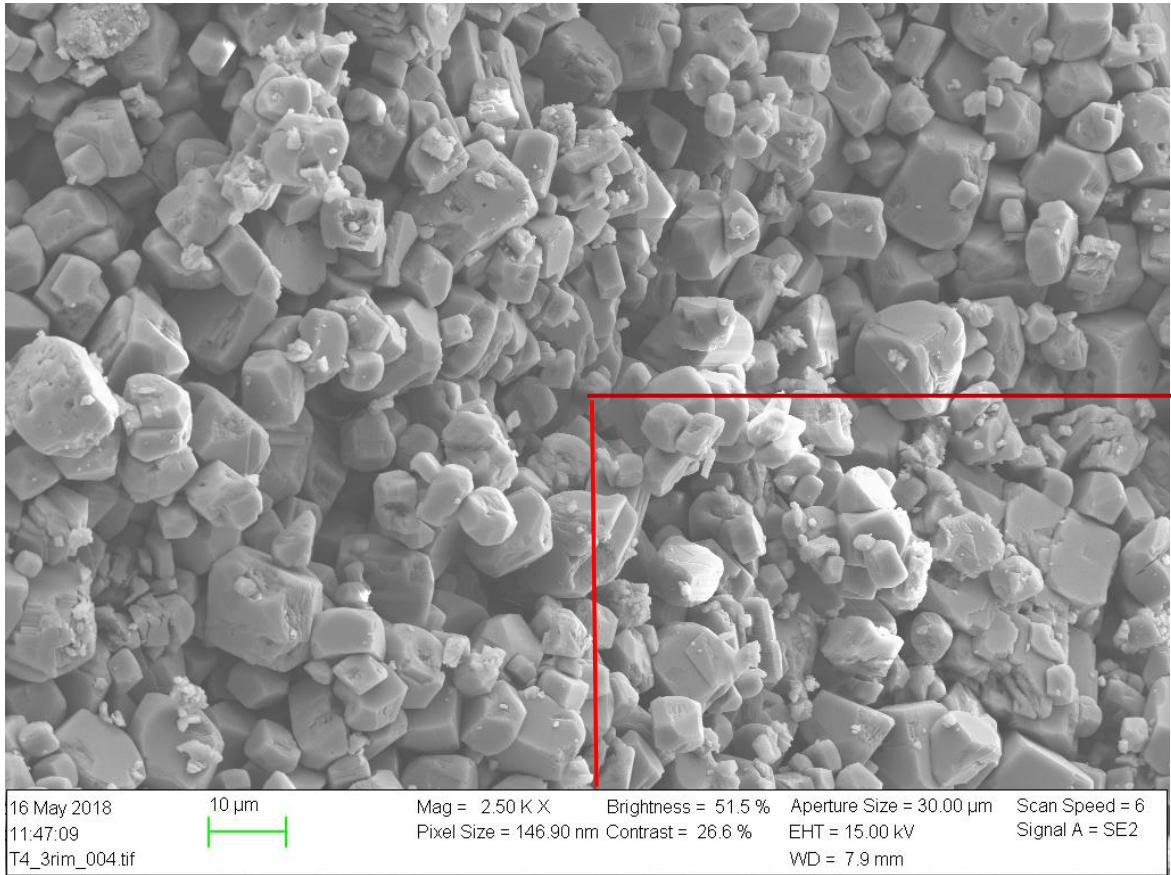


Figure A. 15: SEM image of rim for HP4.

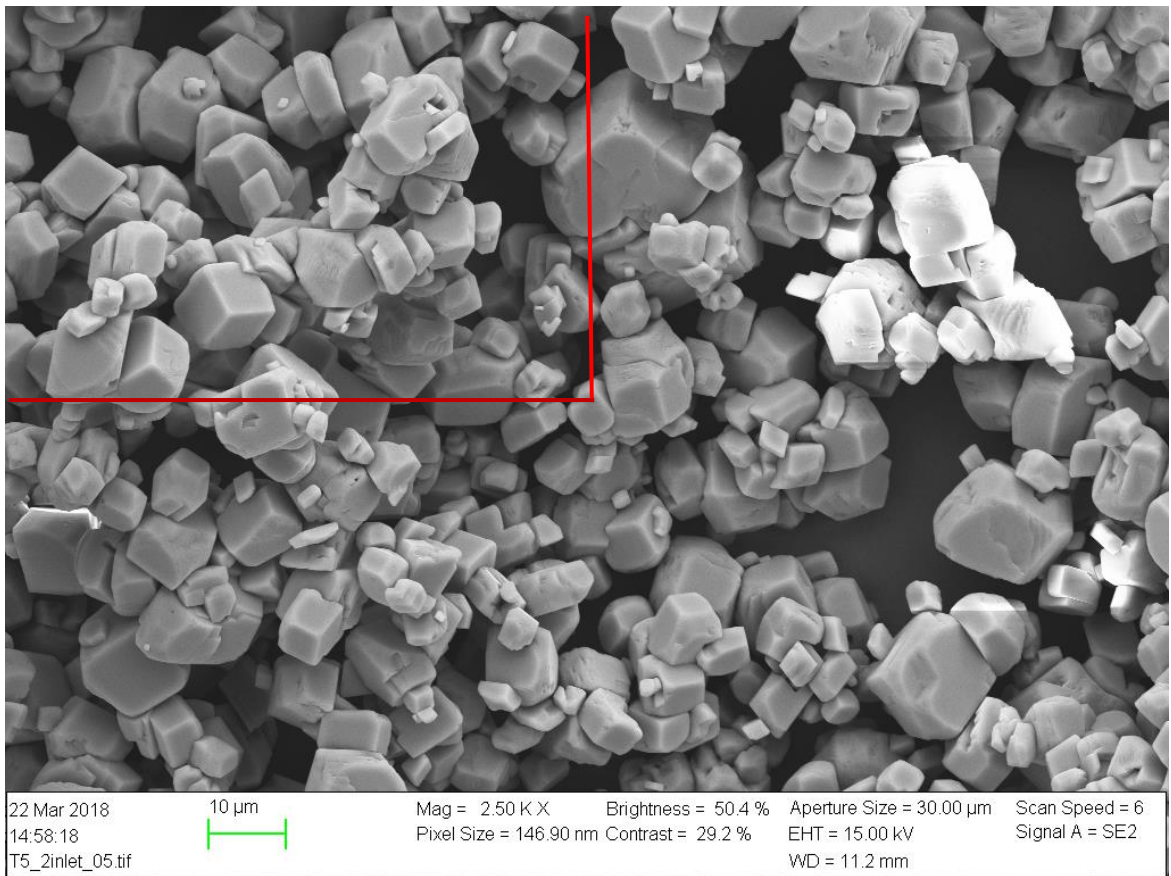


Figure A. 16: SEM image of inlet for LP5.

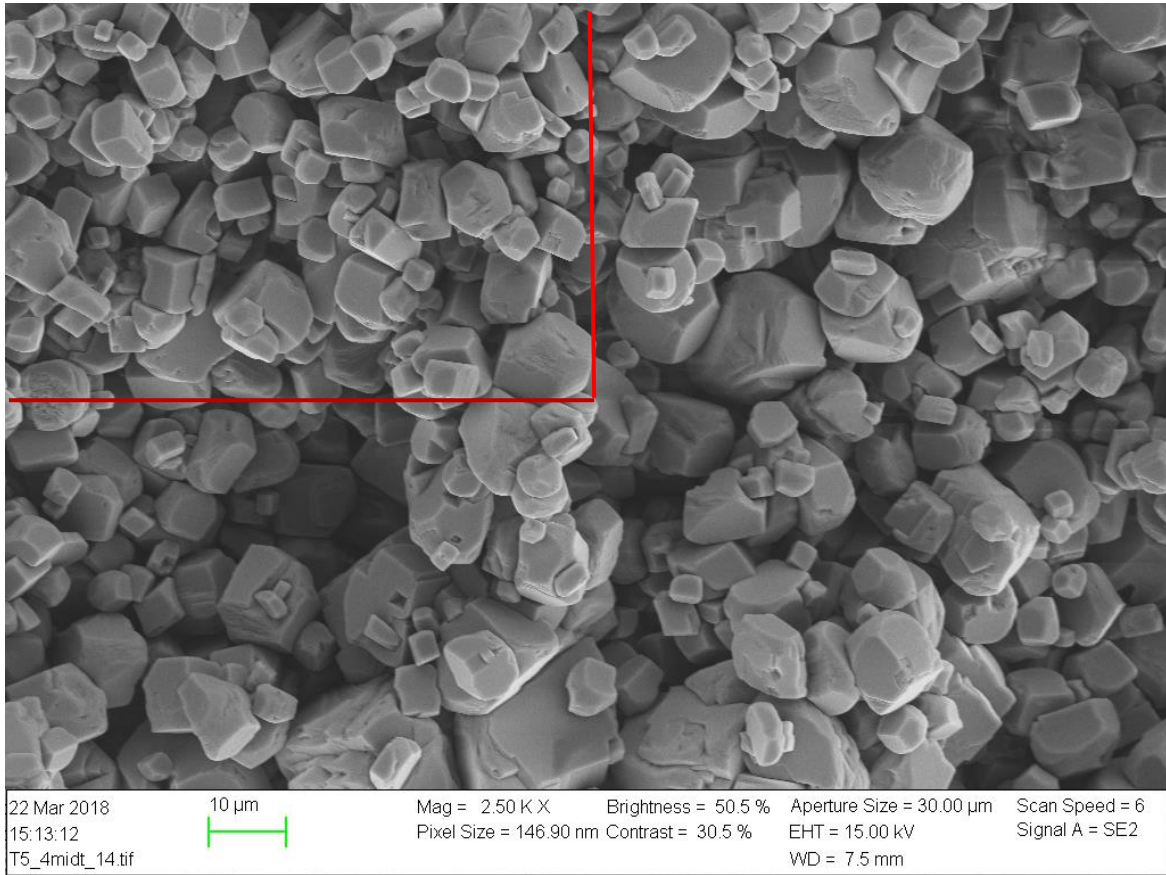


Figure A. 17: SEM image of the middle for LP5.

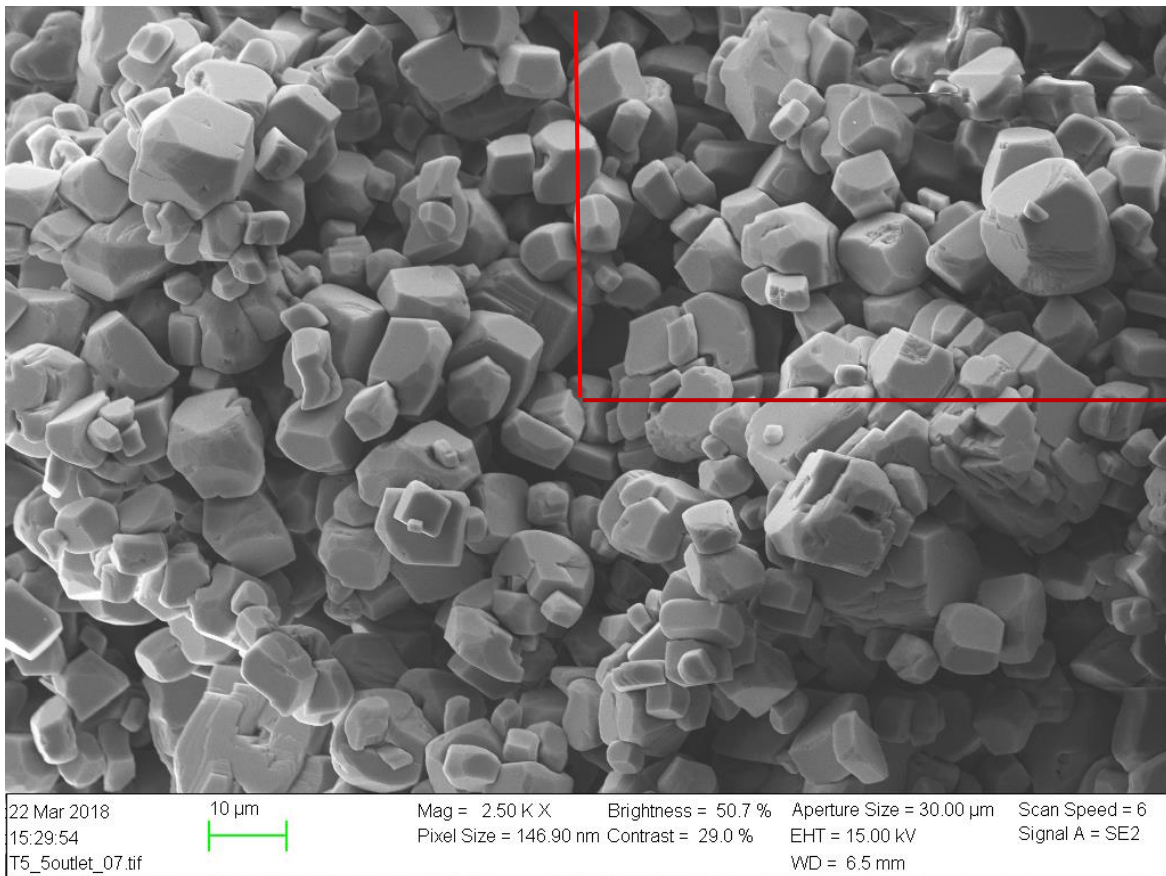


Figure A. 18: SEM image of outlet for LP5.

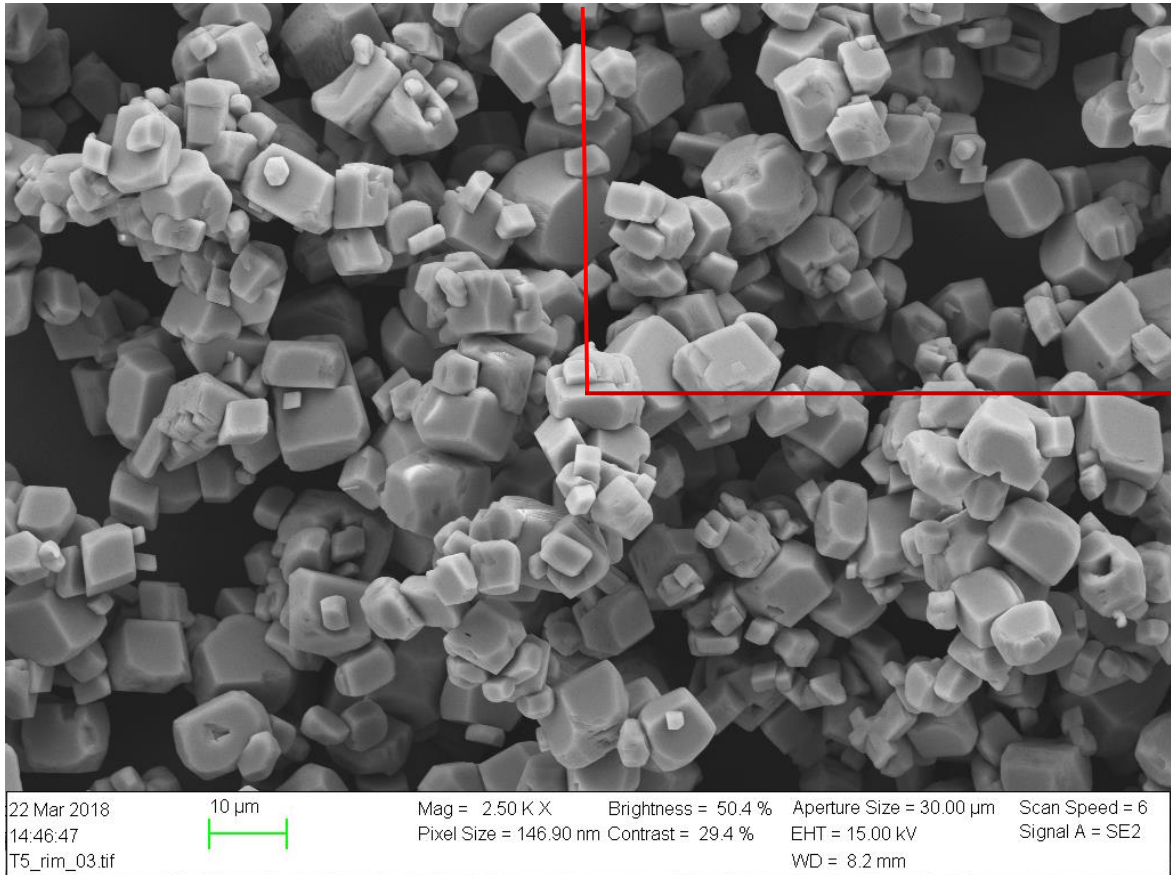


Figure A. 19: SEM image of rim for LP5.

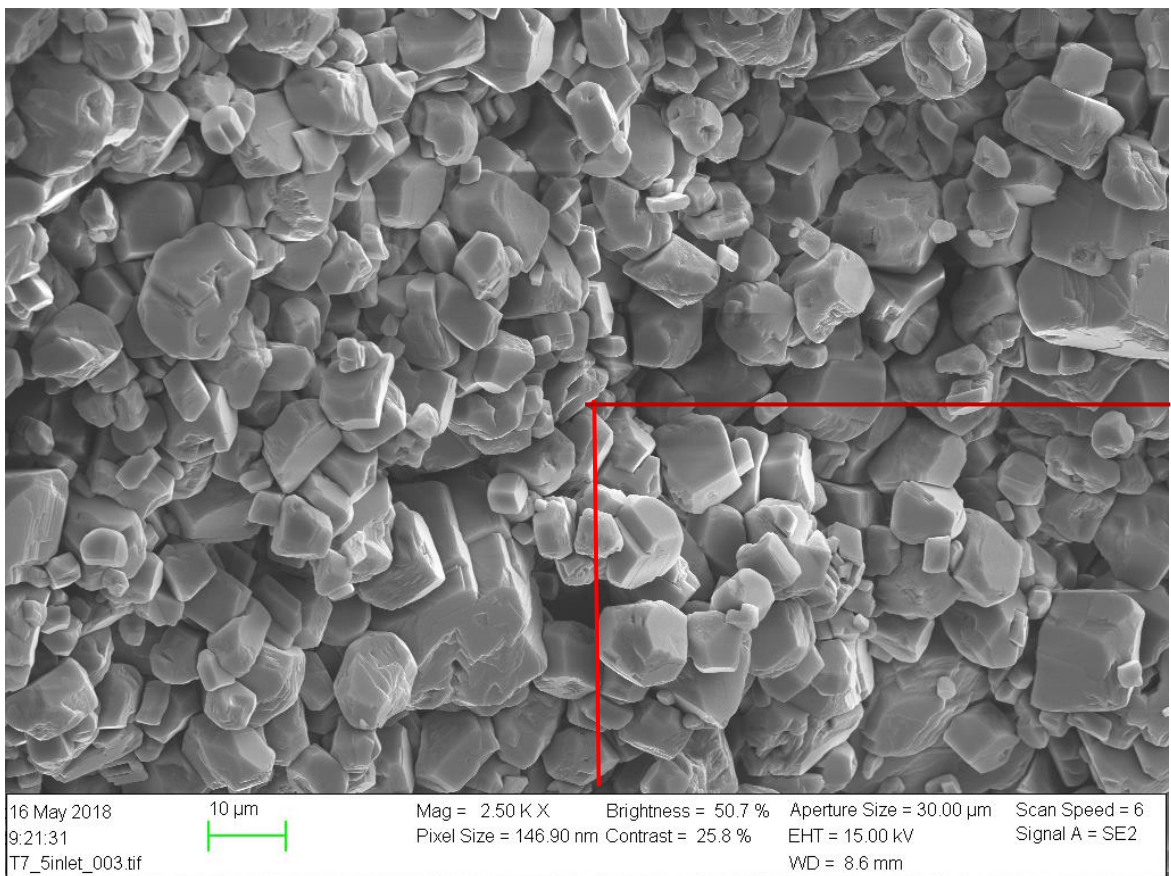


Figure A. 20: SEM image of inlet for HPA7.

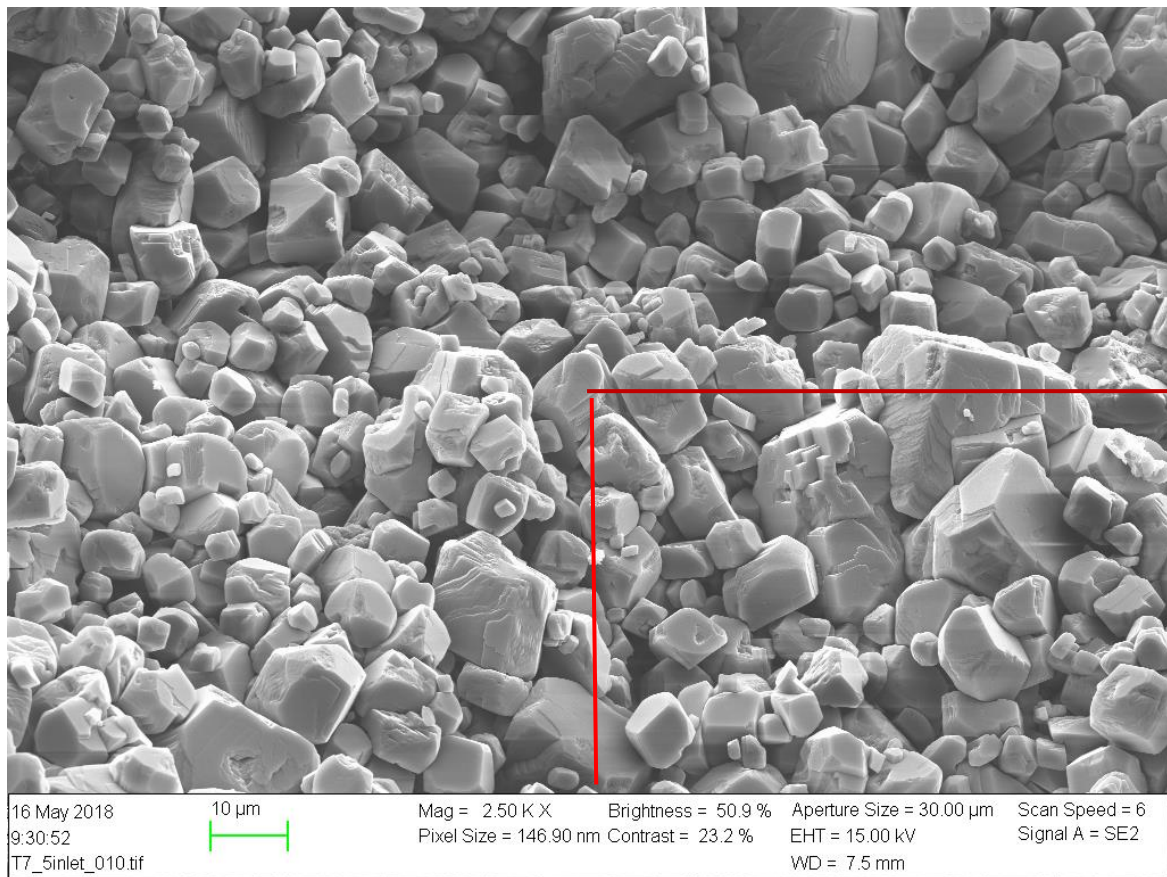


Figure A. 21: SEM image of inlet for HPA7.

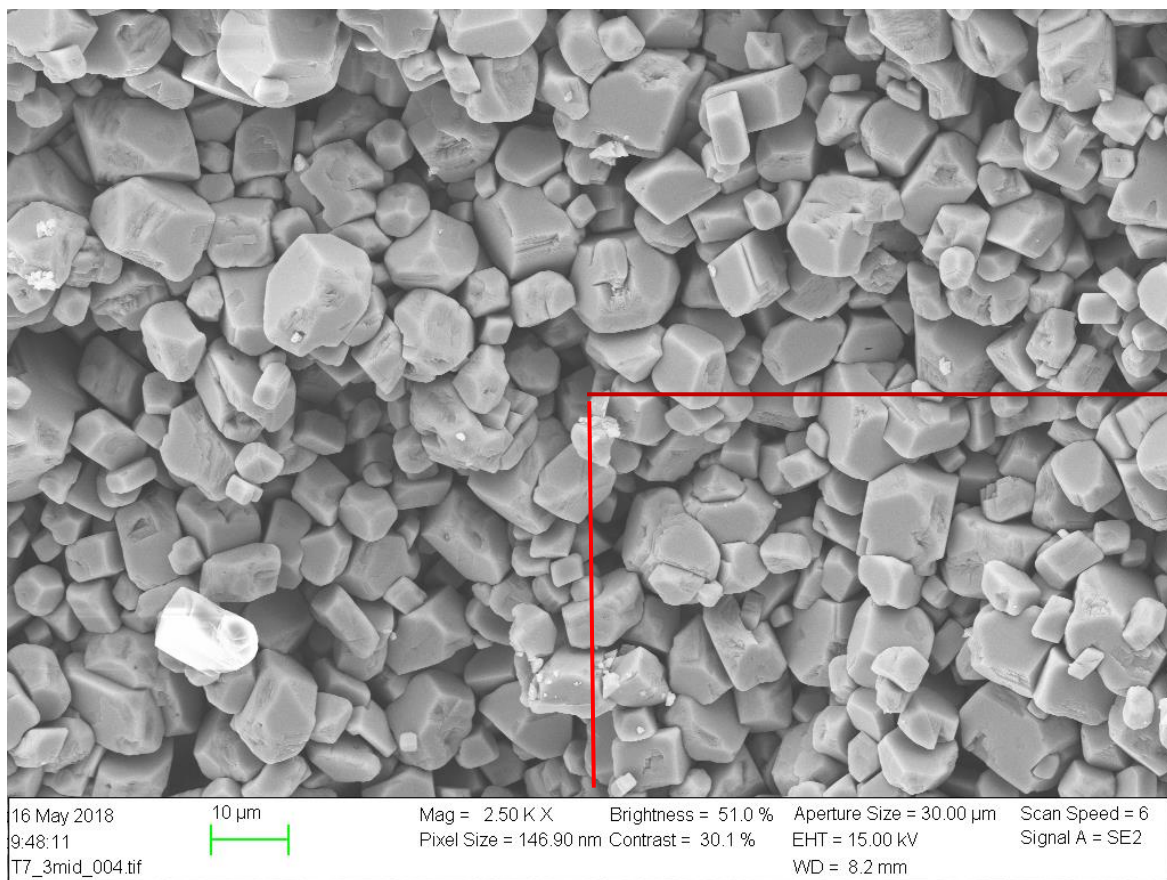


Figure A. 22: SEM image of the middle for HPA7.

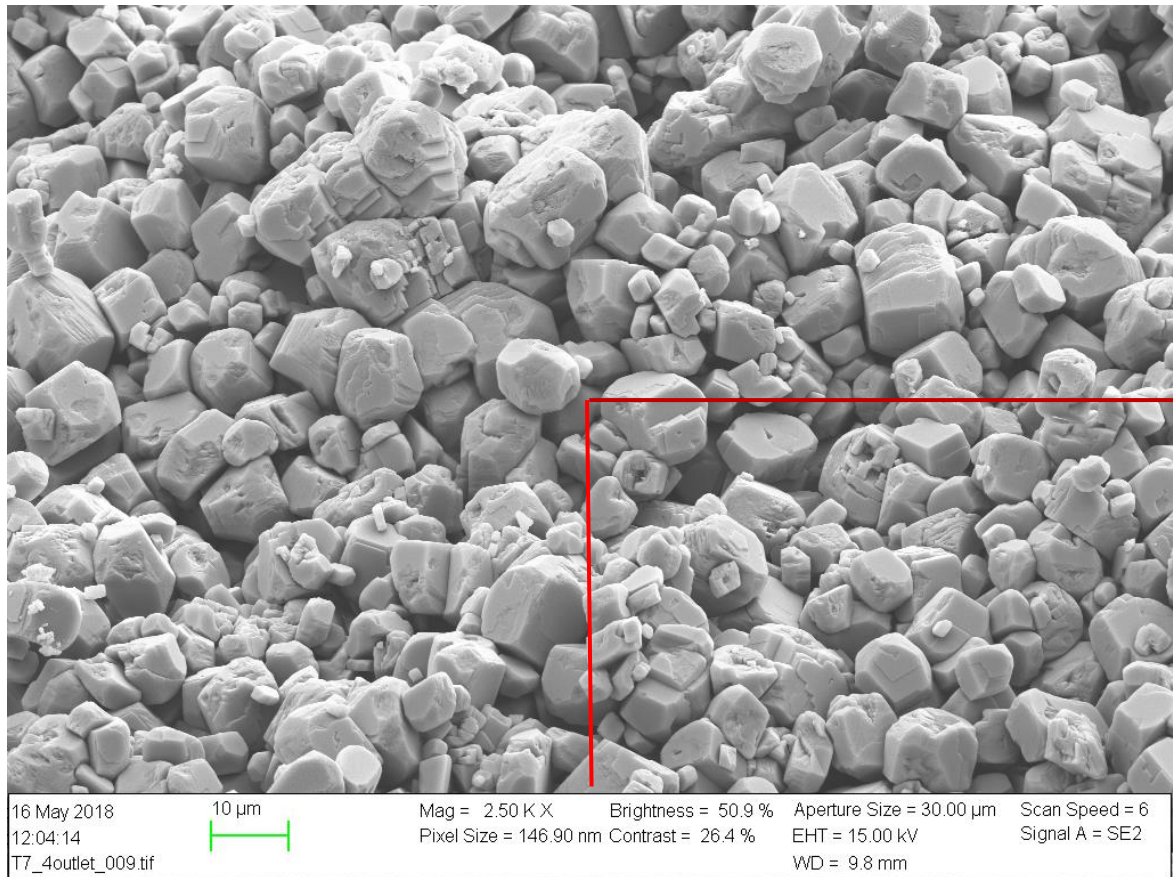


Figure A. 23: SEM image of outlet for HPA7.